N°EDMS: 1132104

UNIVERSITÉ DE PICARDIE JULES VERNE

École Doctorale de la Faculté de Sciences et Santé

Standard and Experimental Approach for Advanced Controls in Cryogenics

Marco Pezzetti

MEMOIRE DE THÈSE
Présenté pour le grade de Docteur, Mention Automatique

Date de soutenance: **18 Octobre 2010**

JURY

Rapporteurs:

Ivan ZELINKA,	*Professeur* Université de Thomas BATA, Zlin République Tchèque
Vladan KONCAR,	*Professeur* ENSAIT, Roubaix France

Examinateurs:

Ahmed RACHID,	*Professeur* (Directeur de thèse) Université de Picardie Jules Verne, Amiens France
Mohammed CHADLI,	*Maître de Conférences* (Directeur de thèse) Université de Picardie Jules Verne, Amiens France
Hervé COPPIER,	*Ingénieur* ESIEE, Amiens France (Président)

To Raquel, Eleonora, Gabriele, Caterina and Rossella

Acknowledgements

This work has been realized thanks to the experience accumulated over more than ten years on the construction, deployment and operation of the LHC cryogenic installations, and has been co-supervised by A. Prof. PhD. Mohammed CHADLI and Prof. PhD. Ahmed RACHID from the University of Picardie Jules Verne (UPJV), Amiens. I am really grateful to all of them for their vision, support, help, patience, and dedication. I feel privileged for having them as supervisors and friends.

I also express my recognition to Prof. Ivan ZELINKA from the University de Thomas BATA-Czech Republic, Prof. Vladan KONCAR from ENSAIT, Roubaix and Ing. Hervé COPPIER from ESIEE, Amiens to accept to review and evaluate this work.

More than ten years ago, when I chose to work for CERN instead of following my dear friend Marco Scussat for a Ph.D. thesis at the EPFL in Lausanne, I though I would never launch myself into such a scientific experience.

Four years ago, when I was at the starting block before the beginning of my Ph.D., I did not know how much a research work of this kind is demanding and challenging. I wish for everyone to experience such an intense occasion of professional and personal growth. For that I am really grateful to Philippe Lebrun, the former leader of the CERN Technology Department, and to his successor Frédérick Bordry for the permission granted, and to Giorgio Passardi and Laurent Tavian, my former and current group leader. Many thanks also to Johan Bremer, Allain Gonidec and the ATLAS collaboration for allowing me to carry out my experimental campaign on their systems.

My thanks goes also to Philippe Gayet, Enrique Blanco, Benjamin Bradu, Edouard Rogez and Czeslaw Fluder for the many fruitful project collaborations and the technical support that have made this experience possible, and to all the Cryogenics Group and the Control & Electricity Section for their help to perform the work properly.

A very special thanks to Vitaliano Inglese and Alexandre Moraux, who spent some time collaborating with me on the final architecture of this project. I feel privileged to have worked with them, brilliant and highly skilled engineers.

I would like to dedicate this thesis to my parents and my brother for instilling into me the strength to pursue my goals and dreams, and specially to my wife, Raquel, for her love and patience during this long period.

Contents

List of Figures

List of Tables

List of symbols

Latin letters

- A : Area $[m^2]$
- a, r, t : Absorbed, Reflectivity, Transmissivity [-]
- $C_x(T)$: Specific heat of x at T $[J \cdot kg^{-1} \cdot K^{-1}]$
- d : Diameter $[m]$
- f : Friction factor [-]
- Gr : Grashof number [-]
- h : Heat transfer coefficient $[W \cdot m^{-2} \cdot k^{-1}]$
- k : Thermal conductivity $[W \cdot m^{-1} \cdot k^{-1}]$
- L : Length $[m]$
- m & n: Integer numbers [-]
- m_x : Mass of x $[kg]$
- M_x : Molar mass of x $[kg \cdot mol^{-1}]$
- Nu : Nüsselt number [-]
- P : Light flux $[lm]$
- p : Pressure $[bar]$
- Pr : Prandtl number [-]
- Q : Heat $[J]$
- R : Ideal gas constant $[8.314\ J \cdot K^{-1} \cdot mol^{-1}]$
- Ra : Rayleigh number [-]
- Re : Reynolds number [-]
- T : Temperature $[K][^\circ C]$
- v : Speed $[m \cdot s^{-1}]$
- V : Volume $[m^3][L]$
- W : Work $[J]$

Greek letters

- α : Accommodation coefficient [-]
- γ : Ratio between C_p and C_v [-]
- ϵ : Effective emissivity [-]
- λ : free path of gas molecules $[m]$
- μ : Viscosity $[Pa \cdot s]$
- σ : Stefan-Boltzmann constant $[5.6704 \cdot 10^{-8} \cdot kg \cdot s^{-3} \cdot K^{-4}]$

- ρ : Density $[kg/m^3]$
- ω : Pulsation $[rad \cdot s^{-1}]$

Subscripts

- c : cold surface
- f : fluid
- g : gas phase
- h : warm surface
- in : inlet flow
- l : liquid phase
- out : outlet flow
- s : contact surface
- sc : screen
- v : saturation temperature
- W : Wall

Abbreviations and acronyms

- $ALICE$: A Large Ion Collider Experiment
- $ARX/ARMA/ARIMA/ARIMAX/CARIMA$: Auto Regressive (Integrated Moving) Average (with eXternal inputs)
- $ATLAS$: A Toroidal LHC ApparatuS
- CCL : Close Control Loop
- $CERN$: European Organization for Nuclear Research
- $CIET$: Cryogenic Instrumentation Expert Tool
- CMS : Compact Muon Solenoid
- $DASSL$: Differential Algebraic System Solver
- DCS : Distribute Control System
- DFB : Distribution Feed Box
- $ECAL$: Electromagnetic CALorimeter
- EWS : Engineering WorkStation
- FBD : Functional Block Diagram
- FEC : Front End Computers
- FPE : Final Predicted Error
- GPC : Generalized Predictive Control
- $HCAL$: Hadron CALorimeter
- HMI : Human Machine Interface
- IL : Instruction List
- $LAr/LKr/LHe/LN2$: Liquid Argon/Krypton/Helium/Nitrogen
- LD : Ladder Diagram
- $LEP(2)$: Large Electro Positron (2)
- $LHC(b)$: Large Hardon Collider (b)
- $LS/RLS/RELS$: Least Square / Recursive Least Square / Recursive Extended Least Square

- LSS : Long Straight Section
- $MAWS$: Modeling Workstation
- MBC : Model Based Control
- $MIMO/SISO$: Multiple Inputs Multiple Outputs / Signle Input Single Output
- MTB : Mobile Test Benches
- NCS : Networked Control System
- ODE : Ordinary Differential Equation
- OLE : Object Linking and Embedding
- OPC : OLE Process Control
- OWS : Operator Workstation
- PDM : Process Device Manager
- $PERL$: Practical Extraction and Report Language
- PFC : Predictive Function Control
- PID : Proportional Integral Derivative
- PLC : Programmable Logic Controller
- $PRBS$: Pseudo Random Binary Signal
- $PROCOS$: PROcess and COntrol Simulator
- $PROFIBUSDP/PA$: Process Field Bus : Decentralized Peripherals / Process Automation
- RF : Radio Frequency
- RIO : Remote Input/Output
- $SCADA$: Supervisory Control And Data Acquisition
- SPS : Super Proton Synchrotron
- ST : Structured Text
- $UNICOS$: UNified Industrial Control System
- UPS : Uninterruptible Power Source
- VCP : Virtual Control Platform

List of publications

2007

"**Process identification through test on cryogenic system**" Marco Pezzetti, Herve Coppier, Mohammed Chadli, Ahmed Rachid. EUROSIM2007 - Federation of European Simulation Societies. University of Ljubljana, Slovenia.

"**Modeling workstation for a Krypton condenser system**" Alexandre Moraux, Marco Pezzetti, Herve Coppier, Ahmed Rachid, Mohammed Chadli. EUROSIM2007 - Ljubljana. Slovenia.

2008

"**Modélisation, simulation et contrôle des installations cryogéniques du CERN**" Benjamin Bradu, Alexandre Moraux, Marco Pezzetti REE Revue de l'électricité et de l'électronique, REE N° 4 Avril 2008.

"**De l'Identification du Modèle au Contrôle : Le MultiContrôleur, Stratégie pour la Régulation Avancée dans les Systèmes Complexes des Expériences du CERN**" Hervé Coppier, Sébastien Cabaret, Marco Pezzetti. CIFA 2008 - Conférence Internationale Francophone d'Automatique Bucarest, Roumanie.

"**The upgrade of the control system for the CERN/NA62 liquid Krypton de-**

tector" Moraux A., Bremer J., Falaleev V., Gonidec A., Passardi G., Pezzetti M. 22nd International Cryogenic Engineering Conference (ICEC 22) and International Cryogenic Materials Conference (ICMC 2008) ICEC22-ICMC2008 , Seoul, Dem. Peo. Rep. of Korea.

"**A simulation study for the virtual commissioning of the CERN central helium liquefier**" Rogez E., Bradu B., Moraux A., Pezzetti M., Gayet P., Coppier H. ICEC22-ICMC2008 , Seoul, Dem. Peo. Rep. of Korea.

"**First cool-down and test at 4.5K of the ATLAS superconducting magnet system assembled in the LHC experimental cavern**" G. Passardi, K. Barth, N. Delruelle, A. Dudarev, F. Haug, O. Pavlov, M. Pezzetti, O. Pirotte, H.H.J. Ten Kate, D.E. Baynham, C. Mayri, R. Pengo, A.Yamamoto ICEC22-ICMC2008 , Seoul, Dem. Peo. Rep. of Korea.

"**Cryogenic characterization of the ATLAS barrel toroid superconducting magnet**" R. Pengo, K. Barth, N. Delruelle, M. Pezzetti, O. Pirotte, G. Passardi, A. Dudarev, and H. ten Kate ICEC22-ICMC2008 , Seoul, Dem. Peo. Rep. of Korea.

"**Design principles and operational results of the cryogenic system for the ATLAS liquid Argon calorimeter**" Fabre C., Bremer J., Chalifour M., Gonidec G., Passardi G., Petit P., Pezzetti M., Wicek F. ICEC22-ICMC2008 , Seoul, Dem. Peo. Rep. of Korea.

2009

"**The Control System for the cryogenics in the LHC tunnel: First Experience and Improvements**" P. Gomes, E. Blanco, J. Casas, C. Fluder, E. Fortescue, P. Le Roux, G. Penacoba, M. Pezzetti, M. Soubiran, A. Tovar, L. Zwalinski. 12th International

Conference On Accelerator And Large Experimental Physics Control Systems Related conference - ICALEPCS 2009, KOBE, JAPAN, Japan.

"**Helium Cryoplant Off-line Commissioning and Operator Training: two Applications of the PROCOS Simulation System at CERN**" M. Pezzetti, B. Bradu, P. Gayet, Julien Vasseur. ICALEPCS2009, Kobe Japan.

"**Advanced control facility for the CERN-UNICOS framework**" M. Pezzetti, D. O. Tavares, H. Coppier. ICALEPCS2009, Kobe Japan.

"**Cooling system for the MERIT high-power target experiment**" F. Haug, H. Pereira, P. Silva, M. Pezzetti, O.Pavlov, O. Pirotte, J. Metselaar, I. Efthymiopoulos, A. Fabich,J. Lettry, H.G. Kirk, K.T. McDonald, P. Titus, and J.R.J Bennett. Cryogenic Engineering Conference and International Cryogenic Materials Conference - CEC/ICMC 2009, Tucson, Arizona, United States Of America.

2010

"**The Development of the Control System for the Cryogenics in the LHC Tunnel**" C. Fluder, E. Blanco-Vinuela, J. Casas-Cubillos, P. Dubert, P. Gomes, M. Pezzetti, A. Tovar-Gonzalez, L. Zwalinski. 12th LSS Symposium, Large Scale Systems: Theory and Applications - IFAC 2010, Villeneuve d'Ascq, France.

Résumé

Le CERN, l'Organisation Européenne pour la Recherche Nucléaire, est un des plus vastes et des plus respectés centres pour la recherche scientifique. Sa raison d'être est la physique fondamentale : la découverte de quoi l'univers est fait et comment il fonctionne. Au CERN, les instruments scientifiques les plus massifs et les plus complexes du monde sont utilisés pour étudier les composants de base de la matière : les particules fondamentales. En étudiant ce qui se passe quand ces particules entrent en collision, les physiciens apprennent plus sur les lois de la nature.

Les instruments utilisés au CERN sont des accélérateurs de particules et des détecteurs. Les accélérateurs projettent des faisceaux de particules à des énergies élevées avant de le faire rentrer en collision entre eux, ou contre des cibles stationnaires. Les détecteurs observent et enregistrent les résultats de ces collisions.

Le Large Hadron Collider (LHC) est l'accélérateur le plus grand et le plus puissant jamais construit. C'est un accélérateur de particules circulaire d'une circonférence de 27 km, localisé approximativement à 100 mètres sous terre, utilisé par les scientifiques pour étudier les particules les plus petites qui existent, le module de construction fondamental de toute chose.

Deux faisceaux de particules subatomiques appelées des "hadrons", qui sont ou des protons ou des ions de plomb, voyagent dans des directions opposées à l'intérieur de l'accélérateur circulaire, gagnant de l'énergie à chaque tour. La machine va être utilisée pour recréer les conditions de l'instant après le Big Bang, en faisant rentrer deux faisceaux en collision directe à une énergie très élevée. Des groupes de scientifiques de part le monde analyseront les particules créées lors de ces collisions en utilisant des détecteurs spéciaux

au sein de plusieurs expériences dédiées au LHC.

Les faisceaux qui circulent dans le LHC sont accélérés par des cavités radio-fréquence (RF) à plus de 99 % de la vitesse de la lumière, atteignant ainsi l'énergie nominale de 7 Tev par faisceau ce qui donne une énergie de collision nominale de 14 TeV. Les faisceaux se rencontrent au centre des énormes détecteurs construits pour récolter les résultats. Les faisceaux sont courbés et dirigés par le biais d'un champ magnétique produit par des aimants dipôles et quadrupôles. Le champ maximal requis afin de permettre un faisceau stable qui ait une assez longue espérance de vie peut atteindre 8.33 T dans les aimants dipôles. Cette valeur est atteinte en utilisant des aimants super-conducteurs avec des bobines en Niobium-Titanium (NbTi) refroidies à 1.9 K pour permettre la circulation d'un courant nominal approximatif de 15 kA. De plus, un fonctionnement sans danger et correct des détecteurs et des cavités RF nécessite des températures cryogéniques. Conséquemment, l'opération de l'accélérateur demande des systèmes cryogéniques capables d'atteindre ces températures extrêmement basses. Le LHC utilise la plus grande installation cryogénique au monde utilisant de l'Hélium comme liquide refroidissant. Cette installation est contrôlée par des "automates programmables" (Programmable Logic Controllers - PLCs) industriels. La réalisation, autant des installations que des systèmes de contrôle, a constitué un grand défi, comme c'était la première fois que ces technologies de pointe étaient utilisées dans un système complexe à si grande échelle.

Motivations

Cette thèse présente la problématique des modèles et des systèmes de contrôle appliqués à certaines installations cryogéniques utilisées au CERN et exploite l'expérience accumulée pendant plus de dix ans lors de la construction, du développement et de la mise en route des installations cryogéniques du LHC.

Un des points les plus importants du travail est la modélisation mathématique des phénomènes physiques des processus cryogéniques. Dans de tels systèmes, le principe de super-

position n'est pas souvent applicable, à cause de fortes non-linéarités dans les relations entre les causes qui agissent sur le système et leurs effets.
Dans des installations à grande échelle comme celles présentées dans ce travail, les possibilités d'expérimentation sont fortement limitées autant par les coûts que par les risques engendrés par la réalisation des installations. C'est pour cette raison que, dans cette thèse, il y aura une importante utilisation de la simulation dans le processus de conception. Néanmoins, il a été possible, exceptionnellement, de réaliser une campagne expérimentale sur un échangeur de chaleur d'azote pour identifier le processus sous contrôle.
Il faut également mentionner que, dans le contexte décrit ci-dessus, à savoir les modèles et le contrôle appliqués à grande échelle sur des systèmes non-linéaires, les techniques traditionnelles et bien établies peuvent poser des problèmes quant à leur application pratique. De plus, on peut développer de nouvelles techniques avancées de modélisation et de contrôle pour optimiser la gestion des installations, avec l'objectif d'augmenter la performance des systèmes contrôlés sur le plan de la fidélité au comportement désiré, réduisant ainsi les effets indésirables qui pourraient à long terme augmenter les coûts de fonctionnement et affecter la disponibilité du système.

Contributions principales

Par rapport à la situation mentionnée ci-dessus, les contrôles appliqués à une grande échelle sur des installations cryogéniques, cette thèse fournit une double contribution:

- Dans le cadre de l'identification standard et des techniques de contrôle, après examen des solutions présentées dans la littérature de haut niveau, cette thèse montre quels genres de problèmes ces approches traditionnelles peuvent causer quand elles sont utilisées à grande échelle, et elle propose une solution par la présentation des activités menées au CERN pour l'identification paramétrique et la conception du contrôle de l'échangeur de chaleur d'azote de l'expérience ATLAS. De cette manière, une synthèse des approches scientifiques et industrielles est fournie, en particulier par rapport à l'implémentation des résultats mathématiques dans les contrôleurs industriels par le biais des objets PLC Schneider. Il est à mentionner que l'échangeur de chaleur n'est habituellement pas disponible pour expérimentation, et que les travaux qui ont été menés ont seulement été possibles grâce à une autorisation exceptionnelle accordée à l'auteur et à ses collaborateurs. Ceci constitue en soi une étude sans précédent et une des principales contributions à cette thèse.

- Une nouvelle approche au contrôle des installations cryogéniques est proposée, incluant les phases (*i*) de modélisation du système par le biais d'équations de bilan , décrivant ainsi l'évolution des débits massiques et du transfert de chaleur dans le laps de temps imparti sous l'hypothèse de l'uniformité spatiale des propriétés physiques, (*ii*) de conception du contrôle et de son implémentation, (*iii*) d'estimation des paramètres, à savoir les délais de communication employés par l'algorithme de contrôle, et (*iv*) des résultats obtenus grâce à la nouvelle approche en comparaison avec ceux obtenus par un contrôleur PID traditionnel. Le modèle est encore amélioré dans l'Appendice A, par l'introduction d'une formulation plus affinée de l'équation en tenant compte des variations des propriétés physiques dans les domaines temporels et spatiaux. Au moment de finaliser ce travail, la phase de modélisation était encore en cours et il était donc impossible d'intégrer les résultats correspondants dans cette thèse. Malgré cela, cette partie joue un rôle central parmi les contributions de cette thèse, comme elle constitue le point de départ pour de plus amples développements des approches de modélisation de contrôle proposées.

Vue d'ensemble de la thèse

Cette thèse est composée de quatre parties principales, qui sont brièvement décrites cidessous.

La **première partie** introduit (*i*) les bases de la cryogénie, tel que les fluides cryogéniques, la théorie de transfert de chaleur, le concept de la thermodynamique, (*ii*) les installations de test cryogéniques et les détecteurs au CERN, y compris les détecteurs ATLAS et CMS, le liquéfacteur central d'Hélium et le calorimètre au Krypton de l'expérience NA62.

La **deuxième partie** donne une vue d'ensemble des techniques standards utilisées pour l'identification du système et la conception des lois de commande, en plus des résultats liés à l'application de ces techniques à l'échangeur de chaleur d'azote pour ATLAS. Notamment, dans la mesure où les techniques d'identification sont utilisées, leurs objectifs et leurs principes sont illustrés, avec une présentation rapide des méthodes de post-traitement du signal, des types de modèles, des algorithmes d'identification ainsi que des procédures de validation. Par la suite, un état de l'art des techniques de contrôle avancées est présenté, y compris le prédicteur de Smith, la commande prédictive généralisée, la commande prédictive fonctionnelle, la commande polynomiale RST. Toutes ces techniques sont présentées selon un point de vue industriel, avec le but de les implémenter sur des PLCs. Dans ce sens, le "Kit d'automatique avancée" du système Mathworks et le "MultiController Object" du système *UNICOS* sont présentés pour (*i*) identifier, valider le modèle, et (*ii*) implémenter le contrôle avancé, respectivement, sur des plateformes industrielles, c'est-à-dire les PLCs de Schneider. Finalement, les résultats des techniques mentionnées ci-dessus appliquées à l'identification et à l'optimisation des contrôleurs PID dans l'échangeur de chaleur d'azote pour ATLAS sont présentés et discutés.

La **troisième partie** présente une nouvelle approche théorique à la modélisation et au contrôle pour des systèmes cryogéniques à grande échelle, dont la formulation est appliquée sur le condensateur liquide à Krypton de l'expérience NA62. Premièrement, un modèle est dérivé d'équations de bilan sous la forme d'équations différentielles ordinaires (ODE) qui décrivent le flux de masse et le transfert de chaleur entre des fluides cryogéniques. La phase de modélisation est suivie d'une proposition d'une stratégie de contrôle avancé, le *Time Delay Control*, dont les performances, obtenues en simulation, est présentée en comparant avec les performances d'une boucle de régulation plus traditionnelle (correction PID), montrant ainsi les améliorations obtenues avec la nouvelle approche. L'implémentation de la solution proposée a demandé une phase d'analyse plus approfondie afin d'estimer statistiquement les délais de communication rencontrés lors de la mise en marche du système ainsi contrôlé. Les résultats de ces analyses sont également

présentés.

La **quatrième partie** présente les principes de programmation et les outils informatiques actuellement utilisés au CERN pour gérer les installations cryogéniques. En particulier, (i) l'approche basée sur les objets du contrôle industriel, et (ii) le système *UNICOS*, développé au sein de l'Organisation afin de fournir une plateforme unifiée qui permette de gérer tous les équipements cryogéniques. A titre d'exemples d'application des principes de programmation mentionné ci-dessus, cette partie de la thèse fournit aussi des informations sur l'installation et la recette du système de réfrigération pour les aimants CMS, tout comme sur une étude de simulation pour la mise en marche virtuelle du liquéfacteur d'Hélium central du CERN. Finalement, la mise en route "offline" de l'installation cryogénique à l'Hélium et la formation des opérateurs sont aussi discutés. Dans ce cas, un environnement de simulation est présenté, permettant la formation des opérateurs sans risques pour les installations et en évitant de devoir arrêter l'opération normale.

Pour terminer l'étude, des **conclusions** sont données à partir du travail théorique et pratique présenté dans les chapitres précédents, avec une vue d'ensemble des **nouvelles perspectives** ouvertes par celui-ci. En particulier, en ce qui concerne des développements futurs, une nouvelle stratégie de modélisation pour le condensateur du NA62 est présentée et développée dans ses aspects fondamentaux (Appendice A). Cette amélioration du travail proposée dans la troisième partie décrit le phénomène qui se produit dans le condensateur par le biais d'équations différentielles partielles, en tenant compte des variations autant dans le domaine temporel que dans le spatial. Une étude plus approfondie sera nécessaire pour évaluer les possibles bénéfices qui peuvent apparaitre de cette approche, et pour vérifier si la complexité additionnelle que cela introduit est compensée par des améliorations significatives autant dans la précision du modèle que dans les possibles perfectionnements de la stratégie de contrôle.

De plus, du travail supplémentaire sera dédié à l'amélioration des outils de simulation utilisés pour la mise en marche "offline" des installations cryogéniques et pour la formation des opérateurs. Cette tâche joue un rôle important dans le cadre des activités futures prévues pour le LHC, comme la machine sera principalement utilisée en mode d'opération stable pour les expériences de physique et il n'y aura pas de temps prévu pour la formation des opérateurs. Dans ce scénario, le développement d'outils de simulation prendra une très grande importance, permettant ainsi de (*i*) former les opérateurs sans risques et sans arrêt de l'opération, (*ii*) améliorer la connaissance des systèmes cryogéniques, et (*iii*) gagner un temps précieux lors du redémarrage des installations en minimisant la probabilité d'erreurs inattendues.

Summary

CERN, the European Organization for Nuclear Research, is one of the world's largest and most respected centres for scientific research. Its business is fundamental physics, finding out what the Universe is made of and how it works. At CERN, the world's largest and most complex scientific instruments are used to study the basic constituents of matter, the fundamental particles. By studying what happens when these particles collide, physicists learn about the laws of Nature.

The instruments used at CERN are particle accelerators and detectors. Accelerators boost beams of particles to high energies before they are made to collide with each other or with stationary targets. Detectors observe and record the results of these collisions.

The Large Hadron Collider (LHC) is the biggest and more powerful particle accelerator ever built. It is a circular particle accelerator with a circumference of 27 km, located about 100 m underground, used by physicists to study the smallest known particles, the fundamental building blocks of all things.

Two beams of subatomic particles called "hadrons", either protons or lead ions, travel in opposite directions inside the circular accelerator, gaining energy with every lap. The machine will be used to recreate the conditions just after the Big Bang, by colliding the two beams head-on at very high energy. Teams of physicists from around the world will analyse the particles created in the collisions using special detectors in a number of experiments dedicated to the LHC.

The beams circulating in the LHC are accelerated by RF cavities to more than 99 % of the speed of light, thus reaching the nominal energy of 7 TeV per beam for a resulting overall

nominal collision energy of 14 TeV. The beams intersect at the centre of the enormous detectors built to collect the results. The beams are bent and focused by means of a magnetic field produced by dipole and quadrupole magnets. The maximum field required in order to attain a stable beam with a sufficiently long life time reaches the peak of 8.33 T inside the dipoles, value reached by means of superconducting magnets whose Niobium-Titanium ($NbTi$) windings are cooled down to 1.9 K to allow the circulation of a nominal current of about 15 kA. In addition to that, also the safe and correct working of detectors and RF cavities need cryogenic temperatures. As a consequence, the operation of the accelerator requires cryogenic systems capable of reaching these extremely low temperatures. In particular, the LHC employs the world's biggest cryogenic installation with Helium as cooling fluid, controlled by industrial Programmable Logic Controllers (PLCs). The realization of both installations and control systems constituted a great challenge, since for the first time cutting-edge technologies were employed on a complex large scale system.

Motivations

This thesis deals with the problem of modeling and control applied to some of the cryogenic plants currently used at CERN, and exploits the experience accumulated over more than ten years on the construction, deployment and operation of the LHC cryogenic installations.

A crucial point of the work lies in the mathematical modeling of the physical phenomena related to the cryogenic processes. In such systems, the superposition principle does not often hold true, because of the strong nonlinearities in the relations between causes acting on the system and their effects.

In large scale installations such as those discussed in this work, the experimentation possibilities are strongly limited both by the costs and by the risks for the plants deriving from their realization. For this reason, in this thesis there will be an extensive use of simulation in the process of control design and simulation. Nonetheless, for the identification of the process under control it was exceptionally possible to carry out an experimental campaign on a Nitrogen heat exchanger.

Furthermore, it is to be pointed out that in the above-described context, i.e. modeling and control applied to large scale nonlinear systems, also traditional well-established techniques may pose relevant problems for their practical application.

In addition to that, new advanced techniques for modeling and control can be developed to optimize the management of the plants, with the purpose of increasing the performance of the controlled system in terms of fidelity to the desired behaviour, thus reducing undesired effects which could on the long term both increase operation costs and affect the availability of the system.

Main contributions

In reference to the aforementioned situation of the controls applied to large scale cryogenic installations, this thesis provides a twofold contribution:

- Within the frame of standard identification and control techniques, after a review of the state-of-the-art solutions proposed in literature, it shows what kind of problems these traditional approaches may pose when used in real large scale applications, and proposes a solution through the presentation of the activities carried out at CERN for parametric identification and control design of the ATLAS Nitrogen heat exchanger. In this way, a synthesis of scientific and industrial approaches is provided, in particular with reference to the implementation of the mathematical results in industrial controllers by means of Schneider PLC objects. It is worth mentioning that the heat exchanger is normally unavailable for experimentation, and that the practical work carried out on it was made possible only by an exceptional authorization granted to the author and his collaborators. This constitutes an unprecedented case study and one of the main contributions of this thesis.

- A novel approach to the control of cryogenic plants is proposed, including the phases of (i) system modeling through balance equations, describing mass flows and heat transfer evolution in the time domain under the assumption of spatial uniformity of the physical properties of interest, (ii) control design and implementation, (iii)

estimation of the parameters, namely communication time delays, employed by the control algorithm, and (*iv*) results obtained thanks to the new approach in comparison with those of a traditional PID controller. The model is further improved in Appendix A, through the introduction of a more refined formulation of the equations taking into account variations of the physical properties both in the time and in the space domains. At the moment of closing this work, the modeling phase was still in progress and it was therefore impossible to include in this dissertation any related results. Anyway, this parts plays a central role among the contributions of the thesis, since it constitutes the starting point of further developments of the proposed modeling and control approaches.

Thesis overview

This thesis is composed of four main parts, briefly described in the following.

The **first chapter** introduces (*i*) the basics of cryogenics, such as cryogenic fluids, heat transfer theory, concepts of thermodynamics, and (*ii*) cryogenic test facilities and detectors at CERN, including the ALTAS and CMS detectors, the central Helium liquefier and the Krypton calorimeter of the NA62 experiment.

The **second chapter** gives an overview of the standard techniques used for system identification and control design, along with the results of the application of such techniques to the ATLAS Nitrogen heat exchanger. In particular, as far as the identification techniques are concerned, their goals and principles are illustrated, along with an overview of methods for signal post-processing, types of models, identification algorithms, and validation procedures. Subsequently, a state of the art on advanced control techniques is presented, including the Smith Predictor-based control, the Generalized Predictive Control, the Predictive Function Control, the R-S-T control. All these techniques are presented with a view to their industrial application, namely to their implementation on PLCs. In this perspective, the "*Advanced Automation Toolkit*" from Mathworks and the "*MultiController*

Object" from the *UNICOS* framework are presented for (*i*) model identification and validation, and (*ii*) advanced control implementation, respectively, on industrial target platforms, namely Schneider PLCs. Finally, the results of the above-mentioned techniques applied to the identification and PID controller optimization in the ATLAS Nitrogen heat exchanger are presented and discussed.

The **third chapter** presents a novel theoretical approach to modeling and control for large scale cryogenic systems, whose formulation is applied to the liquid Krypton condenser of the NA62 experiment. First, a model is derived from balance equations in the form of ordinary differential equations (ODE) describing the mass flow and the heat transfer between cryogenic fluids. The modeling phase is followed by the proposal of an advanced control strategy, the *Time Delay Control*, whose performance obtained in simulation are presented in comparison with those of a more traditional PID-based control loop, thus showing the improvement allowed by the new approach. The implementation of the proposed solution required a further phase of analysis in order to statistically estimate the communication time delays usually encountered during the operation of the system under control. The results of these analysis are also presented.

The **fourth chapter** presents the programming paradigm and the software tools currently used at CERN to handle the cryogenic plants. In particular, (*i*) the object-based approach to industrial control, and (*ii*) the *UNICOS* framework, developed inside the Organization in order to provide a unified platform for the management of all the cryogenic equipments, are discussed. As examples of application of the aforementioned programming paradigm, this part also provides information about the installation and commissioning of the refrigeration system for the CMS magnets, as well as about a simulation study for the virtual commissioning of the CERN central Helium liquefier. Finally, the off-line commissioning of the Helium cryogenic plant and the operator training are discussed. In particular, a simulation environment is presented, which allows the training of the operators on large complex cryogenic systems, without any risk for the installations and any need to stop its normal operation.

The thesis ends with the discussion of the **conclusions** drawn by the theoretical and practical work presented in the previous parts, along with an overview of the new perspectives it has opened. In particular, with regard to the **future developments**, a new modeling strategy for the NA62 condenser is introduced and developed in its basic aspects (Appendix A). This further improvement of the work proposed in the third part describes the phenomena occurring in the condenser through partial differential equation, taking into account variations both in the time and in the space domains. Further investigation will be required to assess the possible benefits deriving from this approach, and to check whether the additional complexity it introduces is balanced by significant improvements both in the model prediction accuracy and in the possible enhancements of the control strategy.

In addition to that, further work will be devoted to the refinement of the simulation tools employed for the off-line commissioning of cryogenic plants and operator training. This task plays an important role in the frame of the future activities planned for the LHC, since the machine will be mostly used in steady state operation for physic experiments and no time will be scheduled for operator training. In this scenario, highest importance will be given to the development of simulation tools giving the opportunity of (*i*) training the operators without risks and stops for the installations, (*ii*) improving the knowledge of cryogenic systems, and (*iii*) saving an important time during plant re-starting by minimizing the probability of unexpected errors.

Chapter 1

Cryogenics and its application at CERN

1.1 Introduction to cryogenics

The word cryogenics literally means *"the production of icy cold"*, from Greek "*kruos*" = cold and "*geneia*" = production, however the term is used today as a synonym for the low-temperature state; it defines, in a general matter, the techniques aimed to produce, to conserve, to distribute and to measure the low temperatures. Moreover, the cryogenic word includes within itself the study of the entire properties of the matter and the phenomena that happens at cryogenic temperatures [1].

It is not well-defined at what point on the temperature scale refrigeration ends and cryogenics begins. The field of cryogenics could be considered when temperatures goes below $-180\ °C$ ($93.15\ K$). This seems a logical dividing line, since the normal boiling points of the so-called permanent gases (such as Helium, Hydrogen, Neon, Nitrogen, Oxygen, and normal air) lie below $-180\ °C$ while the Freon refrigerants, Hydrogen sulfide, and other common refrigerants have boiling points above $-180\ °C$.

In a more operational way [2], it is also defined as the science and technology of temperatures below $120\ K$. The reason for this latter definition can be understood by examining characteristic temperatures of cryogenic fluids (Table 1.1): the limit temperature of $120\ K$

comprehensively includes the normal boiling points of the main atmospheric gases, as well as of methane which constitutes the principal component of natural gas. Today, liquid natural gas (LNG) constitutes one of the largest - and fast-growing - industrial domains of application of cryogenics, together with the liquefaction and separation of air gases. The densification by condensation, and separation by distillation of gases was historically - and remains today - the main driving force for the cryogenic industry, exemplified not only by liquid Oxygen and Nitrogen used in chemical and metallurgical processes, but also by the cryogenic liquid propellants of rocket engines and the proposed use of Hydrogen as a “clean” energy vector in transportation.

Cryogen	Triple point	Normal boiling point	Critical point
Methane	90.7	111.6	190.5
Oxygen	54.4	90.2	154.6
Argon	83.8	87.3	150.9
Nitrogen	63.1	77.3	126.2
Neon	24.6	27.1	44.4
Hydrogen	13.8	20.4	33.2
Helium	2.2*	4.2	5.2

*λ point

Table 1.1: Characteristic temperatures of cryogenic fluids $[K]$.

Historically, the field of cryogenics had a big improvement during World War II when scientists found that metals frozen to low temperatures showed more resistance to wear. Based on this theory of cryogenic hardening, the commercial cryogenic processing industry was founded. This evolved in the 1990s with the fortuitous discovery of superconductivity in parallel with the continuous push of the development of astronomy and particle physics detectors.

1.1.1 Cryogenics fluids

Liquefied gases, such as liquid Nitrogen, liquid Helium and liquid Argon, are used in many cryogenic applications to cool down an apparatus either electronic or mechanics. Liquid

Nitrogen is the most commonly used element in cryogenics as well as liquid Helium, used to reach the lowest attainable temperatures in cryogenics. Liquid Argon and liquid Krypton are commonly used in particle physics detectors for their specific physical proprieties.
At a certain point we could ask ourselves how and how much did we use of these fluids to cool down the cryogenics apparatus ? The simplest way to cool down an apparatus using a cryogenic fluid is to make use of its latent heat of vaporization, e.g. by immersion in a bath of boiling liquid or by passing trough a forced flow heat exchanger. As a consequence, the temperature range of cryogenic fluids that will be exploited is that in which there exists latent heat of vaporization, i.e. between the triple point and the critical point, with a particular interest in the normal boiling point.
The heat balance equation for cooling a mass of, say Aluminium m_{Al} of specific heat $C_{Al}(T)$ at temperature T by vaporizing a mass dm of cryogenic liquid at saturation temperature T_v, latent heat of vaporization L_v and vapour specific heat C (taken as constant), is assuming perfect heat exchange with the liquid and the vapour will be presented as:

$$mAl \cdot C_{Al}(T) \cdot dT = [L_v + C(T - T_v)] \cdot dm \tag{1.1}$$

Hence the specific liquid cryogen requirement for cool-down from temperature T_0

$$\frac{m}{mAl} = \int_{T_0}^{T} \frac{C_{Al}(T)dT}{L_v + C \cdot (T - T_v)} \tag{1.2}$$

The term $C(T - T_v)$ adding to L_v in the denominator brings a strong attenuation to the specific liquid requirement, provided that there is good heat exchange between the solid and the escaping vapor.

1.1.2 Heat transfer

The heat transfer in cryogenics processes are basically the same as for any temperature range. The strong variation of thermal properties of materials and fluids at low temperature however has two consequences: the magnitudes of the thermal processes may be very different from those at room temperature, and the equations representing the model became non-linear. There are three basic mechanisms for transferring heat: conduction, convection and radiation.

In conduction, heat is transported inside solids or fluids at rest by atomic scale processes. In convection, macroscopic movement of a fluid produces the heat transfer. Finally, in radiative heat transfer, energy is transported by electromagnetic radiation, emitted by any surface at $T > 0\ K$, without need of matter's support.

The basic laws for the flow of heat Q through an area A or onto a surface A in the three modes are Fourier's law for conduction is $\dot{Q} = -kAgradT$, general law for convection (free or forced) is $\dot{Q} = hA(T_w - T_f)$ and Stefan-Boltzmann's law for radiation $\dot{Q} = \sigma\varepsilon A(T_h^4 - T_c^4)$ where k is the thermal conductivity of the medium, h is the heat exchange coefficient, T_w the wall and T_f the fluid temperature, $\sigma = 5.67\text{x}10^{-8}\ W \cdot m^{-2} \cdot K^{-4}$ Stefan-Boltzmann's constant, ε an effective emissivity, T_h the warm surface and the T_c the cold surface temperature.

Conduction

Conduction can be defined by a general law as :

$$\dot{Q} = k(T)A\frac{dT}{dx} \tag{1.3}$$

expressing proportionality of heat flux with thermal gradient (where the term k, thermal conductivity coefficient of the material depends mostly on temperature). By integration of the Fourier's law we obtain:

$$\dot{Q} = \frac{A}{L}\int_{T_c}^{T_h} kdT \tag{1.4}$$

in one dimensional case of time independent heat flow through a cross section $A(x)$ over a length L, between a warm temperature T_h and a cold temperature T_c. Conduction model definition specifies the conduction in solid material or conduction in fluid.

In solid conduction heat carriers are delocalized electrons and phonons, the elementary excitations of the atomic lattice. At low temperature, the thermal conductivity associated with phonons varies with T^3, whereas for electrons, it varies linearly with T. Generally, good electrical conductors are also good thermal conductors, although the best thermal conductors, diamond and sapphire, are electrical insulators. Heat transmission at low temperature is hindered by electron-defect and phonon-defect scattering, limiting the mean free path of the heat carriers: as a result, a pure metal is a better conductor than its alloys. Treatments modifying the defect's content of a metal affect its thermal conductivity: cold work reduces it, annealing enhances it. At higher temperature, it is electron-phonon and phonon-phonon scattering which limit the mean free path, such that the differences between pure metals and dilute ones vanish.

In fluid or gases conduction, heat transmission, between two surfaces separated by gas, obeys two different regimes according to the ratio between the mean free path of gas molecules λ and the distance L between the two surfaces (Table 1.2). For $\lambda << L$, the viscous regime, heat transmission is described in terms of thermal conduction k, which is independent of pressure. The heat flux is therefore inversely proportional to wall distance. Decreasing the residual gas pressure, the molecular regime is reached as $\lambda >> L$.

[Pa]	$1x10^{-6}$	$1x10^{-4}$	$1x10^{-2}$	1	$1x10^{2}$
Ar	$6.3x10^{3}$	$6.3x10^{1}$	0.63	$6.3x10^{-3}$	$6.3x10^{-5}$
Air	$6.1x10^{3}$	$6.1x10^{1}$	0.61	$6.1x10^{-3}$	$6.1x10^{-5}$
N_2	$6.0x10^{3}$	$6.0x10^{1}$	0.60	$6.0x10^{-3}$	$6.0x10^{-5}$
He	$1.77x10^{4}$	$1.77x10^{2}$	1.77	$1.77x10^{-3}$	$1.77x10^{-4}$

Table 1.2: λ at 300 K for different gases, in $[cm]$.

The molecules travel undisturbed from the warm to the cold surface and heat transfer becomes proportional to residual gas pressure and independent of wall distance. Kinetic gas theory predicts the mean free path at temperature T $[K]$, pressure p $[Pa]$ and viscosity μ $[Pa \cdot s]$, for a gas of molar mass M $[g \cdot mol^{-1}]$ as being equal to:

$$\lambda = 115 \cdot \frac{\mu}{p} \cdot \sqrt{\frac{T}{M}} \tag{1.5}$$

In the viscous regime, the thermal conductivity coefficient is:

$$K = \frac{1}{3} \cdot \rho \left(\frac{8RT}{\pi M} \right)^{1\backslash 2} \lambda C_V \tag{1.6}$$

T [K]	^{4}He	H_2	O_2	N_2	Ar
300	$1.56x10^{-3}$	$1.92x10^{-3}$	$2.63x10^{-4}$	$2.6x10^{-4}$	$1.8x10^{-4}$
80	$0.64x10^{-3}$	$0.60x10^{-3}$		$0.76x10^{-4}$	$0.6x10^{-4}$(90 K)
20	$0.26x10^{-3}$	$0.16x10^{-3}$			
5	$0.10x10^{-3}$				

Table 1.3: Thermal conductivity k $[W \cdot cm^{-1} \cdot K^{-1}]$.

In the molecular regime, the heat transfer between two surfaces at temperature T_1 and T_2 is (by Kennard's law):

$$\dot{Q} = A_1\alpha \left(\frac{\gamma+1}{\gamma-1}\right) \left(\frac{R}{8\pi}\right)^{1/2} \frac{p}{\sqrt{MT}} (T_2 - T_1) \tag{1.7}$$

with $\gamma = Cp/Cv$, R the ideal gas constant, A_1 the surface receiving the heat flow and α an accommodation coefficient. In general, liquids are bad thermal conductors, with the important exception of superfluid Helium (solution currently used for the LHC cryogenic).

Radiation

Radiation is present in any surface (absorbed and emitted) in the form of electromagnetic radiation, depending on wavelength and direction. For an incident light flux P, a fraction a is absorbed, a fraction t (transmissivity) traverses the body, and a fraction r (reflectivity) is reflected back. Energy conservation requires the sum $a + t + r$ to be equal to 1. A body is called black when its surface absorbs all of the incident flux. Per definition, the absorptivity a is then equal to 1. Blackbody radiation strongly and only depends on the temperature of the emitting body, with the maximum of the power spectrum given by Wien's law :

$$\lambda_{\max} = \frac{2898}{T}[\mu m \cdot K^{-1}] \tag{1.8}$$

and the total power radiated given by Stefan-Boltzmann's law :

$$E_b = \sigma A T^4 \tag{1.9}$$

with $\sigma = 5.67\text{x}10^{-8}[W \cdot m^{-2} \cdot K^{-4}]$.

The radiating heat by a surface (approximation defined as "$gray$" bodies, with an emissivity $\varepsilon < 1$) will be :

$$\text{Q} = \varepsilon\sigma \text{AT}^4 \tag{1.10}$$

For real materials, emissivity depends on wavelength and direction, however, many real surfaces satisfy reasonably well the diffuse-gray approximation. It has been observed that clean, well-polished metallic surfaces have small emissivities, whereas non-metallic surfaces have high emissivities. The emissivity it is a function also of temperature: for metals, it decreases with decreasing temperature and is almost proportional to T at cryogenic temperature. For non-metals, the emissivity may decrease or increase with temperature, and in particular it increases with decreasing temperature for organic materials.

Convection

Taking into account the diversity and complexity of convection processes we will focus only in useful relations valid in the most common cryogenic cases. The general law of convection heat transfer has the following form :

$$\dot{Q} = h(T_s - T_f) \tag{1.11}$$

where T_f is the temperature in the bulk of the fluid and T_s the temperature of the surface in contact with it. The engineering problem consists in determining the exchange coefficient h. In forced convection high density and low viscosity of cryogenic fluids often result in flows with high Reynolds number Re. The Nüsselt number Nu which characterizes the efficiency of convective heat transfer relative to conduction in the fluid, is an increasing function of the Prandtl Pr and Reynolds numbers, respectively representing the ratio of mass to heat transport, and the ratio of inertial to viscous forces :

$$\mathrm{N\,u} = \mathrm{f(Pr, Re)} \tag{1.12}$$

The case of natural convection at low temperature however deserves particular mention, as this mechanism, usually weak at room temperature except on very large scales, becomes dominant in cryogenic equipment. In this case, the Nüsselt number is an increasing function of the Prandtl Pr and Grashof Gr numbers, with the latter representing the ratio of buoyancy to viscous forces:

$$\mathrm{N\,u} = \mathrm{f(Pr, Gr)} \tag{1.13}$$

For gases, while Pr is about constant and independent of temperature, Gr is proportional to the heated volume and indicates whether these local fluid flows are laminar or turbulent, with the associated low or high heat transfer rate.

Natural convection occurs when the fluid movement has its origin in the expansion and ascension of heated sections of fluid. The useful dimensionless groups are Nu, Pr and Gr. A relation of the type $Nu = f(Gr, Pr)$ permits to calculate the exchange coefficient h in his empirical forms :

$$\mathrm{Nu} = \mathrm{a(Gr \cdot Pr)^n} = \mathrm{a \cdot Ra^n} \tag{1.14}$$

where the Rayleigh number $Ra = GrPr$ appears.

In monophasic forced convection problems three dimensionless numbers are applied : Nu, Re and Pr. A relation of the type $Nu = f(Re, Pr)$ permits to infer h, the exchange coefficient:

$$\mathrm{Nu} = \mathrm{f(Re, Pr)} = \mathrm{a \cdot F \cdot Re^m \cdot Pr^n} \tag{1.15}$$

Exchange in laminar flow inside a horizontal tube takes the name of Sieder and Tate formula, the one valid for turbulent flow is the well-known Colburn formula. The pressure drop along a segment L of a tube is determined by the friction force:

$$\frac{\mathrm{dp}}{\mathrm{dx}} = \frac{\rho v^2}{2}\frac{4f}{d} \tag{1.16}$$

In two-phase convection, both natural and forced, the actual heat transfer rate is due to a combination of bubble formation and motion near the walls and the direct sweeping of the heated surface by the fluid. Due to significant density changes in the two-phase regime, or to pressure-drop change, instabilities and oscillations may occur.

1.1.3 Basic thermodynamics for cryogenics

Cryogenics temperatures are achieved by letting a working fluid absorbs heat at low temperatures and rejects it at higher temperatures during a series of cyclic thermodynamic transformations, called thermodynamic cycles.

A predominant estimator for all low-temperature process considerations is the Carnot factor which defines the maximum amount of work that can be extracted from a process operating between two temperature levels. In fact, the Carnot factor is a direct consequence of combining the first and second law of thermodynamics.

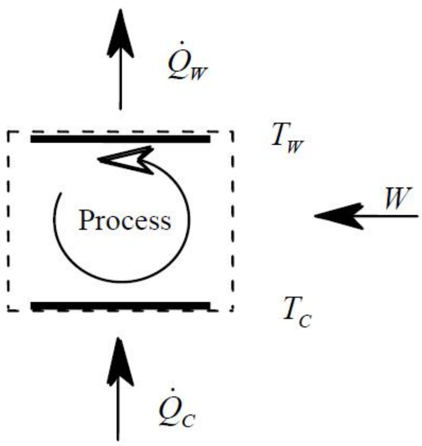

Figure 1.1: Thermal energy from any temperature to a higher temperature level.

The conservation of energy (expressed by the first law of thermodynamics)

$$\dot{Q}_w + \dot{Q}_c + W = 0 \tag{1.17}$$

and the definition of the second law of thermodynamics

$$\frac{\dot{Q}_w}{T_w} + \frac{\dot{Q}_c}{T_c} \leq 0 \tag{1.18}$$

bring to

$$W \geq \dot{Q}_c \left(\frac{T_w}{T_c} - 1 \right) \tag{1.19}$$

where the Carnot factor is

$$\left(\frac{T_w}{T_c} - 1\right) \tag{1.20}$$

Besides defining the minimum work necessary to extract heat in a reversible process, the Carnot factor clearly demonstrates why in any cryogenic system heat entering the low temperature level should be limited to the minimum. The refrigeration work in real systems is always above the limit given by the Carnot factor due to the inevitable irreversibilities.

Within the number of different phase diagram for fluids, the temperature-entropy $(T-s)$ diagram is the most practical to illustrate the different cycles used for the closed cryogenic processes. In a $(T-s)$ diagram the reversibly exchanged heat for any change of state is represented by the area under the path for the change of state. This allows to compare the heat exchanged for different process changes. For low-temperature application it is may be convenient to use a $(T-s)$ diagram with a logarithmic temperature scale. In this case for any ideal gas the isochors, isobars, and isenthalps are straight lines; moreover the isenthalps coincide with the isotherms. The disadvantage of the logarithmic temperature scale is that the area under the path for a change of state does not represent the reversibly exchanged heat.

1.2 Cryogenic Detectors and Test Facilities at CERN

This Section provides an overview of the CERN cryogenic detectors and test facilities on which we will base the methodologies presented in the following of this thesis.
In particular, two LHC experiments are introduced: ATLAS and CMS, with details on their cryogenic detectors, main purposes and basic requirements. Afterwards, the CERN central Helium liquefier is presented. Finally, an overview of the NA62 experiment is provided.

1.2.1 Introduction

The European Organization for Nuclear Research (CERN), has now become the widest cryogenic test facility in the world, with the Large Hadron Collider (LHC), a 26.7 km circumference superconducting accelerator equipped with high-field magnets operating in superfluid Helium below 1.9 K, as well as the two biggest (ever built) cryogenic detectors operating in liquid Helium 4.5 K and liquid Argon at 89.3 K [3].

The LHC cryogenic system is the quasi-isothermal magnet cooling scheme, in which flowing two-phase saturated superfluid Helium removes the heat load from the $36'000$ t cold mass, immersed in some 400 m^3 static pressurised superfluid Helium. The LHC also makes use of supercritical Helium for non-isothermal cooling of the beam screens which intercept most of the dynamic heat loads at higher temperature.
LHC has two general-purpose cryogenics detectors CMS and ATLAS, which are designed to detect the Higgs particle as well as a host of new particles, such as supersymmetric partners of the standard family of elementary particles. The collisions will also produce copious amounts of top quarks, be a B physics factory and have large amounts of W's and Z's [4].
Particle Detectors track and identify all the particles that have been produced by the resulting collision of two beams circulating through an accelerator. A particle is fully identified when it is well known its charge and its mass.

The calculation of the mass of a particle, in principle, can be calculate if it is known its momentum and either its speed or its energy. However, for a particle moving close to the speed of light any small uncertainty in momentum or energy makes it difficult to determine its mass from these two, so we need to measure speed too. A multi-layer detector is used to identify particles. Each layer gives different informations about the "event". Computer calculations based on the information from all the layers reconstruct the positions of particle tracks and identify the momentum, energy, and speed of as many as possible of the particles produced in the event.[5].
ATLAS detector (point 1 of the LHC accelerator) use two kind of cryogenic fluid Helium for the superconducting magnet and housed more then 9 m^3 of liquid Argon for the inner calorimeter; CMS detector (point 5) use only liquid Helium to refrigerate the biggest solenoid superconducting magnet.

Refrigeration for the LHC is produced in eight large refrigerators, each with an equivalent capacity of about 18 kW at 4.5 K, completed by 1.8 K refrigeration units making use of several stages of hydrodynamic cold compressors. The cryogenic fluids are distributed to the cryomagnet strings by a compound cryogenic distribution line circling the tunnel. The refrigeration for the detectors is produce with 3 large Helium refrigeration with an equivalent capacity of about 6 kW at 4.5 K and 60 kW at 60 K for ATLAS and 1.2 kW at 4.5 K for CMS, and one Nitrogen refrigerator of 60 kW at 78 K for the ATLAS Argon cryogenic facility.

1.2.2 The ATLAS detector

ATLAS "A Toroidal Lhc ApparatuS" is a general-purpose p-p spectrometer designed to exploit the full discovery potential of the LHC (Fig. 1.2). The detector concept and its physics potential have been presented in the Technical Proposal [6] in 1994 and in different Technical Design Reports [7]. ATLAS consists of four major components (Fig.s 1.3 and 1.4): a inner tracker (measures the momentum of each charged particle), a liquid Argon calorimeter (measures the energies carried by the particles) composed by two end-caps

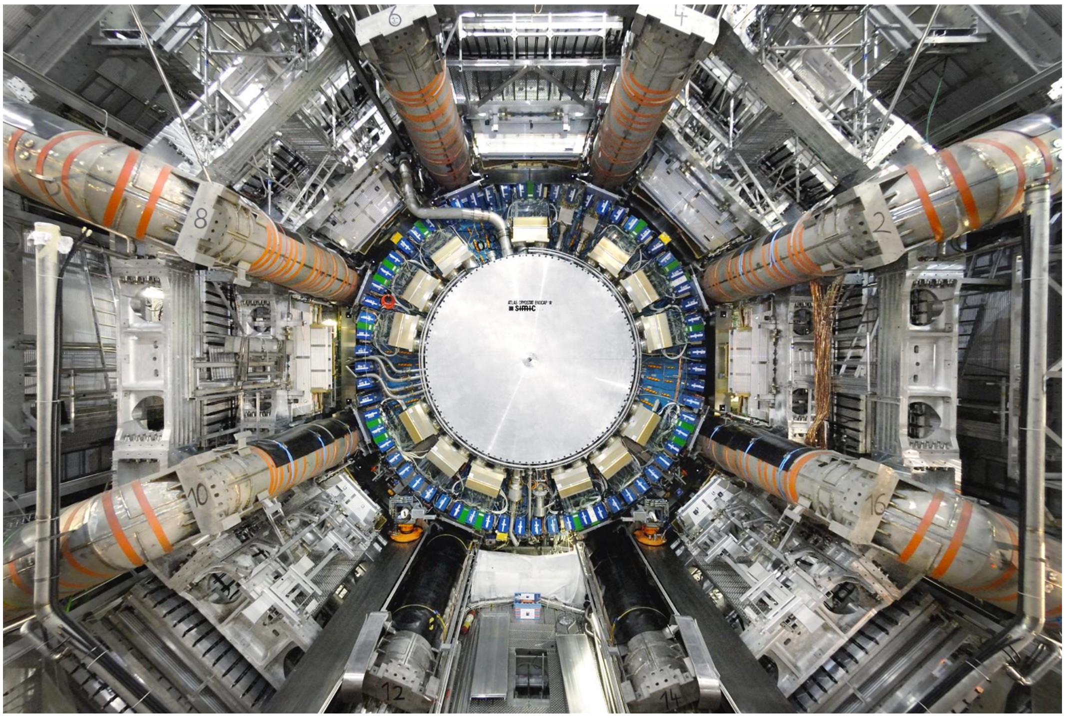

Figure 1.2: The ATLAS detector.

and one barrel, a muon spectrometer (identifies and measures muons), a magnet system (bending charged particles for momentum measurement). The detector will be installed 100 m under ground level in the cavern Ux15, at the interaction point 1 of the LHC. The interactions in the ATLAS detectors will create an enormous dataflow. To digest this data we need to have a trigger system capable of selecting 100 interesting events per second out of 1 billion others, a data acquisition system (channeling the data from the detectors to the storage) and a computing system capable of analyse 1 billion events recorded per year. For a high resolution of the detectors, a very high magnetic field is essential.

ATLAS Barrel Calorimeter

The barrel electromagnetic calorimeter consists of two identical half-wheels separated by a 4 mm gap (Fig. 1.5). Each wheel is divided in 16 modules, made of 64 accordion-shaped particle absorber plates, interleaved with copper electrodes. The absorbers are made of lead plates sandwiched between stainless-steel sheets, which are glued by resin-

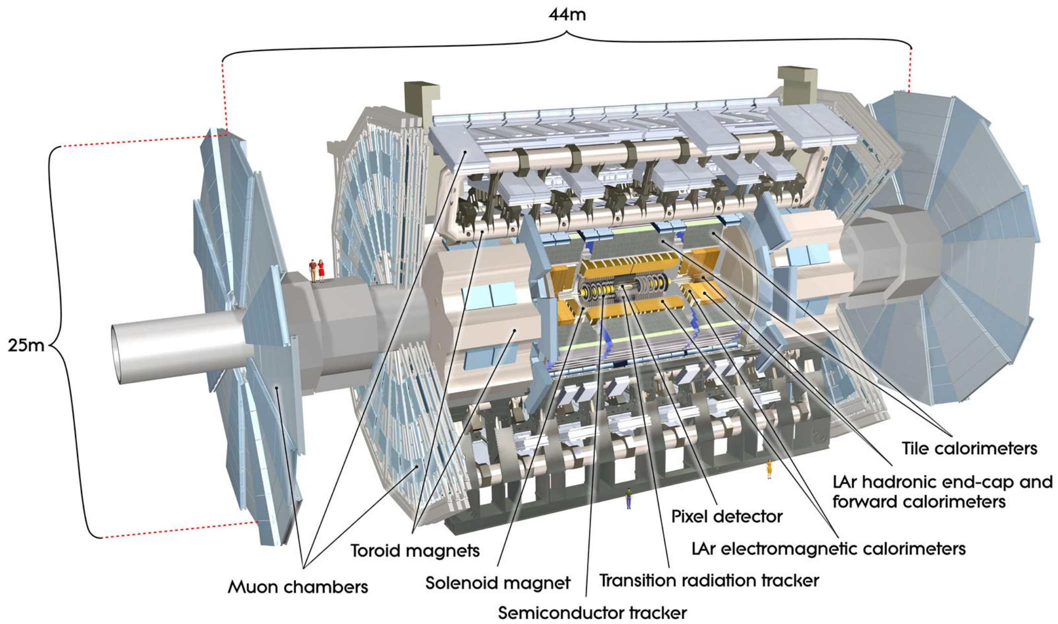

Figure 1.3: Main components of the ATLAS detector.

impregnated glass-fiber fabric. At the inner and outer edges, each absorber in encased in a G10 glass-epoxy composite precision bar. The outer G10 bars are fixed to 7 stainless-steel outer rings which support and give rigidity to the wheel. At the inner radius, the G10 bars are fixed to 8 composite inner rings which define the inner geometry of the wheel.

The presampler, built from thin glass-epoxy shells, acts as a thin active layer of liquid Argon, which provides a first sampling of the electromagnetic showers in front of the EM barrel. The electromagnetic barrel calorimeter is housed in the barrel cryostat made of aluminium. In addition, it supports and provides the vacuum for the central superconducting solenoid coil which generates the magnetic field for the inner tracker. The warm vessel forms a hollow cylinder which contains a similarly shaped cold vessel. The outer cold cylinder is 6.5 m long and has a diameter of 4.3 m. Each calorimeter wheel is supported on two aluminium sliding rails connected to the outer rings. The sliding rails are in turn posed on a counter rail connected to the cold vessel. The wheels and cryostat rails are only fixed together at the extremities of the cryostat. There are 32 signal and 1

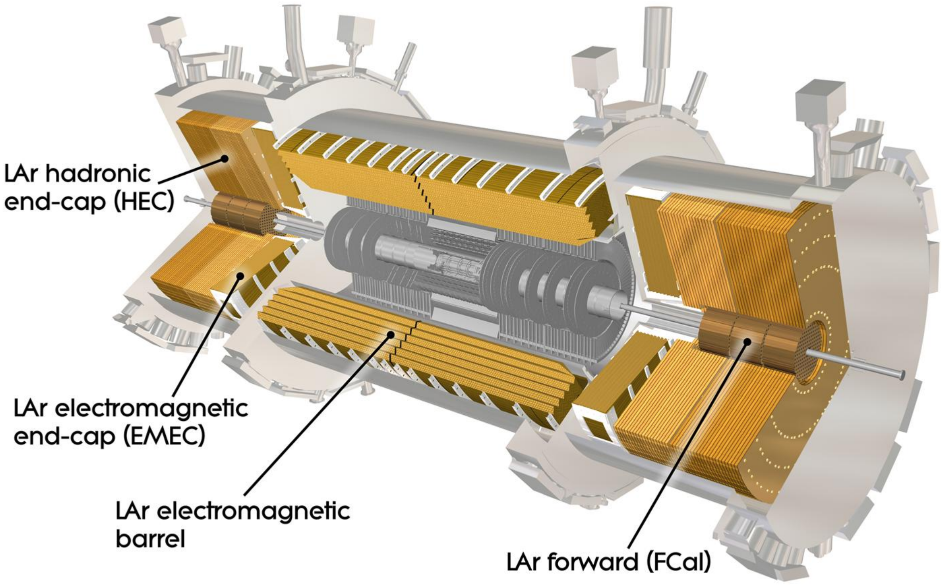

Figure 1.4: Liquid Argon cryogenic system for the ATLAS detector.

high-voltage feedthroughs for each half-barrel distributed radially around each end of the cryostat. Each signal feedthrough brings a total of 2′000 signal, monitoring and calibra-

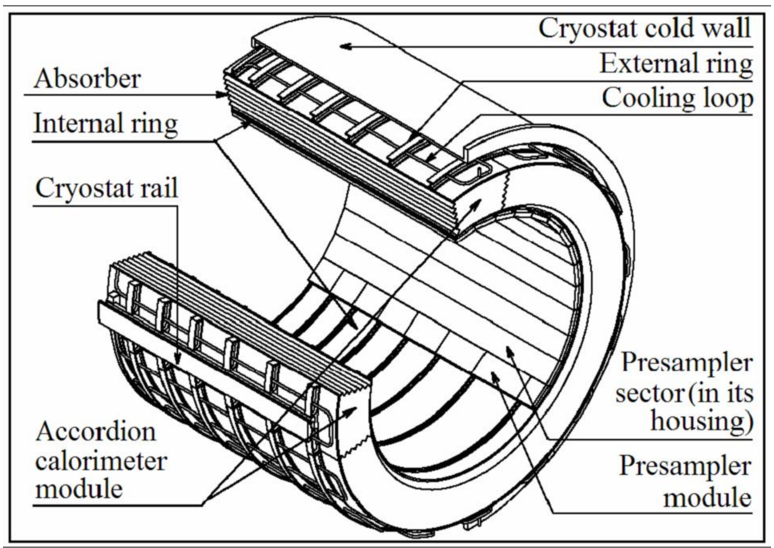

Figure 1.5: General layout of one barrel half-wheel.

tion cables through an independent insulation vacuum, out of the liquid Argon bath. The barrel cryostat weights about $203t$ when filled with liquid. Four heat exchangers made of 20/22 mm diameter stainless-steel pipe each with a length of about 60 m are integrated in the calorimeter outer rings. They are symmetrically distributed around each detector wheel: one at the upper half and one at the lower. One additional heat exchanger shaped in loops is placed at each cryostat extremity, close to the feedthroughs.

The ATLAS Liquid Argon Cryogenics Calorimeter The central part of the ATLAS detector, the liquid Argon calorimeter, consists of the barrel and two end-cap detectors with cold masses of 120 t and 2x219 t. They are housed in three independent cryostats filled with 40 m^3 and 2x19 m^3 of liquid Argon (LAr) respectively. The cryostats are cooled by evaporating liquid Nitrogen (LN_2) circulating in cooling loops placed in the LAr baths. The LN_2 pressure of, and flow through, each individual cooling loop it is regulated with the use of valves placed in intermediate valve boxes.

In normal operation the evaporated Nitrogen will be re-liquefied by a Nitrogen refrigerator into a 15 m^3 LN_2 phase separator, both placed underground. Two 50 m^3 LN_2 storage tanks placed at the surface are holding the Nitrogen to be used for the cooling of the calorimeter in case of problems with the refrigerator. The liquid Argon will stay, under normal circumstances, in the cryostats over a 15 year period. In case of an emergency the liquid can be emptied into two underground 50 m^3 LAr storage tanks.

The cryogenic system of the Liquid Argon Calorimeter has been separated into four main parts: an internal cryogenics, concerning the elements integrated in the cryostats. A proximity cryogenics, concerning the elements directly connected to the cryostats like the expansion vessels, regulation valve boxes and cryo-lines. A external cryogenics, concerning elements considered as external services, a LN_2 refrigerator for reliquefaction of Nitrogen gas, the LN_2 storage tanks, LN_2 circulators, LAr storage tanks, LAr pumps and cryolines linking the surface to the cavern. As all the cryogenics system it has been provide a vacuum system.

Maintaining the temperature of the liquid in sensitive parts of the calorimeters uniform and stable with time is extremely important since temperature variations directly affect energy measurements. During normal operation the temperature of the liquid Argon bath in the cryostats must be (*i*) maintained constant at 87.3 K, (*ii*) the temperature gradient across the bath must be less than 0.7 K; besides, (*iii*) the formation of gas bubbles, which are detrimental to the functioning of the detectors, must be prevented. Finally, (*iv*) the purity of the Argon must be below 2 ppm of Oxygen volume equivalent.

Temperature stability requirements : subcooling Maintaining the temperature of the liquid in the active parts of the calorimeters uniform and stable with time is an extremely important goal, since temperature variations directly affect energy measurements. The proposed system is based on the use of subcooled liquid Argon. For safety reasons (see below) each cryostat is connected by a large (and long) horizontal pipe to an overflow vessel (Fig. 1.6). The gas pressure above the liquid surface in the overflow vessels will be regulated to typically 1.25 bar using a LN_2 heat exchanger. The associated temperature of the liquid Argon close to the surface is 89.3 K (See Fig. 1.7). Thermally speaking the overflow vessel is essentially isolated from the liquid baths in each of the three main cryostats. LN_2 cooling loops, installed in each cryostat will be used to compensate the heat leaks, and to maintain the baths at the same temperature as on the surface. This is between 3 to 7 K below the equilibrium temperature of liquid Argon at the top or bottom of the cryostat.

The temperature of the subcooled volume can be lowered down to 87.3 K, which is the minimum to avoid the freezing of liquid Argon in the region of the heat exchangers. We give ourselves the conservative target of 0.66 K between any two points in the sensitive volume, at any time during operation. Ultimately, our aim is to achieve a factor of two

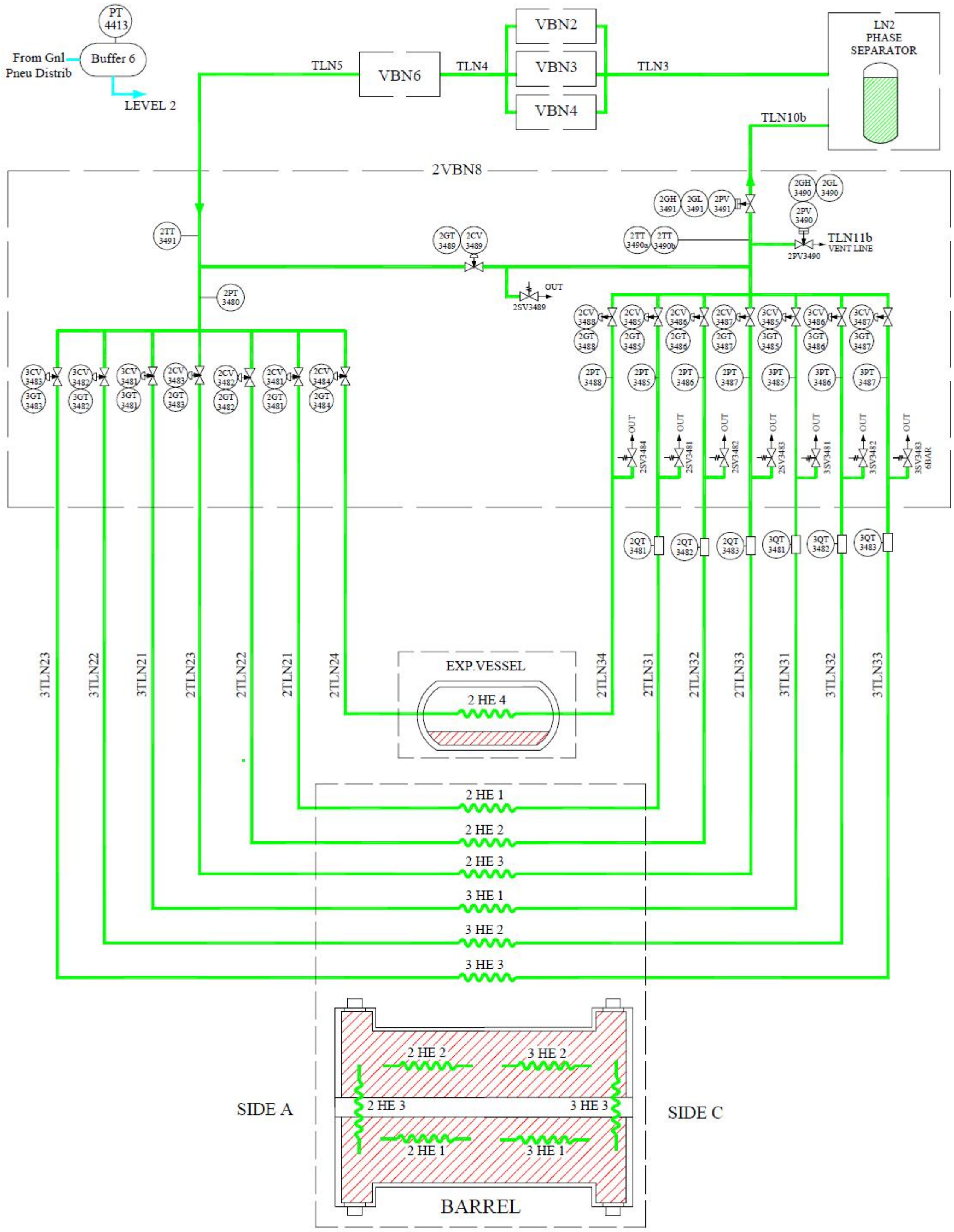

Figure 1.6: Process Instrumentation diagram.

better than this, in order to be able to satisfy the requirements on the constant term in energy measurements without correction.

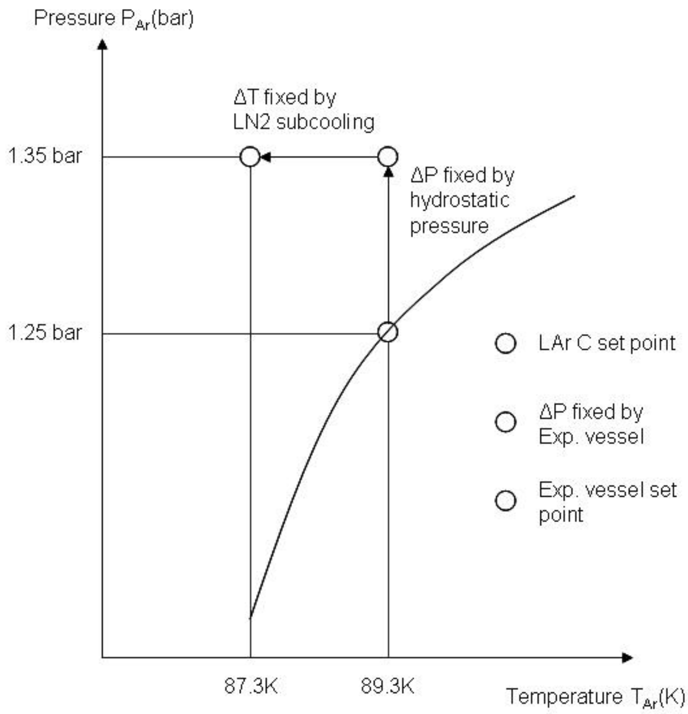

Figure 1.7: Properties of liquid Argon.

Temperature and Pressure of LAr Normal working temperature 89.3 K
Pressure of saturated vapour 1.25 $bar\ abs.$
Density $\rho = 1381\ kg \cdot m^{-3}$
Set point of safety device 1.7 $bar\ abs.$
The minimum working temperature is 87.3 K.

Model overview

As described in the previous section, the main objective, through a cryogenics approach is: (i) to maintain the liquid Argon at liquid state without bubbles; (ii) to ensure a gradients less than 0.7 K across the Argon bath; (iii) the temperature of the liquid Argon bath in the cryostats must be maintained constant at 87.3 K. The set point is defined by a precise pressure and temperature in the cryostat. One can be controlled by a liquid Nitrogen flow in heat exchangers and the other one by the level of liquid Argon in an extension vessel which allow fixing a hydrostatic pressure. The gas pressure above the liquid surface in the expansion vessel must be regulated to 1.25 *bar* (89.3 K), using the heat exchanger place in the gaseous volume. In order to prevent the formation of gas bubbles in the cryostats, the temperature of the Argon bath was lowered in the Argon bath to create a sub-cooled liquid. To satisfy all the requirements, a complex structure of valves, pumps was created. All the CERN cryogenics experimental infrastructure have to be controlled real time by means of a system based on an advanced control technique. In the following a standard approach to the problem of the control modeling are presented. Subsequently a novel approach is proposed.

1.2.3 The CMS detector

The first simulation test was based on the cryogenic system of a CERN experiment: CMS (Compact Muon Solenoid). CMS is one of the biggest particle detector of the LHC. Approximately 2′300 people from 159 scientific institutes are in collaboration for this project. The complete detector is cylindrical, 21 m long and 16 m diameter and weigh approximately 12′500 t.

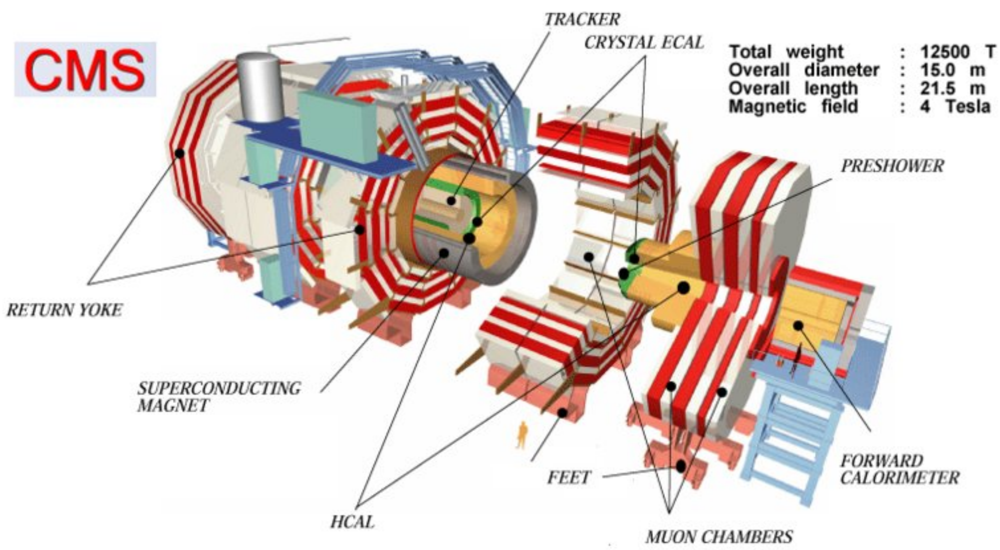

Figure 1.8: The CMS experiment.

The main objective of the CMS experiment is to discover the Higgs boson but also to look for evidence of physics beyond the standard model, such as supersymmetry, or extra dimensions and the study aspects of heavy ion collisions. CMS was designed to detect energies and momenta of particles which are produced from proton-proton collisions (photons, electrons, muons...) in the LHC. There are four layers of detections represented in the Figure 1.8 :

- The Tracker, in the center of the detector, able to detect charged particles
- The Electromagnetic Calorimeter (ECAL) to measure precisely the energies of electrons and photons
- The Hadron Calorimeter (HCAL) to measure energies of hadrons (protons, neutrons, kaons, pions)
- The Muon Detectors and return yoke which allow to identify muons.

Moreover, CMS has a high-magnetic field solenoid [8] in order to deviate charged particles. Hence, the ratio charge/mass can be deduced from the curved track of particles in the magnetic field. This magnet consists of a 4 t central field, 6 m free bore, and 12.5 m length, superconducting solenoid, enclosed in an iron yoke, which is also used for muon detection [9]. It is the biggest and most powerful superconducting magnet ever built, with an inductance of 14 H and a nominal current of $19'500$ A, giving a total stored energy of 2.7 GJ (equivalent to about half-a-tonne of TNT). The magnet is composed of five module coil using aluminum-stabilized as conductor [10].

CMS cryogenic system

The CMS refrigerator (Fig. 1.9) has to cool the 225 t cold mass of the superconducting coil down to 4.5 K by means of a thermosyphon cooling circuit [11]. The required cooling power shall be provided by a dedicated Helium refrigeration system which has by now been installed in a temporary position inside the CMS assembly hall [12, 11]. After the commissioning and the fine tuning by the means of a test cryostat, the Helium refrigeration system has been connected to the CMS solenoid in order to allow the full cryogenic testing of the solenoid. Upon completion of the surface tests of the solenoid, the cold box has been moved to its final position in the service cavern adjacent to the CMS experimental cavern. The CMS cryogenic system is composed of several units, as follows:

- A *compressor station* located at the surface which compress gaseous Helium from 1.03 bar to 18 bar at 300 K with two oil-lubricated screw compressors in series providing a mass flow of 207 $g \cdot s^{-1}$.

- A *coldbox* provided by Air-Liquide to cooldown Helium from 300 K until 4.5 K at 1.25 bar. It is located underground in a cavern close to the magnet and it has a cooling capacity of 800 W at 4.5K for the magnet, 4.5 kW between 60 K and 80 K for the thermal shield of the screens and 4 $g \cdot s^{-1}$ liquefaction for the current leads simultaneously. The cooling scheme of the refrigerator is based on a Claude cycle, 6 heat-exchangers, 3 expansion-turbines, cryogenic valves and one phase separator are used. A Nitrogen precooler can also be used to start the cooldown until 100 K. The scheme of the coldbox is shown in Figure 1.9 on the left side.

- An *intermediate cryostat* of 6 m^3 to allow the system an uninterrupted supply of liquid Helium in case of failure.

- A *Coil Cryogenic System* situated above the magnet for the Helium supply of the coil (see Figure 1.9, right side). It is composed of a phase separator of 900 L connected to cooling sub-circuits via a chimney. The Helium flow is driven by a natural thermosyphon principle.

At the present stage, the study is limited to the coldbox, the intermediate cryostat and the magnet together. The compressor station is considered perfect under constant boundary conditions.

The CMS experiment and its cryogenic unit are currently in the CMS cavern at 100 m underground on the accelerator trajectory since June 2007. Two main simulations have been effectuated :

- The first one is the simulation of a complete cooldown of the cold-box connected to the superconducting magnet and the thermal shields using the intermediate cryostat.

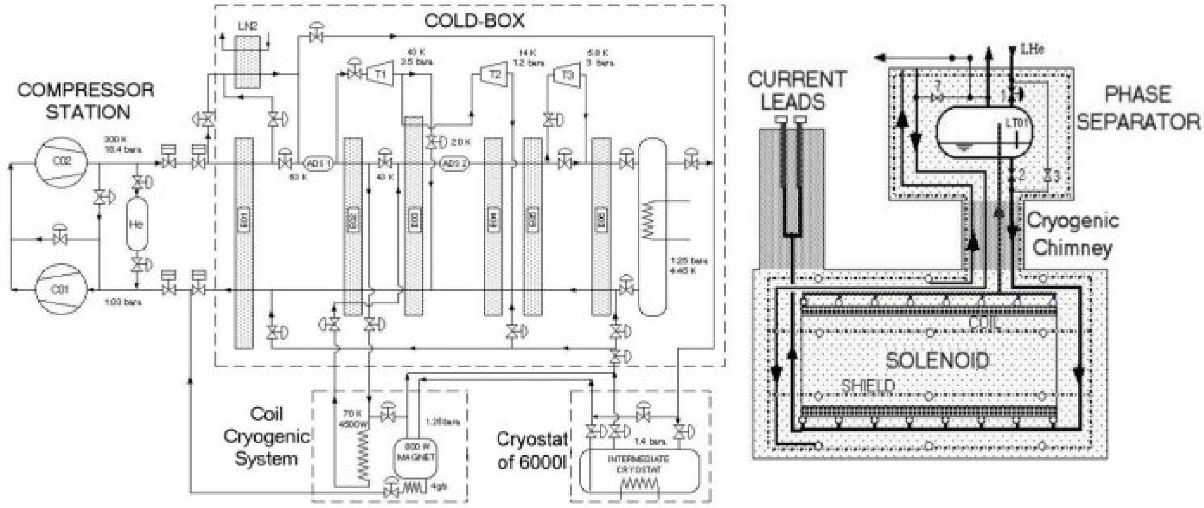

Figure 1.9: The CMS coldbox and the Coil Cryogenic System.

Simulation results were validated with a test carried out in February 2006 at the surface.

- The second simulation is done for the coldbox alone, the superconducting magnet and thermal shields are not connected. Simulated results are compared with the test campaign of August 2007 effectuated in the cavern.

During the real tests, some valves have been forced and some set-points were changed by operators to optimize the cooldown or to see how the coldbox behaves. Most of these manual actions were not taken into account in the simulations where the control is automatically done by the PLC program.

1.2.4 The central Helium liquifier at the CERN Cryolab

The CERN cryogenics experimental infrastructure includes several cryogenic plants. These plants are spread through out different experimental areas around the CERN sites. In order to ensure safety and reliability as required by the operation team, to enhance ease of operation and to provide long-term durability, CERN has undertaken a major upgrade using the experience gained during the construction of the LHC cryogenic control system

Figure 1.10: The CMS coldbox during the installation.

within the *UNICOS* framework [13]. The CERN Central Liquefier plant produces all year long liquid Helium at 4.5 K for distribution via mobile dewars to CERN-wide users. The Helium liquefier is composed of several units:

- A compressor station which compresses gaseous Helium from 1.1 bar to 12.5 bar.
- A TCF50 coldbox provided by Linde® cooling down Helium from 300 K until 4.5 K with a $2g \cdot s^{-1}$ liquefaction rate. The scheme of the coldbox is shown in Fig. 1.11.
- An intermediate 5 m^3 dewar to stock the liquid Helium before distribution in small dewars.
- A liquid Helium distribution box dispatching the Helium dewars.

The compressor pressure is auto-controlled and can provide 80 $g \cdot s^{-1}$ of Helium to the coldbox at room temperature. The cold box circuit consist of 6 heat exchangers, 2 turbines and a Joule-Thomson valve, see Fig. 1.11. The speeds of the turbines are controlled at around 3.4 kHz.

1.2.5 The liquid Krypton calorimeter NA62

The NA62 experiment is a continuation of the CERN kaon research program and particularly the NA48 experiment which was designed in the early 90's to measure the direct CP

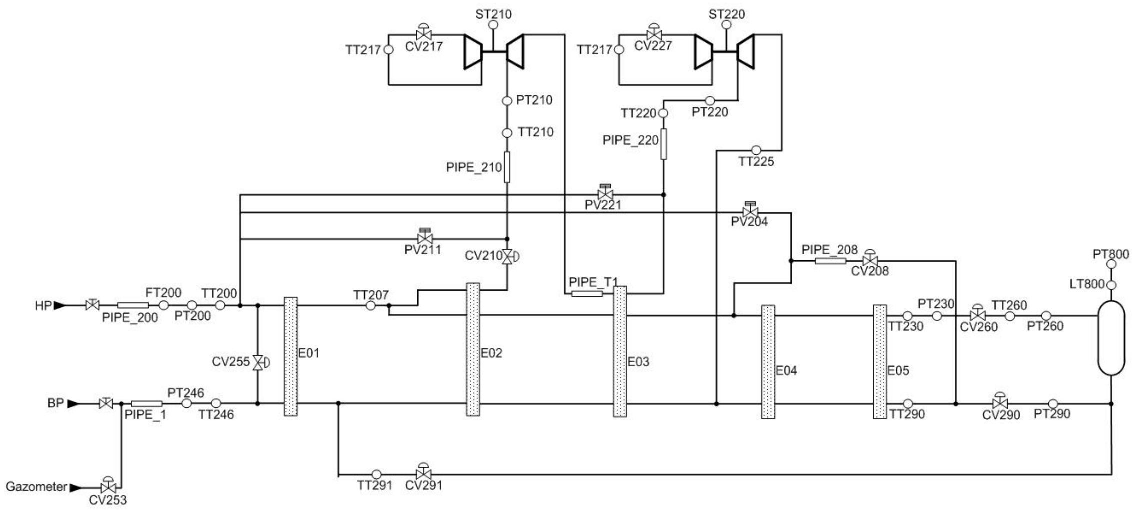

Figure 1.11: The TCF50 model.

violation [14] with a very high precision. An important component of the experimental setup is an electromagnetic calorimeter filled with 9 m^3 of high-purity liquid Krypton at 120 K. Its associated cryogenic system aims at providing a very high reliability and stable thermal conditions with temperature stabilization better than 0.1 K. The upgrade of the cryogenic control system was motivated by the need of ensuring its durability and standardization for the long term fixed-target physics program at the CERN Super Proton Synchrotron (SPS). At the creation of the NA48 experiment, the purpose of the electromagnetic calorimeter was to reconstruct kaons neutral decays using a quasi homogeneous liquid Krypton (LKr) ionization chamber to combine good energy, position, and time resolution [15]. The cryogenic system consists basically of a vacuum insulated calorimeter cryostat, a Krypton storage dewar to ensure loss-free storage for long idle period, and two Nitrogen dewars (see 1.12).

Purifying and specific cooling devices have been integrated to maintain the liquid Krypton at a relevant impurity level and to guarantee high-grade thermal stability. Liquid transfer is generally achieved with a centrifugal pump and several filters are dedicated to Krypton purification either in the liquid or in the gas phase. The calorimeter is further equipped with a cool down/warm up unit. To compensate static and dynamic heat loads produced by cold electronics, solid conduction, and power cables entering the liquid, a Krypton

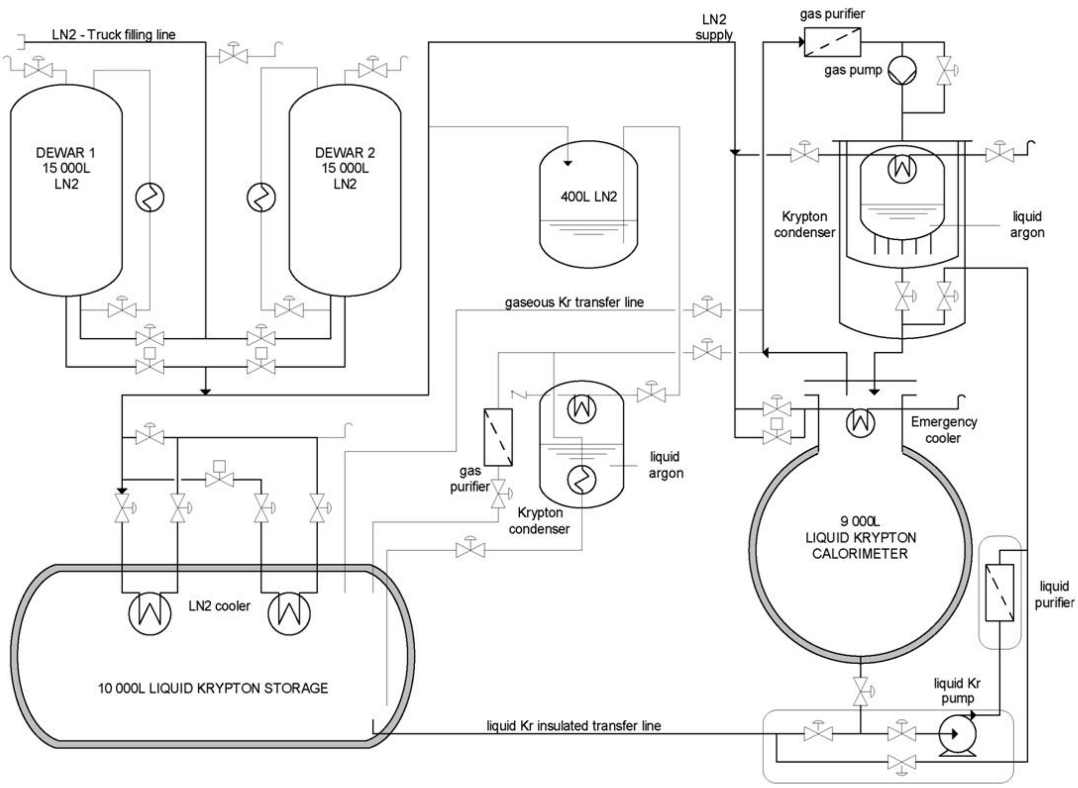

Figure 1.12: Simplified cryogenic flow scheme.

condenser using liquid Argon as intermediate coolant has been installed. Argon in itself is further cooled by liquid Nitrogen evaporation. Nitrogen heat exchangers, located in the gas space of the calorimeter and the storage dewar, provide emergency solutions in cases of unforeseen pressure rises. To prevent any critical situation which, in the worst case, could lead to a Krypton loss, several redundancies have been performed on the apparatus and on its consecrated control. Consequently, both cold water and compressed air supply systems can be switched to external sources, and inlet valves for emergency coolers are duplicated. Concerning the control system, most of important temperature and pressure sensors are doubled, and the low voltage supply is backed up by an UPS giving autonomy of six hours, and by a diesel generator. The first commissioning took place in 1994, and the cryogenic system has since operated to provide optimal conditions inside the calorimeter for 14 years of physics exploitation.

Chapter 2

Standard approach

2.1 State of the art

This Section provides an overview of the control systems for cryogenics, along with hardware and software tools normally employed for their realization, such as PLC-*SCADA* solutions, PID control loops, process identification techniques.
A crucial point of the discussion is the introduction of *UNICOS* (Unified Industrial COntrol System), a software framework developed at CERN, which (*i*) allows the use of more advanced control techniques (such as Smith predictor, PFC, RST, GPC) through the *Multicontroller* object, (*ii*) provides a powerful human-machine interface, and (*iii*) is conceived as a standard platform for the management of the CERN automation systems. Results obtained in simulation by means of the "*Advanced Automation Tool Kit*" are also provided. In particular, a comparison between PID and *Multicontroller* is carried out to show that the latter can easily outperform the more traditional PID in typical application scenarios.

2.1.1 Introduction

The Cryogenic controls deal with the development of the control system for the cryogenics. The control systems are based on PLC (Programmable Logic Controller) technology. With the aim of standardize the PLC programming, the group has developed the UNICOS framework [13] It is an object oriented development for industrial process control technologies based on PLC-*SCADA* solutions. The first *UNICOS* framework version was

able to provide PID control loops. The PID controller is simple and reliable and is able to solve up to 80 per cent of control loop systems. In cryogenics environments the PID controller is sometimes insufficient to solve critical problems (inverse response, long dead times, non-linear systems).To overcome this limit the *MultiController* object, presented in this Chapter, has been integrated in the latest *UNICOS* framework to offer various advanced control loop strategies. It gives to the user a series of advanced control algorithms: Smith Predictor, PFC, RST and GPC. Additionally the *MultiController* offers full tuning possibilities via a Human Machine Interface (HMI).
Since also the process identification is a key point to elaborate the control signal, an advanced tool suite named "*Advanced Automation Tool Kit*" was included allowing several control functionalities to work in a PLC environment. It provides PLC objects for system simulation, online system identification, and online system recording processes. The *MultiController* combined with the "*Advanced Automation Tool Kit*" gives to the process engineer a complete solution to tune a system with advanced controllers. For its importance, in the following, the main theoretical aspects of the parametric identification for process modeling are presented.

2.1.2 Identification

To control a process, particularly with a predictive control, it is necessary to have a mathematical model of the process. An identification is a transformation of the natural laws in equations. Two approaches are possible:

- Using the physical equations of the system (Mass conservation, energy conservation...) which are generally complex differential equations.
- Exciting the process by inputs, measuring the outputs and deducing an empirical model upon these observations: parametrical identification.

The first method needs to have an important knowledge of the process and moreover disturbances on electrical signals (noise) can not be expressed. The different parameters

obtained with this method are physical constants generally not very well-known.
The second method, which will be explained in this report, allows a good reliability in taking care on all possible disturbances applied on the system. The result of this identification is a mathematical model where the different parameters do not have any physical significations. This model can be represented continuously or discreetly by different way as transfer functions, states spaces, step responses, pulse responses...

Identification goal and principle

The principle of the parametrical identification is to extract a mathematical model from observations. Thus, it is important to have a basic knowledge of the process. It is necessary to choose a model type. For this, we have to select the properties of the models:

- SISO or MIMO model. Which inputs ? Which outputs ? Which disturbances ?
- Linear or non-linear model (and what is non-linear about what ?)
- Continuous or discreet model
- Independent or regressive model: for a regressive model the model output y_m depends on the process output y_p
- Deterministic or stochastic model

Then, in order to obtain a model with a good reliability, it is important to excite all frequencies, so, the signal applied to the process input have to be rich in frequencies (i.e.: having a large spectrum). One of the best signal, very rich in frequency is a Pseudo Random Binary Signal (PRBS) (Fig. 2.1). This signal can be set at two distinctive values (e.g.: 1 and -1) where the order of apparition of these two values is generated by a random function during a fixed period. Then, this sequence is repeated.
When there are multiple inputs in a MIMO system, all inputs have to be uncorrelated. If two inputs (u_1 and u_2) are correlated, it exists an infinity of solutions for the two models $M_1 = \frac{y_1}{u_1}$ and $M_2 = y_1 u_2$. For example, if $u_1 = \alpha \cdot u_2$ then $y = M_1 \cdot u_1 + M_2 \cdot u_2 =$

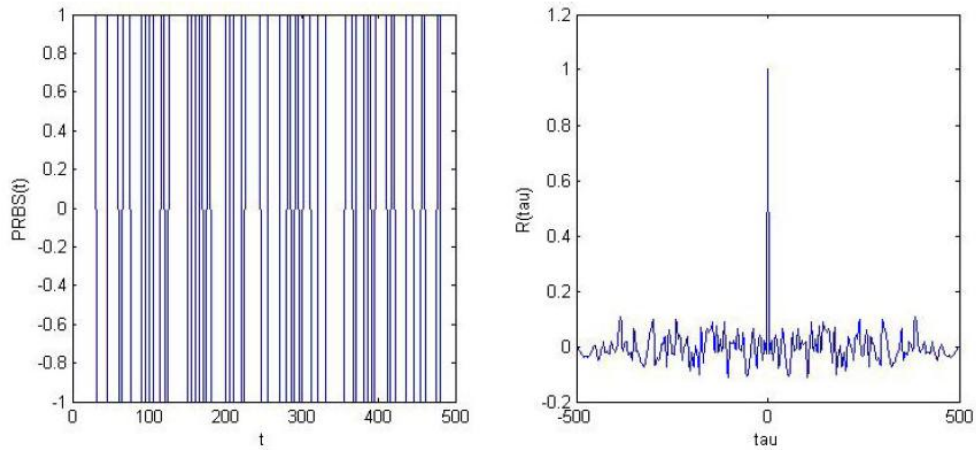

Figure 2.1: A PRBS signal and its autocorrelation.

$(\alpha \cdot M_1 + M_2) \cdot u_2$ and there are a lot of different solutions to find M_1 and M_2. Moreover, exciting one input with the other constant and vice-versa is not a good solution either. First, the time of the test and of the resolution will be longer and secondly, the dynamic of the process is not well evaluated, it is not representative of a normal process operation. So, the best method is to excite the process with all inputs together and all input signals have to be uncorrelated. That is why it is important to develop a test protocol to have a good precision in the model. In Fig. 2.2, the identification procedure is resumed [16]:

- Determination of the test protocol: Properties of the excitation signal to cover all interesting frequencies, the ratio signal/noise must be important enough and the number of measurements must be relevant for the test (> 1000).
- Determination of the model structure: there are a lot of models to describe a dynamic behaviour and the model has to be adapted to the process. The model order and the delays have to be determined too.
- Parameters identification: choice of an algorithm to solve the problem and minimizing errors between process and model.
- The validation of the model is very important. It consists of different tests to validate the model. If the model is wrong, it is necessary to come back on previous

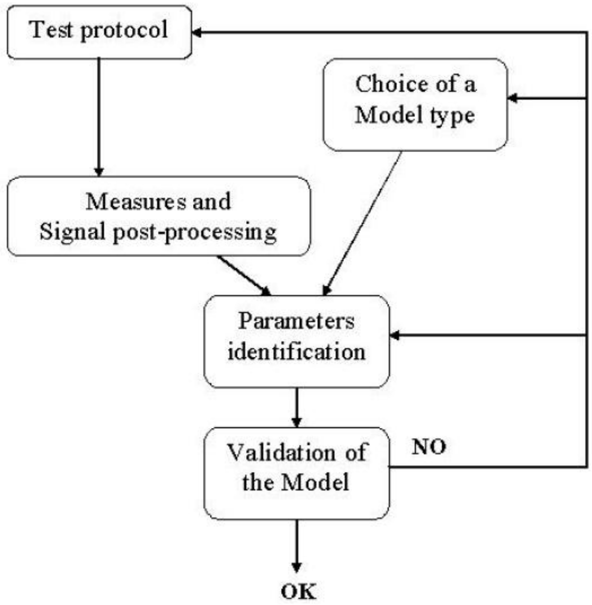

Figure 2.2: Identification procedure.

steps.

Identification procedure Passing through the scheme of Fig. 2.2, the identification procedure is defined by the following steps: (i) define a test protocol; (ii) measure the signals and post processing; (iii) define a model type and order; (iv) identify the parameter; (v) validate the model. In the following each block is discussed.

Signal post-processing After having made a data acquisition from the process, it is necessary to filtering signals, define a sample time and analyze signals correlations in order to have correct signals to beginning the identification.

Sampling time and integrator. The sampling frequency can be reduced according to the dynamic of the process. Of course, the Shannon-Nyquist theorem has to be respected.
If the process contains integrators, it is possible to remove them by derivating the output signals to identify the process without them (a transfer function contains N integrators if there are N poles $z = 1$ or $p = 0$). It means that the process is not stable. The goal of this manipulation is to remove an eventual bias. If the process contains a pole equal to $z = 1$,

the identification will not give a pole strictly equal to 1. Hence a bias is introduced, it is better to identify the process without the integrator (moreover the order of the model is reduced) and to add it later in multiplying the denominator of the transfer function by $(1 - q^{-1})$.

Signal corrections. To perform an identification, the signal must be filtered with different filters. Moreover, to keep the dynamical behaviour between the filtered values, it is a parallelled filter which is applied between the manipulated and controlled variables. The different filters are:

- A high-pass filter with a turn-over pulsation $\omega = 0\ rad/sec$ in order to remove the continuous component.
- A high-pass filter to remove the low-frequencies dues to the external environment (external temperature...) and not dues to the inputs.
- A low-pass filter to remove the noise. The turn-over pulsation must be superior of the input frequency in order not to loose information.

Signal analysis. After all signal post-processing, it is important to check the correlations of signals before the identification (correlations between the output and each input, correlations between the different inputs, the autocorrelations of all signals).
The correlation between 2 signals y and u represents the dependency between the value of y at the instant t and the value of u at the instant $t - \tau$. This relation is defined as:

$$R_{yx}(\tau) = E\{y(t) \cdot u(t-\tau)\} \approx \frac{1}{N-1} \sum_{i=\tau}^{N} y(i) \cdot u(i-\tau) \tag{2.1}$$

The autocorrelation of a signal u represents the self-dependance of the signal between the instants t and $t - \tau$.

$$R_{u}(\tau) = E\{u(t) \cdot u(t-\tau)\} \approx \frac{1}{N-1} \sum_{i=\tau}^{N} u(i) \cdot u(i-\tau) \tag{2.2}$$

As we said previously, all inputs have to be uncorrelated between themselves and their autocorrelations have to be more or less close to a white noise. The autocorrelation of a white noise is a Dirac impulsion, hence, it is a stationary signal (his autocorrelation function not depends of the time) and moreover, the knowledge of the signal value at the instant t does not bring any information about the value at the instant $t + \tau$: a white noise is completely uncorrelated. This signal doest not exist in the nature and cannot be generated (his variance is infinite) but it can be approached by a discreet white noise generated numerically (Fig. 2.3). Generally, a white noise cannot be applied on a real

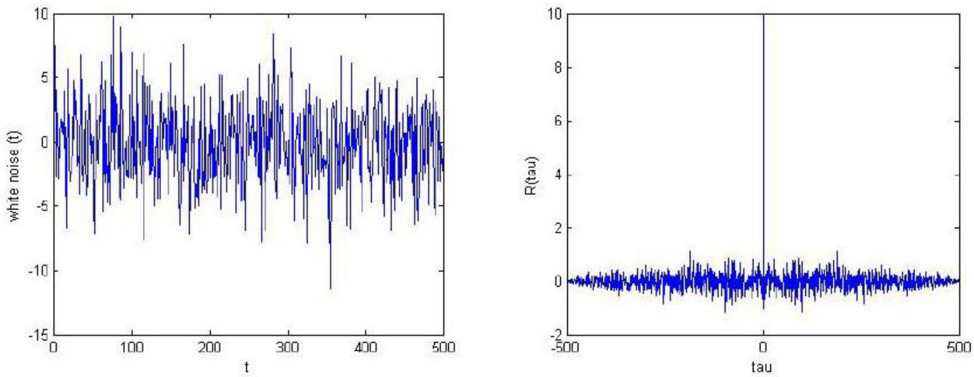

Figure 2.3: Discreet white noise simulated and its autocorrelation.

process directly, because of the actuators, that is why we are using a PRBS signal (Fig. 2.1). The autocorrelation of a PRBS is a weighted sum of Dirac impulsions. For a PRBS signal with a pseudo-period T and an amplitude between $+a$ and $-a$, the autocorrelation of a PRBS is equal to $R_{PRBS}(\tau) = a^2$ when $\tau = k\Delta T$ and $R_{PRBS}(\tau) = -\frac{a^2}{T}$ elsewhere. The advantages of a PRBS are multiple:

- The sum of the signal on one period is 1 and its average is near 0.
- Its autocorrelation is close to a discrete white noise
- The process can be permanently excited if the PRBS is well calculated.

Now, it is important to know what are the different correlations between the input and output variables. In Open loop, the relation between inputs and outputs is:

$$y(t) = \sum_{i=1}^{N} h_i \cdot u(t-i) + v(t) \Leftrightarrow y(t) \cdot u(t-j) = \sum_{i=1}^{N} h_i \cdot u(t-i) \cdot u(t-j) + v(t) \cdot u(t-j) \tag{2.3}$$

Where the h_i are the coefficients of the impulse response. So, to calculate the correlation between y and u:

$$R_{yu}(j) = E\{y(t) \cdot u(t-j)\} = E\left\{\sum_{i=1}^{N} h_i \cdot u(t-i) \cdot u(t-j)\right\} + E\left\{v(t) \cdot u(t-j)\right\} \quad (2.4)$$

Moreover:

$$E\left\{\sum_{i=1}^{N} h_i \cdot u(t-i) \cdot u(t-j)\right\} = \sum_{i=1}^{N} h_i \cdot E\{u(t-i) \cdot u(t-j)\} = \sum_{i=1}^{N} h_i \cdot R_u(j-i) \quad (2.5)$$

In open-loop, the input u and the perturbation v are uncorrelated: $Ev(t) \cdot u(t-j) = R_{vu}(j) = 0$

Finally we obtain:

$$R_{yu}(j) = \sum_{i=1}^{N} h_i \cdot R_u(j-i) \quad (2.6)$$

So, the output y is correlated to u in open-loop via the equation (2.6).

In closed-loop, u can be correlated with v because of y which is dependent of u and v (Fig. 2.4). So in close loop $Ev(t) \cdot u(t-j) = R_{vu}(j) \neq 0$ and:

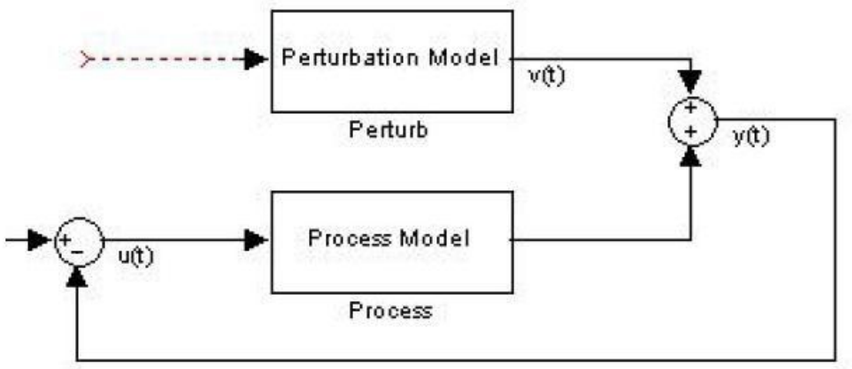

Figure 2.4: Model Structure in closed-loop.

$$R_{yu}(j) = \sum_{i=1}^{N} h_i \cdot R_u(j-i) + R_{uv} \quad (2.7)$$

Model types There are a lot of different mathematical model types. A model can be regressive or not. A model is regressive when the output value at the instant t, $y(t)$, depends on the previous values $y(t-i)$. Moreover, the model can include non measurable perturbation or noise $\zeta(t)$. In order to realize a predictive control, three main models are used:

- The pulse response
- The step response
- Transfer function in z

In identification, the coefficients to find are generally put in a vector (or in a matrix with MIMO systems) called θ and the observations of the system (previous values of inputs and outputs) in a vector (or in a matrix) called $\varphi(t)$. For a MIMO system, $\Phi = [\varphi_1^T ... \varphi_n^T]^T$ for n outputs.
So, the system can be represented in a matrix equality:

$$y_m(t) = \varphi \cdot \theta + \zeta(t) \tag{2.8}$$

Pulse response. In this model, the model output $y_m(t)$ depends on previous values of the different inputs and eventually of a noise $\zeta(t)$, for M inputs:

$$y_m(t) = \sum_{k=1}^{M} \sum_{i=1}^{\infty} h_{ki} \cdot u_k(t-i) + \zeta(t) \approx \sum_{k=1}^{M} \sum_{i=1}^{N} h_{ki} \cdot u_k(t-i) + \zeta(t) \tag{2.9}$$

with a significative value of N according to the process. The coefficients h_i represent the pulse response of the process. The different vectors in a SISO system are:

$$\begin{cases} \varphi = [u(t-1) ... u(t-N)]^T \\ \theta = [h_1 ... h_N]^T \end{cases}$$

Step response. The difference in the step response is that the output y_m depends on the variation of the input $\Delta u = (1 - q^{-1}) \cdot u$, for M inputs:

$$y_m(t) = \sum_{k=1}^{M} \sum_{i=1}^{N} g_{ki} \cdot \Delta u_k(t-i) + \zeta(t) \tag{2.10}$$

and the coefficients g_i represent the step response of the process. The different vectors in a SISO system are:

$$\begin{cases} \varphi = [\Delta u(t-1) ... \Delta u(t-N)]^T \\ \theta = [g_1 ... g_N]^T \end{cases}$$

Transfer function. There are different types of transfer functions according to the process. The first model which can be used is an ARX model (Auto Regressive with eXternal inputs). It is an auto regressive model containing a white noise $\zeta(t)$ with a null average. Moreover the model includes a pure delay where k is the number (an integer) of sampling time (T) representing the delay $d = k\Delta T$.

$$y(t) = q^{-k} \cdot \frac{B(q^{-1})}{A(q^{-1})} \cdot u(t) + \zeta(t) \tag{2.11}$$

Another model is the ARMAX (Auto Regressive Moving Average with eXternal inputs) model. It is a regressive model where the non measurable disturbances are assimilated to white noise $\zeta(t)$ filtered by a transfer function with a moving average:

$$y(t) = q^{-k} \cdot \frac{B(q^{-1})}{A(q^{-1})} \cdot u(t) + \frac{T(q^{-1})}{A(q^{-1})} \cdot \zeta(t) \tag{2.12}$$

It's also possible to integrate the noise directly to obtain an ARIMAX model (or CARIMA model):

$$y(t) = q^{-k} \cdot \frac{B(q^{-1})}{A(q^{-1})} \cdot u(t) + \frac{T(q^{-1})}{\Delta \cdot A(q^{-1})} \cdot \zeta(t) \tag{2.13}$$

Δ corresponds to the differential operator. The polynomial $T(q^{-1})$ is often equal to 1 but can be different according to the noise model. This point will be explained later. The different vectors in a SISO system are:

$$\begin{cases} \varphi = [y(t-1)...y(t-N_1)u(t-1)...u(t-N_2)]^T \\ \theta = [a_1...a_{N_1}b_1...b_{N_2}]^T \end{cases}$$

Model order. To proceed at the identification, the order of the model and the pure delay have to be known beforehand when the model is a transfer function and the number of samples retained for the step/impulse response too. For the pure delay, it is easy to find it during a step test in open-loop: it is the delay between the beginning of the step and the beginning of the process response. Concerning the order of $A(q^{-1})$ and $B(q^{-1})$, there is not law except the shape of the response and the experience. To choose the number of samples in the impulse/step response, a hundred of samples can be retained but it depends on the process velocity and on the sampling time.

Identification The identification consists in finding all parameters θ of the model from the measurements φ to minimize the errors between the model output and the process output. Once the measurement data are obtained and the model is fixed, the algorithms to estimate the parameters could be applied. The most used method to solve this problem is the Least Squares algorithm (LS). A recursive version also exists (RLS).

LS algorithm. The LS algorithm allows to minimize the function V which represents the sum of the quadratic errors ε^2:

$$V = \frac{1}{N} \sum_{k=1}^{N} (y(t) - y_m(t))^2 = \frac{1}{N} \sum_{k=1}^{N} \left(y(t) - \phi^T \cdot \theta\right)^2 \tag{2.14}$$

So, if the system to identify has a model $y = \phi \cdot \theta$ (there is not any noise or disturbance), the optimal θ can be calculated with the pseudo-inverse of ϕ:

$$\hat{\theta} = \left[\phi^T \cdot \phi\right]^{-1} \cdot \theta^T \cdot y \tag{2.15}$$

Of course, $[\phi^T \cdot \phi]$ has to be invertible.
If the model is an ARX model (equation (2.11)), containing a white noise with a null average, the LS algorithm provides a consistent identification without any bias [16] and the solution $\hat{\theta}$ has the same expression. On the other hand, if the model is an ARMAX or ARIMAX model (see equations (2.12) and (2.13)), the solution will contain a bias because of the average of $\frac{T(q^{-1})}{A(q^{-1})} \cdot \zeta(t)$ which is not null. To identity an ARIMAX model, the RELS algorithm has to be used. However, the solution can be more or less exact with the LS algorithm if the noise level is very weak (weak variance). The advantage of the LS algorithm is that it is fast to solve and so, can be used for real-time identification.

RLS algorithm. The RLS algorithm is the recursive algorithm of LS. So, the memory and the time of calculation are more important. It is not well adapted for a real-time identification but it is a performing algorithm for on-line identification. The algorithm is the following for each sampling time k [16]:

$$\begin{cases} \hat{\theta} = \hat{\theta}_{k-1} + K_k \cdot \varepsilon_k \\ \varepsilon_k = \left(y_k - \hat{\theta}_{k-1}^T \cdot \varphi_k \right) \\ K_k = \frac{P_{k-1} \cdot \varphi_k}{1 + \varphi_k^T \cdot P_{k-1} \cdot \varphi_k} \\ P_k = P_{k-1} - \frac{P_{k-1} \cdot \varphi_k \varphi_k^T \cdot P_{k-1}}{1 + \varphi_k^T \cdot P_{k-1} \cdot \varphi_k} \end{cases}$$

$\hat{\theta}_k$ contains the parameters to identify, ε_k is the error between the real output and estimation calculated, K_k represents the adaptation gain Matrix which moves during the time and if the algorithm converges, $K_k \longmapsto 0$.

There are other versions of the RLS which are modified. For example, it could be better to not take into account the first iterations of the algorithm in order to forget old values progressively. For this, a forget coefficient λ is inserted and the matrix P_k becomes:

$$P_k = \frac{1}{\lambda} \left[P_{k-1} - \frac{P_{k-1} \cdot \varphi_k \varphi_k^T \cdot P_{k-1}}{1 + \varphi_k^T \cdot P_{k-1} \cdot \varphi_k} \right]$$

with $0 < \lambda \leq 1$. When $\lambda = 1$ it is the classical RLS algorithm but when $\lambda \neq 1$, the errors are weighted by a coefficient λ^{k-t}.

RELS algorithm. The RELS algorithm (Recursive Extended Least Square) is also called PEM algorithm (Prediction Error Method). This algorithm allows to perform a consistent identification without any bias when the model is an ARMAX or ARIMAX model (see equations (2.12) and (2.13)). The principle of this method is to include the polynomial coefficients of $T(q^{-1})$ of the noise in the vector $\theta = [\hat{a}_i, b_i, t_i]$. In consequence, we have to add in the observation vector φ the past values of the noise:

$$\varphi = [y(t-1)...y(t-n), u(t-1)...u(t-m), \zeta(t-1)...\zeta(t-r)]^T \tag{2.16}$$

Of course, these values cannot be measured, that is why this algorithm calculates the estimated noise $\hat{\zeta}(t)$ thanks to the process model with a recursive relation (it is a predictor):

$$\hat{\zeta}(t) = y(t) + \sum_{i=1}^{n} \hat{a}_i \cdot y(t-i) - \sum_{i=1}^{m} \hat{b}_i \cdot u(t-k-i) - \sum_{i=1}^{m} \hat{t}_i \cdot \hat{\zeta}(t-i) \tag{2.17}$$

The final algorithm is the same as the RLS or the modified RLS algorithm but θ and φ are augmented. Moreover the predictor $\hat{\zeta}(t) = \varepsilon(t)$.

Recursive Maximum likelihood (RML) method. The RML is an upgrade method of the RELS principle for ARMAX plants [17]. The aim is to reduce the correlation between the predictive error and the observation vector by filtering the measured vector with $1/\hat{C}(t, q^{-1})$, with $\hat{C}(t, q^{-1})$ the estimation of $C(t)$.
The parameter vector and the measures vector are then defined by:

$$\begin{array}{l} \phi(t)^T = \dfrac{1}{\hat{C}(t, q^{-1})} * \\ \left[\begin{array}{ccccccccc} -y(t) & ... & -y(t - n_A + 1) & u(t-d) & ... & u(t - d + n_B + 1) & \varepsilon(t) & ... & \varepsilon(t - n_C + 1) \end{array} \right] \\ \hat{\theta}(t)^T = \left[\begin{array}{ccccccccc} \hat{a}_1(t) & ... & \hat{a}_{n_A}(t) & \hat{b}_1(t) & ... & \hat{b}_{n_B}(t) & \hat{c}_1(t) & ... & \hat{c}_{n_C}(t) \end{array} \right] \end{array} \tag{2.18}$$

Validation of the model After having obtained a model, it is necessary to validate this model with different tests. The data used for the validation must be different from the data which have been used with the identification algorithm. If the data are the same, the validation is useless.

Qualitative verification. The first test is a visual verification checking if the model outputs have the same shape as the process outputs for different types of excitation at the input. Be careful, this test is necessary but not sufficient to validate the model.
Statistic tests. The error between the process output and the model output is called residue: $\varepsilon(t) = y(t) - y_m(t)$. This residue has to be close to a white noise with a null average and has to be uncorrelated with the different inputs. So it is necessary to calculate the average of the residue, its autocorrelation R_ε and its correlation with each input $R_{\varepsilon u}$.
Parameters distortion. The question is: How to change the parameters at an instant t to have a perfect model at this instant (i.e.: the residue is null)? To be sure that the model obtained is a good model, the parameters calculated by the algorithm have to be not very

distorted during the time to obtain a perfect model. It is a sign of credibility.

2.1.3 *Multicontroller* object design

Due to the need of advanced control loop strategies the *MultiController* object has been designed. It is an object programming solution for PLCs and *SCADA* systems and offers many advantages in terms of usability, functionality and extensibility [18]. The object design is the result of requests from multiple users and previous experience with existing PID controllers.

Multiple algorithms in a unique monolithic object - a simple object evolution

The *MultiController* object has a single interface for all regulation algorithms. The object structure is implemented with a set of parameters used for all possible algorithms (Fig. 2.5). The way the parameters are treated is dependant on the selected regulation method. The same parameters can be used differently by each advanced control strategy. This design allows the addition of new control loop algorithms without changing the object interface.

An efficient tuning mechanism and a unique HMI with different views

The object development process is a twofold task. On one hand it consists of building a PLC object with the core implementation of the algorithms. On the other hand it deals with the HMI and its possibilities in terms of tuning and parameterized options [19].
The object programming approach of the *MultiController* through the *SCADA* schema is a single monolithic representation by means of a custom faceplate, a unique set of trends, and a unique recipe mechanism. It allows for a global control of the regulation loop via one centralized object representation in the HMI using different views (Fig. 2.6).

2.1.4 Advanced Control Algorithms In *Multicontroller* Object

The *MultiController* object has the following advanced control algorithms implemented: Smith Predictor, RST, PFC, and GPC (PID algorithm is also integrated into the *MultiController*, but is not considered as an advanced feature of the object).

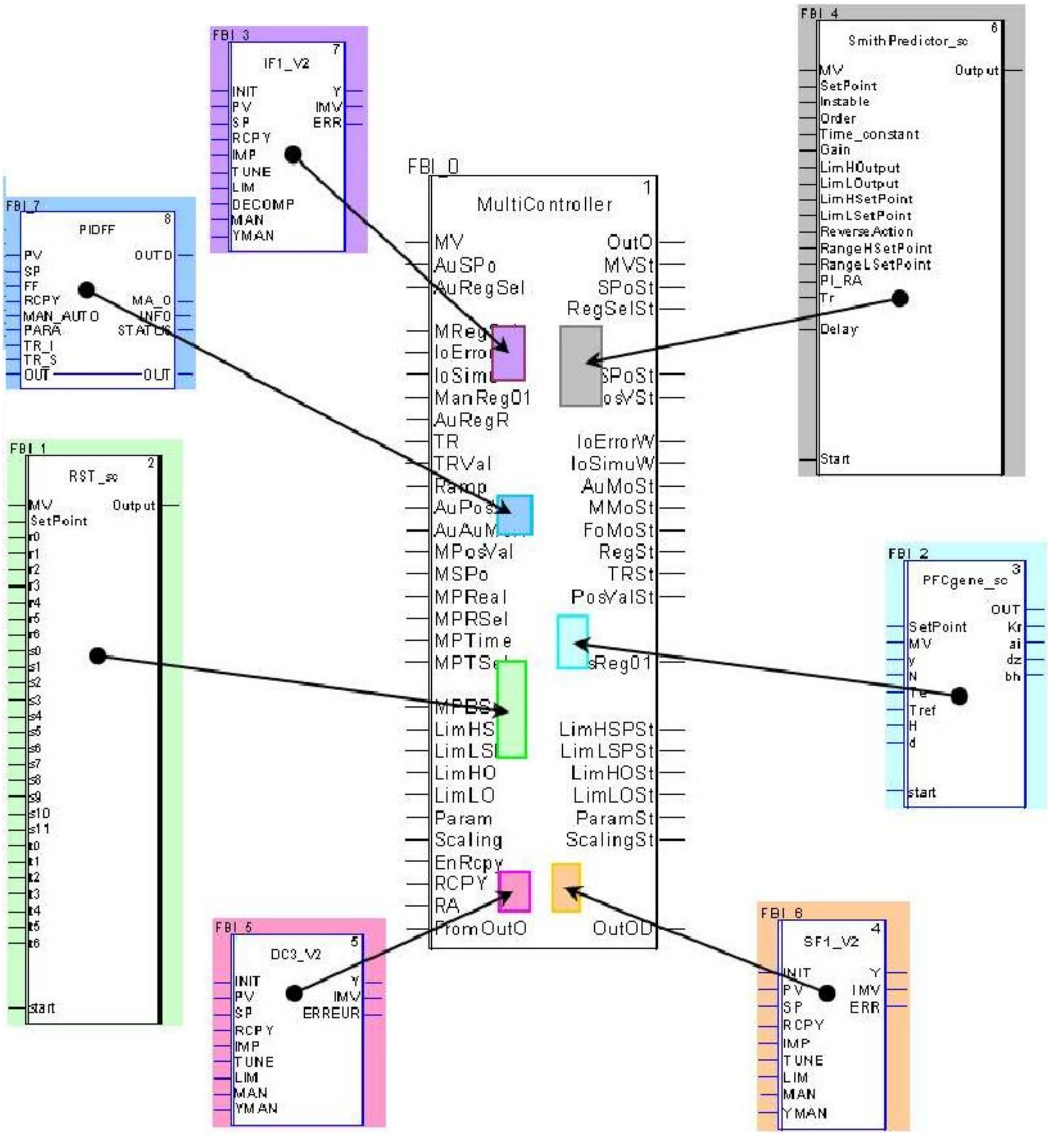

Figure 2.5: *MultiController* object in a Schneider PLC.

Smith Predictor

Classical Smith Predictor structure The Smith Predictor has been proposed [20] to compensate systems with long dead-times. It consists of finding a fictive structure (Fig. 2.7) so that the delay is concealed from the closed loop system.

The smith Predictor can be represented so that R(p) sees F(p) (Fig. 2.8).

Second order system application. The system G is represented by:

$$G(p) = \frac{G_s e^{-\tau p}}{(1 + Tp)^2} \tag{2.19}$$

In this particular case R is a PI corrector and S is a dead-time compensator. The Smith Predictor applied for a second order is shown in Fig. 2.9.

The closed loop response is then:

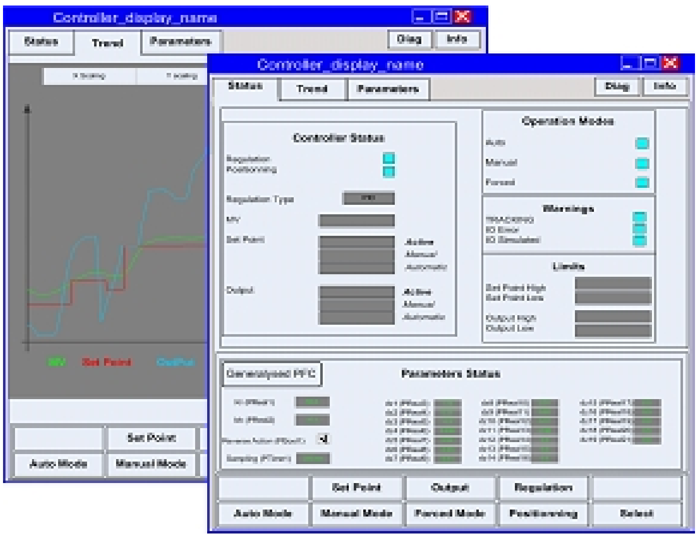

Figure 2.6: *MultiController* faceplate (status and trend views).

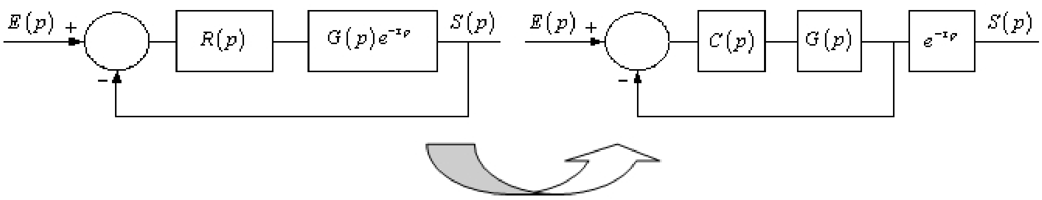

Figure 2.7: Smith Predictor principle: “from a real to a fictive structure”.

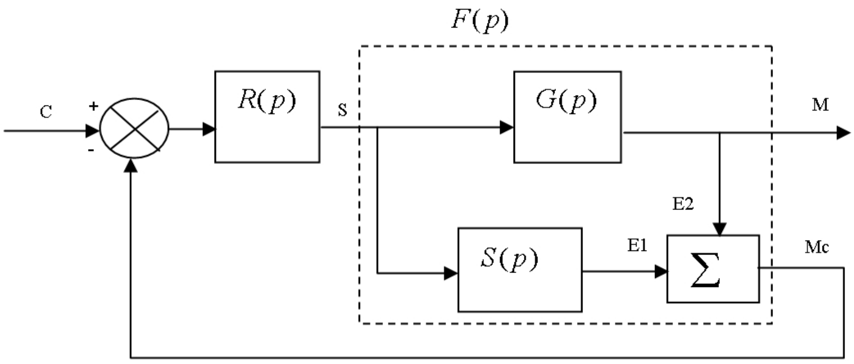

Figure 2.8: Second order Smith Predictor functional view.

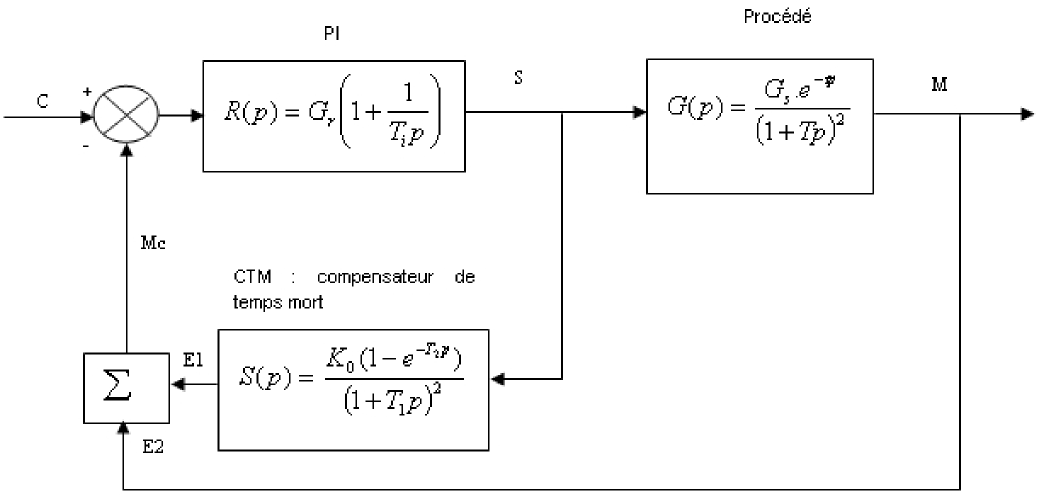

Figure 2.9: Smith Predictor applied for a second order system.

$$H_{CloseLoop} = \frac{1}{1 + \frac{T}{G_s G_{PI}}p + \frac{T^2}{G_s G_{PI}}p^2} = \left.\frac{1}{1 + \frac{2\xi}{w_n}p + \frac{1}{w_n^2}p^2}\right|_{\substack{K_0 = G_s \\ T_{PI} = T}} \tag{2.20}$$

Modified Smith Predictor for integrator with long delay The structure proposed by Matausek [21] is a simple and straightforward modification of the Smith Predictor for integrator systems with long dead-time (Fig. 2.10). It allows a fast setpoint response and a satisfactory load disturbance rejection.

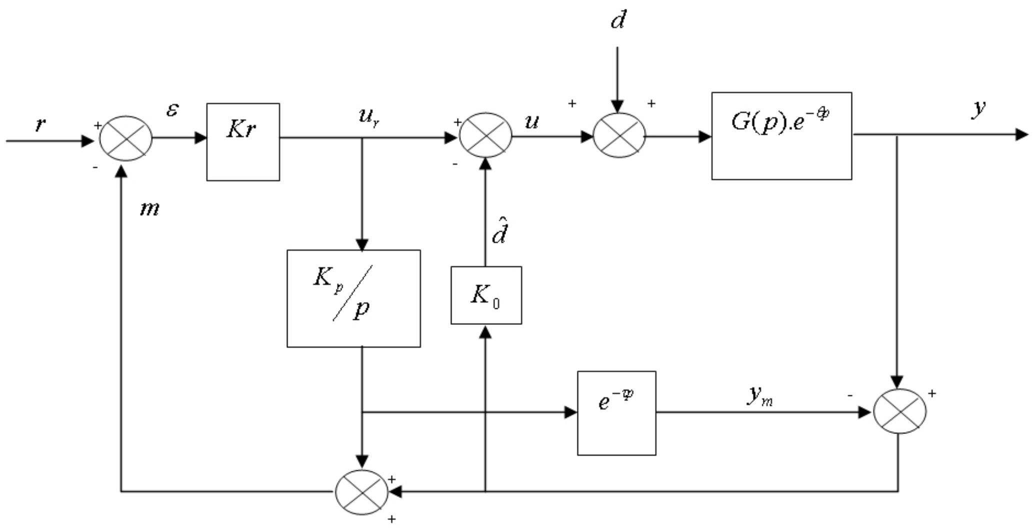

Figure 2.10: Smith Predictor applied for a second order system.

The process is considered so that:

$$G(p) = \frac{K_p}{p} \quad ; \quad \tau = \theta \tag{2.21}$$

Moreover the load $H_d(p)$ and setpoint $H_r(p)$ contributions present the good disturbance rejection $(0, t \to \infty)$ and no steady state error:

$$H_r(p) = \frac{K_p.K_r.e^{-\tau p}}{1 + K_p.K_r}$$
$$H_d(p) = \frac{K_p.\left[p + K_p K_r \left(1 - e^{-\tau p}\right)\right].e^{-\tau p}}{\left(p + K_p.K_r\right).\left(p + K_p.K_0.e^{-\tau p}\right)} \tag{2.22}$$

The tuning proposed by Matausek is:

$$K_0 = \frac{\pi}{2.K_p.\tau} \quad ; \quad K_r = \frac{1}{K_p.T_r} \tag{2.23}$$

Generalized Predictive Control

The Generalized Predictive Control (GPC) proposed by Clarke et al. [22, 23] is a Model Based Control (MBC) strategy. The idea of GPC is to calculate a future sequence of control signals in such a way that it minimizes a cost function over a prediction horizon.

The j-step ahead predictor $y(t+j)$ From a particular operating point, even a non-linear system locally-linearized model as a CARIMA form [24]:

$$A(q^{-1})y(t) = B(q^{-1})u(t-1) + C(q^{-1})\frac{\xi(t)}{\Delta(q^{-1})} \tag{2.24}$$

where $\xi(t)$ is an uncorrelated random sequence and Δ the differential operator $1 - q^{-1}$. From (2.24) we derive the j-step ahead predictor $y(t+j)$:

$$\begin{aligned} y(t+j) = {} & \underbrace{F_j(q^{-1})y(t) + H_j(q^{-1})\Delta u(t-1)}_{Past} + \\ & + \underbrace{G_j(q^{-1})\Delta u(t+j-1) + J_j(q^{-1})\xi(t)}_{Future} \end{aligned} \tag{2.25}$$

The Diophantine equations From (2.24) and (2.25) we obtain

$$A(q^{-1})J_j(q^{-1})\Delta(q^{-1})y(t+j) = B(q^{-1})J_j(q^{-1})\Delta u(t+j-1) + \xi(t)J_j(q^{-1})$$

$$[1 - q^{-j}F_j(q^{-1})]y(t+j) = [G_j(q^{-1}) + q^{-j}H_j(q^{-1})]\Delta u(t+j-1) + J_j(q^{-1})\xi(t+1) \tag{2.26}$$

have the following Diophantine equations to be solved:

$$A(q^{-1})J_j(q^{-1})\Delta(q^{-1}) + q^{-j}F_j(q^{-1}) = 1$$

$$B(q^{-1})J_j(q^{-1}) = G_j(q^{-1}) + q^{-j}H_j(q^{-1}) \tag{2.27}$$

The cost function

The cost function J is defined to set up the future control sequence:

$$J = \sum_{j=N_1}^{N_2} (y(t+j) - w(t+j))^2 + \lambda \sum_{j=1}^{N_u} \Delta u(t+j-1)^2 \tag{2.28}$$

The matrix representation of an optimum j-step ahead predictor

$w(t+j)$ is the setpoint at (t+j), N_1 is the minimum costing horizon, N_2 is the maximum costing horizon, N_u is the prediction horizon and λ is the control-weighting coefficient. The optimum j-step-ahead prediction [25] is given by:

$$\hat{y} = if(q^{-1}).y(t) + G.\tilde{u} + ih(q^{-1}).\Delta u(t-1) \tag{2.29}$$

with

$$if(q^{-1}) = \begin{bmatrix} F_{N_1}(q^{-1}) & ... & F_{N_2}(q^{-1}) \end{bmatrix}^T$$

$$ih(q^{-1}) = \begin{bmatrix} H_{N_1}(q^{-1}) & ... & H_{N_2}(q^{-1}) \end{bmatrix}^T$$

$$\tilde{u} = \begin{bmatrix} \Delta u(t) & ... & \Delta u(t+N_u-1) \end{bmatrix}^T$$

$$G = \begin{bmatrix} g_{N_1}^{N_1} & g_{N_1-1}^{N_1} & ... & ... \\ g_{N_1+1}^{N_1+1} & g_{N_1}^{N_1+1} & ... & ... \\ ... & ... & ... & ... \\ g_{N_2}^{N_2} & g_{N_2-1}^{N_2} & ... & g_{N_2-N_u+1}^{N_2} \end{bmatrix} \tag{2.30}$$

The expectation of the cost-function of (2.28) can be written as:

$$J = \left[if(q^{-1}).y(t) + G.\tilde{u} + ih(q^{-1}).\Delta u(t-1) - w\right]^T$$

$$\left[if(q^{-1}).y(t) + G.\tilde{u} + ih(q^{-1}).\Delta u(t-1) - w\right] + \lambda.\tilde{u}^T\tilde{u} \tag{2.31}$$

Cost function minimization - control increment signal

The objective of GPC is to compute the future control sequence $u(t), u(t+1), ...$, in such a way that the optimal j-step-ahead predictor is driven close to $w(t+j)$ [24, 25]. This is accomplished by minimizing the cost function and making the gradient of J:

$$\frac{\partial}{\partial u}\left[if(q^{-1}).y(t) + G.\tilde{u} + ih(q^{-1}).\Delta u(t-1) - w\right]^T = G^T$$
$$\Rightarrow \tilde{u} = M.\left[w - if(q^{-1}).y(t) - ih(q^{-1}).\Delta u(t-1)\right] \quad (2.32)$$

with

$$M = Q.G^T = \left[G^T.G + \lambda.I_{N_u}\right]^{-1}.G^T \quad (2.33)$$

Only the first value of the sequence of $\tilde{u}$ will be used to be compliant with the GPC strategy which repeats the procedure at each sampling time. The optimal control increment signal is then:

$$\Delta u_{opt}(t) = m_1^T.\left[w - if(q^{-1}).y(t) - ih(q^{-1}).\Delta u(t-1)\right] \quad (2.34)$$

with m_1, the first line of M.

Predictive Function Control

The Predictive Function Control (PFC) principles were introduced in the early 1980's [24, 26]. It applies the same predictive strategy developed for the General Predictive Control (GPC) but uses different concepts to achieve the control signal. Giving the set point on a receding horizon, the predicted process output will reach the future setpoint following a reference trajectory (Fig. 2.11). Additionally the PFC uses a model to build the control signal [27, 28].

The control signal v is then determinated using the base functions defined as follows:

$$v(n+i) = \sum_{k=0}^{k_M} \mu_k U_{Bk}(i) \quad (2.35)$$

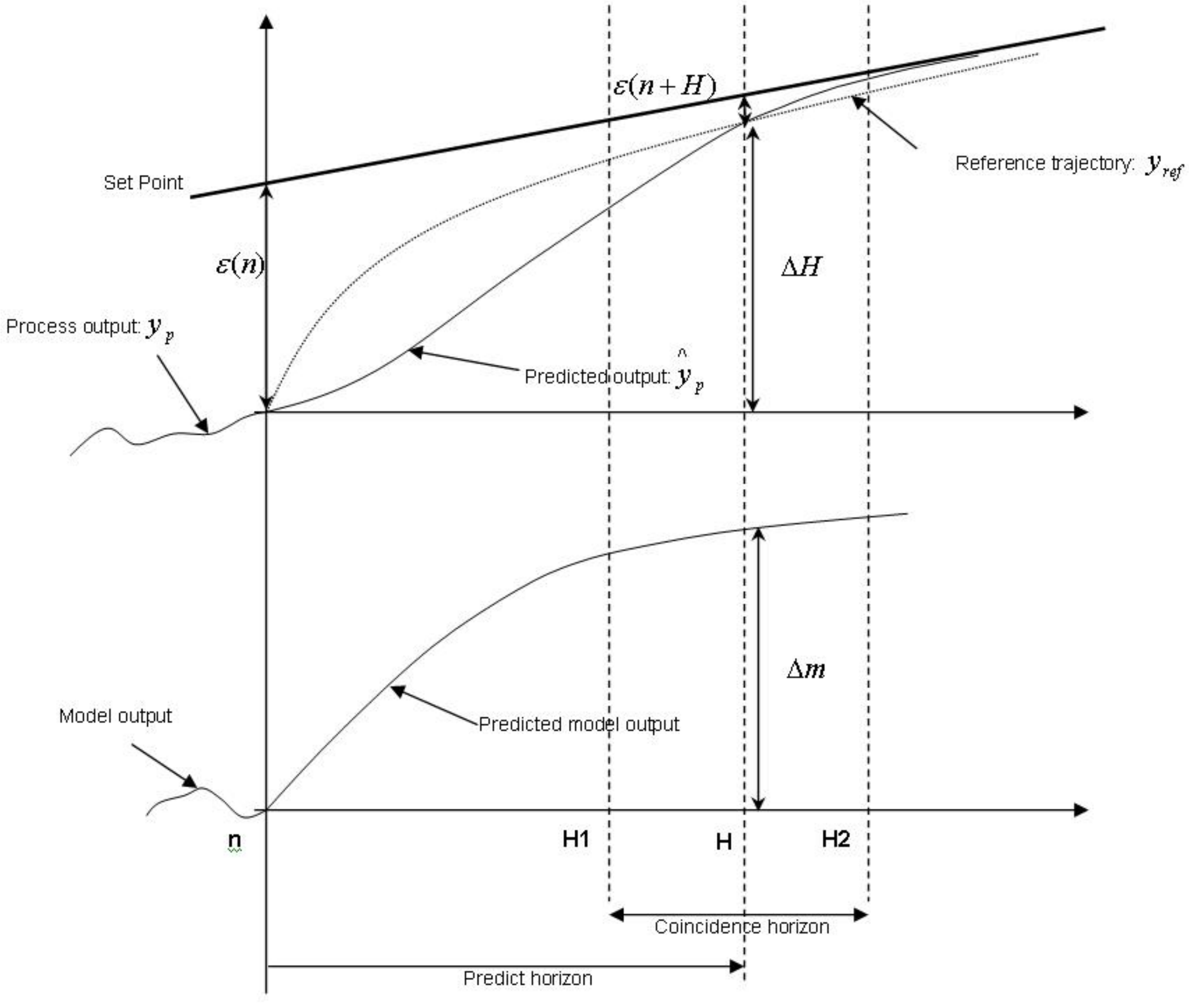

Figure 2.11: Predictive Function Control principles.

First order system application Consider the process output y_p modeled by a first order system given by $S(n)$ with a reference trajectory $\epsilon(n)$ and an exponential decrement λ:

$$S(n) = a_m S(n-1) + K(1-a_m)E(n-1)\Big|_{a_m = e^{-T_e/T}} = S(n)_L + S(n)_F$$
$$\varepsilon(n) = \mathrm{e}^{-n^{T_e}/T}$$
$$\varepsilon(n+H) = \varepsilon(n).\lambda^H \tag{2.36}$$

At a predict coincidence point H we have:

$$\varepsilon(n) = C(n) - s(n) = C(n) - y_p(n)$$
$$\varepsilon(n+H) = C(n) - y_{reference}(n+H)$$
$$\Delta H = y_{reference}(n+H) - y_p(n) \tag{2.37}$$

The command equation becomes:

$$(C(n) - y_p(n)) \,.\, \left(1 - \lambda^H\right) = S_M(n+H) - S_M(n) \tag{2.38}$$

Considering a step function for the base function, we build the control signal $v(n)$:

$$v(n) = \frac{(C(n) - y_p(n)) \,.\, \left(1 - \lambda^H\right) + S_M(n) - a_m^h S_M(n)}{K(1 - a_m^h)} \tag{2.39}$$

Generalized PFC The generalized PFC is applicable for asymptotic stable systems given by its convolute representation (so called MA systems):

$$y_p(n) = a_1^p.u(n-1) + ... + a_i^p.u(n-i) + ... + a_N^p.u(n-N) = \sum_{i=1}^{N} a_i^p.u(n-i) \tag{2.40}$$

The model is then:

$$y_M(n) = \sum_{i=1}^{N} a_i^M.u(n-i) \tag{2.41}$$

If the step function is the base function at a unique coincidence point H, the equation (2.41) can be split:

$$y_M(n+H) = \underbrace{u(n).\sum_{i=1}^{H} a_i^M}_{Future} + \underbrace{\sum_{i=H+1}^{N} a_i^M.u(n-i+H)}_{Past} \tag{2.42}$$

Using the reference trajectory defined in (2.36) we obtain the control signal $u(n)$:

$$u(n) = \frac{(C(n) - y_p(n)).\left(1-\lambda^H\right) - A_H^T.U(n) + A^T.U(n)}{\sum_{i=1}^{H} a_i^M} \tag{2.43}$$

with

$$A_H^T = \left\{a_{H+1}^M, ..., a_N^M\right\}$$

$$A^T = \left\{a_1^M, ..., a_N^M\right\}$$

$$U^T(n) = \{u(n-1), u(n-2), ..., u(n-N+H)\} \tag{2.44}$$

RST Controller

The RST controller representation is extremely useful for PLC implementation due to its simple structure [29]. The polynomial approach in q overcomes the usual inconvenience introduced by the sampling time (Fig. 2.12).

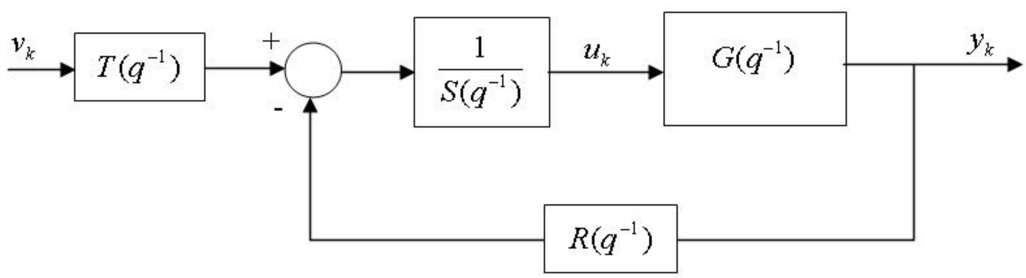

Figure 2.12: The RST controller.

The RST controller is driven by the following equation:

$$S(q^{-1}).u_k = T(q^{-1}).\nu_k - R(q^{-1}).y_k \tag{2.45}$$

The RST controller is often used to calculate robust closed loop response by pole placement. The structured control signal introduced by the RST representation is done so that any controller can be represented through the RST formalized schema.
As an example, the RST representation of the GPC can be found; from equation (2.34) we can see that:

$$\Delta u_{opt}(t)\left[1 + m_1^T.ih(q^{-1}).q^{-1}\right] = m_1^T.\left[q^{N_1}...q^{N_2}\right]^T w(t) - m_1^T.if(q^{-1}).y(t) \tag{2.46}$$

So by identification with (2.45) we obtain the RST form of the GPC controller:

$$\begin{cases} S(q^{-1}) = \Delta.\left[1 + m_1^T.ih(q^{-1}).q^{-1}\right] \\ R(q^{-1}) = m_1^T.if(q^{-1}) \\ T(q) = m_1^T.\left[\begin{array}{ccc} q^{N_1} & ... & q^{N_2} \end{array}\right] \end{cases} \tag{2.47}$$

2.1.5 The "*Advanced Automation Tool Kit*"

The model identification and the validation processes are usually offline workarounds [17, 30, 31]. Matlab/Simulink® from Mathworks [32] company is one of the best simulation tools to accomplish theses tasks. However the online approach is not supported.
The principle of the "*Advanced Automation Tool Kit*" consists on making the online identification and modeling processes trough a PLC environment. By an object oriented development the user is able to determinate the basics tasks needed for the model identification and its validation.

The model identification for Schneider PLC objects

In this section the main points of the identification algorithms implemented for the Schneider PLC objects are highlighted.

The input sequence for the data acquisition Clearly the Maximum Length Sequence is the ideal input signal for the process identification. However, the sequence of three steps is most of the time sufficient to identify the dynamic behaviour of the system. Following this assumption the "*Advanced Automation Tool Kit*" provides an object build in the ST language for Schneider PLCs. It produces a three step sequence signal with determinate time scales (Fig. 2.13).

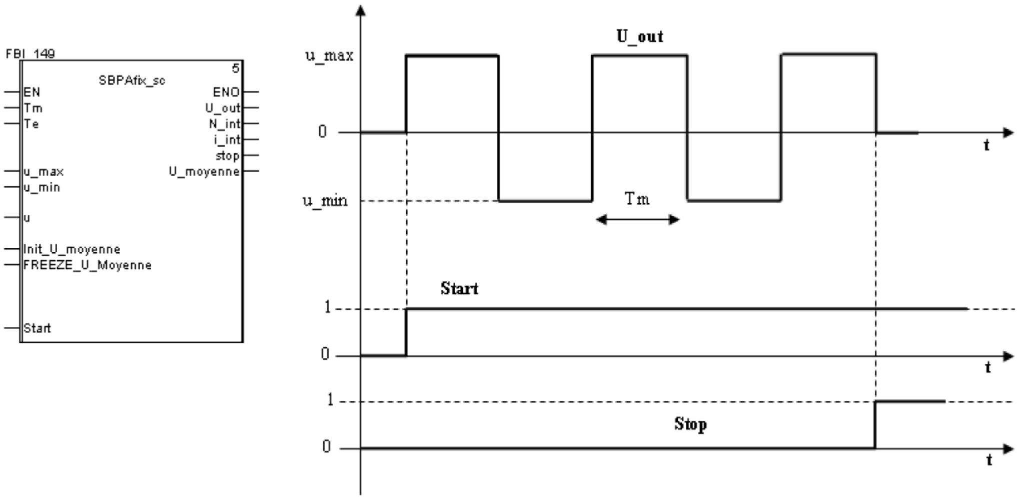

Figure 2.13: A three step sequence signal for Schneider PLC object.

The Recursive Last Square (RLS) method The RLS method is based on the linear regression [17]. This principle in automation is especially built for the estimation of ARMA system parameters plants as shown in 2.1.2

The Schneider "MCR_sc" object implements the RLS identification method (Fig. 2.14).

The Recursive Extended Last Square (RELS) method The RELS method uses the last square criteria from RLS method but adapted for ARMAX plants [17] as shown in 2.1.2.

The online identification for the RELS method in the Schneider "MCE_sc" object implements available through (Fig. 2.14).

Recursive Maximum likelihood (RML) method The RML is shown in 2.1.2. The Schneider "MVR_sc" object implements the online identification for the RML method (Fig. 2.14).

The model validation Schneider PLC objects

During the modeling phase the process is validated before any further corrections. In this objective, the "*Advanced Automation Tool Kit*" provides three objects which helps user to choose the correct decision.

The model order validation The model order validation test proposed by the "*Advanced Automation Tool Kit*" uses the manipulation of the information matrix Q_m and Q'_m defined below [33]:

$$Q_m = \frac{1}{N}\sum_{k=1}^{N}\begin{bmatrix} u(k) \\ u(k+1) \\ u(k-1) \\ u(k+2) \\ .. \\ u(k-m+1) \\ u(k+m) \end{bmatrix}\begin{bmatrix} y(k+1) & u(k+1) & .. & y(k+m) & u(k+m) \end{bmatrix}$$

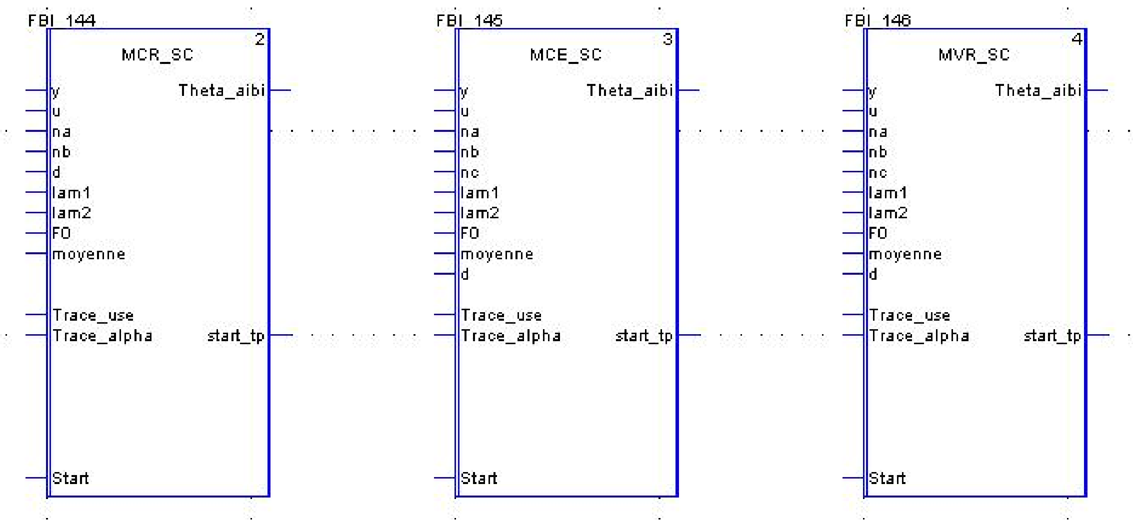

Figure 2.14: Online identification methods under Schneider PLC object.

$$Q'_m = \frac{1}{N}\sum_{k=1}^{N}\begin{bmatrix} u(k) \\ u(k+1) \\ u(k-1) \\ u(k+2) \\ .. \\ .. \\ u(k-m+1) \end{bmatrix}\begin{bmatrix} y(k+1) & u(k+1) & .. & .. & y(k+m) \end{bmatrix} \tag{2.48}$$

The method consists on building the determinant and doing the following calculus:

$$RDI(m) = \left|\frac{\det(Q_m)}{\det(Q_{m+1})}\right| \quad RI(m) = \left|\frac{\det(Q'_{m+1})}{\det(Q_m)}\right| \tag{2.49}$$

The system order n is found when RDI increases and when RI decreases (significantly for both).

The Schneider "RDI_sc" performs this test. It is implemented up to the third order. This limitation is due to the PLC software which is sufficient for most industrial systems (Fig. 2.15).

The whiteness test The "*Advanced Automation Tool Kit*" provides the possibility to simulate a model by using an object named "SimuSysteme_sc". This PLC object is able to simulate ARMA and ARMAX systems (see Fig. 2.14).

2.1.6 Advanced Control Implementation in PLC

The PLC programming concept is a cyclic execution process. The diversity of process control applications have also led to the introduction of the multi program cyclic principle for PLCs by means of four standard languages available through the IEC61131-3 norm [34]: the Instruction List (IL), the Structured Text (ST), the Ladder Diagram (LD) and the Functional Block Diagram (FBD). The IEC61131-3 norm proposes sharing the use of a program unit defined in one language by any of the others.

The advanced control algorithm implementation is not restricted by any of the four standard languages provided for PLCs. However the object programming development should take into account the cyclic nature of the PLC execution.

The advanced control algorithms are set up by using the cyclic execution as a sampling time reference. The algorithms are then developed with emphasis on the sampling aspect commonly defined in the automation processes. The use of the ST language is a good compromise to deal with complex implementations such as loops and recursive mechanisms.

As a practical example the recursive first order system (without dead-time) implementation in ST language is written as follow:

```
Te_in_Real := TIME_TO_REAL(Te_system);
TETA_in_Real := TIME_TO_REAL(TETA_POSR);
Ap := EXP_REAL((-Te_in_real)/(TETA_in_real));
Bp := 1.0 - Ap;
Output_FOWDT := (Ap*Output_FOWDT) + (Bp*GAIN_POSR*Input_FOWDT);
```

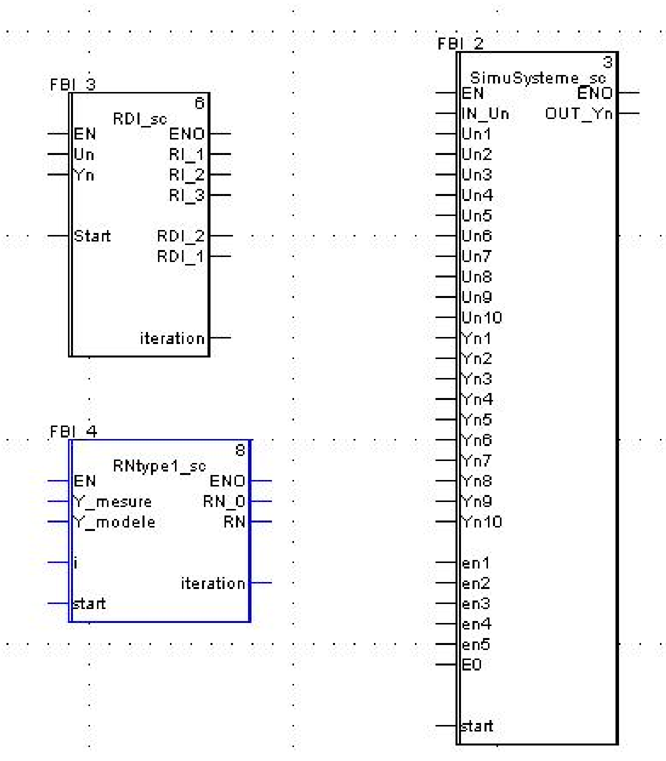

Figure 2.15: Model validation methods under Schneider PLC object.

While using the ST language for implementation, the FBD language is optimal for testing. By synchronizing the object to a pre-determined fixed sampling time, the process is able to work with sampling behaviour in such a way that it satisfies the discrete implementation of the internal advanced algorithm implementations. The FBD language is a powerful validation test environment for the object integration phase. It allows online visualization of the pertinent variables and parameters (see the example Fig. 2.16).

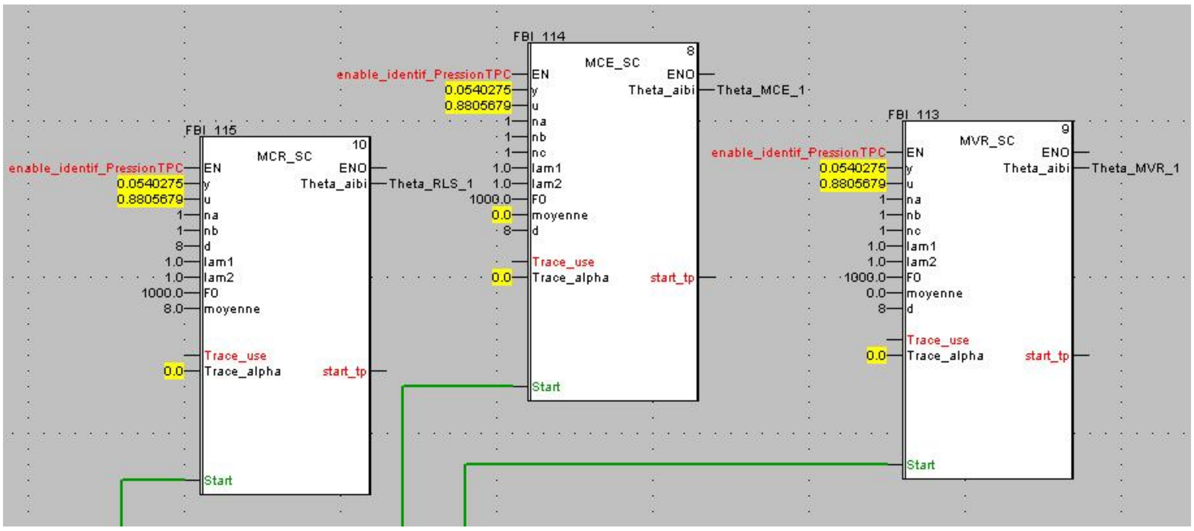

Figure 2.16: Online identification with Schneider DFB's of the *Advanced Automation Tool Kit*.

2.1.7 Experimental Results

Online identification with the "*Advanced Automation Tool Kit*"

Tests have been done for a pressure regulation system so that it is an unstable system of order one with time delay of four seconds. The model to be found has the expression (ARMAX):

$$y(t+1)_{Model} = -a_1 y(t) + b_1 u(t-8) + e(t+1) + c_1 e(t)|_{T_e=0.5s} \tag{2.50}$$

The process identification is done trough two different experimental protocols:

- Under Matlab with the classical RELS and RLM algorithms (offline treatment)

- Under the Schneider PLC environment (online treatment)

We obtain the following models:

$$
\begin{aligned}
y(t+1)_{Matlab\_RELS} &= 0.9999y(t) + 0.0005476u(t-8) + e(t+1) - 0.2411e(t) \\
y(t+1)_{Matlab\_RLM} &= 0.9476y(t) + 0.0005676u(t-8) + e(t+1) - 0.0656e(t) \\
y(t+1)_{PLC\_RELS} &= 1.00031y(t) + 0.000567u(t-8) + e(t+1) - 0.256e(t) \\
y(t+1)_{PLC\_RLM} &= 0.95448y(t) + 0.00066u(t-8) + e(t+1) - 0.063e(t) \qquad (2.51)
\end{aligned}
$$

The PLC results highlight the power of the online identification introduced by the "*Advanced Automation Tool Kit*". The equations (2.51) show the similar results between Matlab algorithms and Schneider objects. In addition the estimated evolution of the model parameters (Fig. 2.17 to 2.20) follows the same behaviour so that this experimental identification expresses clearly the validity of the PLC objects for the model identification.

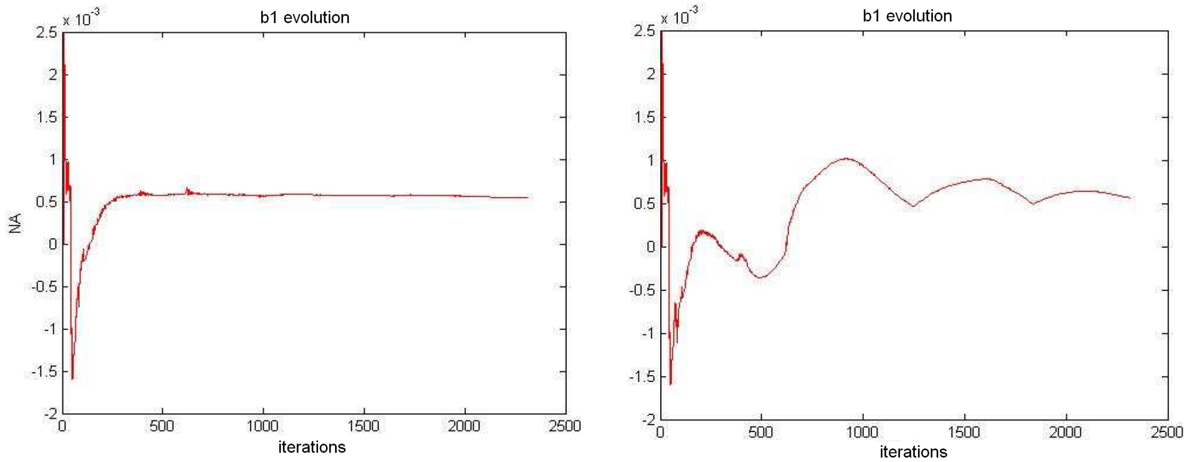

Figure 2.17: b_1 estimation along the Matlab identification process for RELS and RLM methods.

MultiController application to a second order with dead time

The first object implementation of the *MultiController* into a Schneider PLC solution (Unity) has produced valuable results. The *MultiController* has introduced advanced

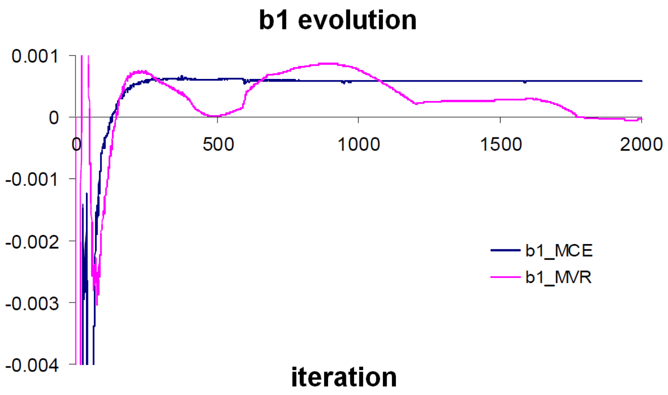

Figure 2.18: b_1 estimation along the PLC identification process for RELS and RLM methods.

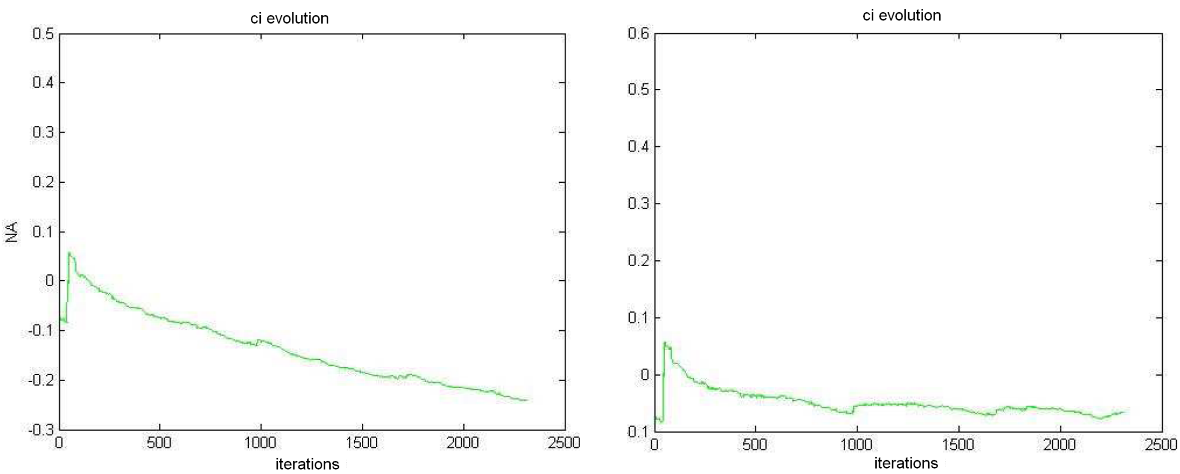

Figure 2.19: c_1 estimation along the Matlab identification process for RELS and RLM methods.

control algorithms for the large scale *UNICOS* framework project. It offers to experimental plants a way to use new controllers.

The system is represented by this model:

$$G(z) = \frac{0.1269z^{-1} + 0.09614z^{-2}}{1 - 1.323z^{-1} + 0.4346z^{-2}} . z^{-3} \Big|_{T_e=1s} \quad (2.52)$$

Here are the settings of the *MultiController* algorithms:

PID	***Smith Predictor***	***PFC***	***GPC***
K=0.26	T=4.25s	TS=1s, H=1	N1=4
Ti=3.25s	G=2	TRBF=5s	N2=20
	Delay=3s	Km=2	Nu=1
		Tm=4.25	Lambda=0
		Delay=3s	Te=1s

Fig.s 2.21 and 2.22 show the process output signal and the control signal in a system driven by (2.52) with several control algorithms given by the *MultiController* object.

This application clearly shows the possibilities of the *MultiController*. The PID controller introduced an overshoot. On the contrary, the Smith Predictor and the PFC controller are

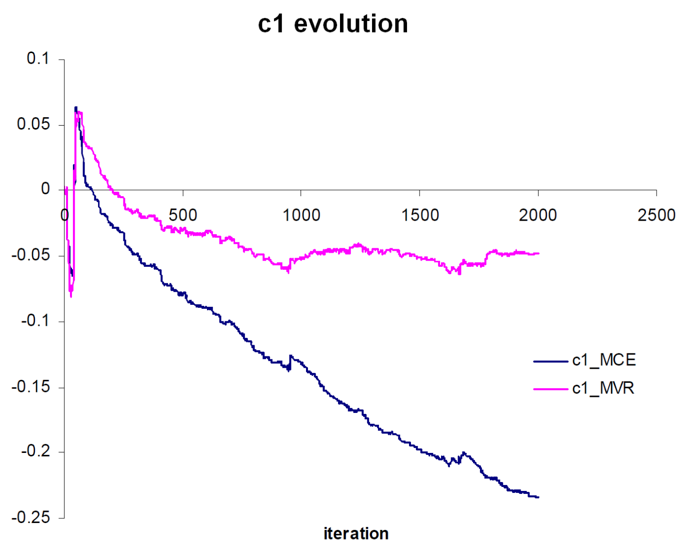

Figure 2.20: c_1 estimation along the PLC identification process for RELS and RLM methods.

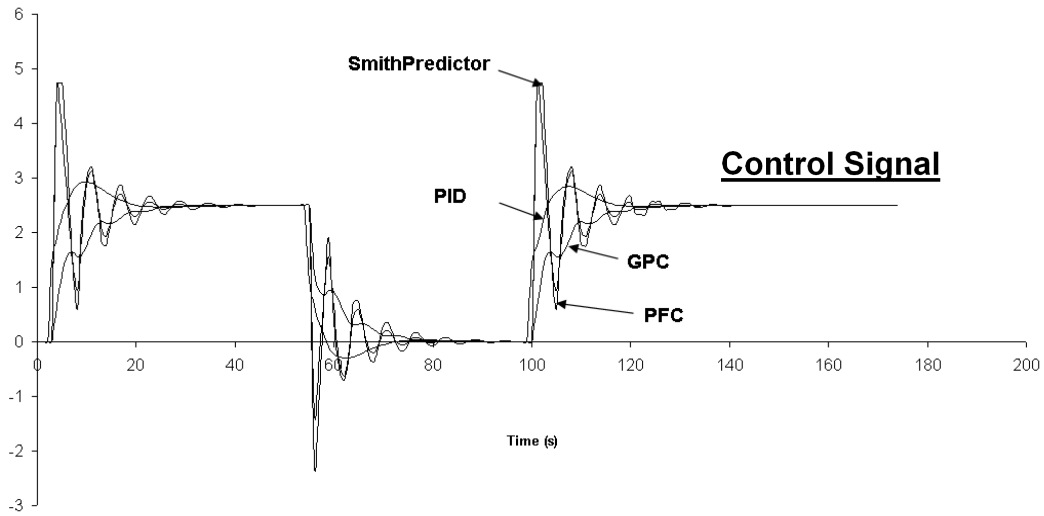

Figure 2.21: *MultiController* application - control signal.

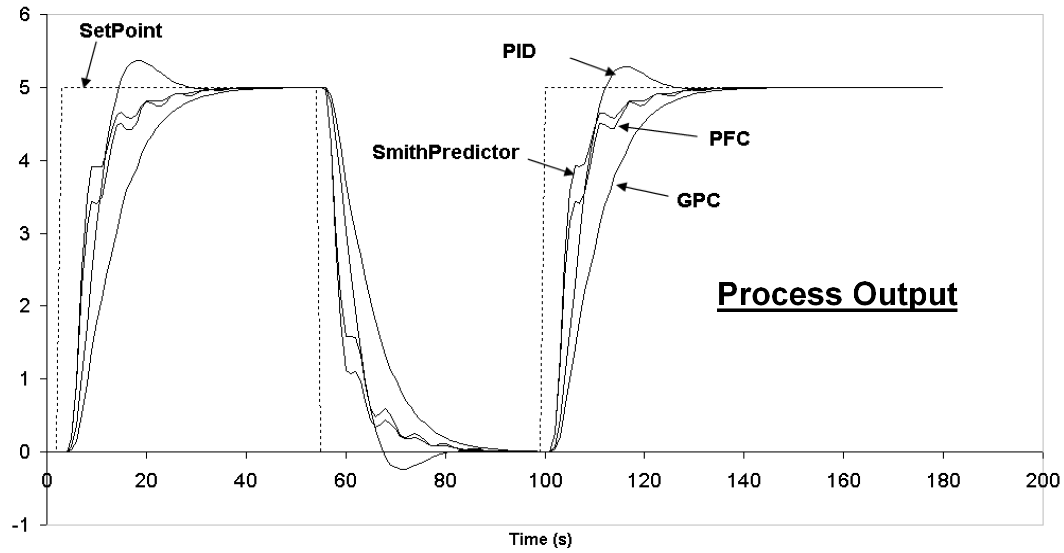

Figure 2.22: *MultiController* application - process output.

both well adapted for speed process output response without the PID inconvenience. The control signals of those solutions do not converge gently but can be acceptable in some circumstances. Finally, the GPC controller produces a smooth process output response.

2.1.8 Discussion

The *MultiController* object of the *UNICOS* framework is the combination of an efficient object programming process and advanced control features. By its robust design, this object is able to capture tuning parameters of all control algorithms through a single custom HMI.

The PLC object implementation follows the IEC61131-3 norm by means of coding the advanced algorithm in ST language. It also takes into account the cyclic nature of a PLC execution process through the program.

The "*Advanced Automation Tool Kit*" is a set of advanced control features developed in addition to the *MultiController* object. It allows the use of a PLC environment to do online identification and online validation steps. This work demonstrated the validity of the package proposed for Schneider PLC's under the Unity software.

The *MultiController* object implementation gives alternative solutions to standard PID controllers and increases the available control solutions to solve non-negligible complex problems. The Smith Predictor solution is able to solve dead time problems. The RST controller can be used to obtain robust closed loop responses. The *MultiController* also shows the powerful use of predictive algorithms for control loop system under PLC.

The advanced algorithms proposed by the *MultiController* object provide control loop solutions that enable the process control engineer to have access to more expert automation tools in a PLC-*SCADA* based environment.

2.2 Identification and PID optimization in ATLAS Nitrogen heat exchanger

UNICOS is the CERN object-based control standard for the cryogenics of the LHC and its experiments. It includes a variety of embedded functions, dedicated specifically to cryogenic processes. To enlarge the capabilities of the standard, in this Section it is proposed to integrate the parametric identification step in the control system of large scale cryogenic plants. Different methods of parametrical identification are reviewed and tested, and the results are combined with the main purpose of finding a good compromise between ease of use and performance of the solution for model identification. The study focuses on identification protocol for large delayed system, the measurement consistency and correlation between different inputs and outputs. Finally, a Smith predictor-based control architecture employing the identified internal model is proposed to cope with the large delays of the system.

2.2.1 Introduction

The CERN *UNICOS* framework is currently the standard used in the ATLAS experiment. In this standard the current object used for control loops is a PI controller (no derivative term), this is a not mere coincidence , in the cryogenic "industry", operators are apprehensive about derivative action and its response to noise, especially when the actuators involved are valves. This *UNICOS* controller is suitable most of the time for cryogenics process and they are optimized by the operation team with "try & error" methodology. This astonishing fact is common for industrial control engineers which do not use any identification guideline, although an urgent need for efficient and effective identification methods in process control industry is required. A possible reason for this is the failure of the technology transfer of identification technology as a whole, researchers focus most of their efforts on parameter estimation and convergence analysis, while few study test design and model validation the part close to model application. Another reason could lead in identification toolboxes approach, most of the time very flexible and does not get along with practical control engineers who do not have academic training in system identification.

This part present the explicit design of the different step using the CERN/UNICOS standard control system on large scale cryogenic systems for recursive identification and optimisation method including data acquisition, filtering, modeling, uncertainty estimation and tuning methods for applied cryogenics PI controller, to enlarge the capabilities of the standard. Different approaches of parametrical identification (single and multivariable) have been experimented; a synergy between an industrial and a scientific solution has been combined. The main objective of the research is to find a compromise between an easy-to-use solution and a good level of fidelity in model's outputs for cryogenic. The study focuses on generalized identification protocol for large delayed system, the measurement consistency and on correlation between different inputs and outputs.

2.2.2 Experimental system

In the central part of the ATLAS detector is located the liquid Argon calorimeter: a barrel calorimeter and two end-cap detectors with respectively 120 t and 2x219 t cold masses. They are housed in three independent cryostats filled with 40 m^3 and 2 x 19 m^3 of liquid Argon at 88 K. The cryogenic system chosen for the tests is the central barrel calorimeter (see Fig. 2.23).

The cooling system of the cryostat relay on 7 liquid Nitrogen heat exchangers; 6 heat exchangers are positioned in circular geometry around the calorimeter immerged in the liquid Ar and 1 positioned in the gaseous volume of the expansion vessel to control the Ar saturated pressure. Heat exchangers in the Ar bath control the δT of the sub-cooled liquid to obtain the best operating point avoiding bubbles formation in the bath [35], as shown in Fig. 2.24.

The expansion vessel is located 2.8 m [7] above the calorimeter to move the operating point away from the saturation curve in fixing a ΔP, refer to the Eq. 2.53:

$$\Delta P = ((P_{sat,EV} - P_{Ar,bath})) \tag{2.53}$$

The LN_2 (Liquid Nitrogen) flows and pressures within each cooling loop are regulated by respectively inlet and outlet control valves. The LN_2 flows must always be sufficient to maintain the wet area along the entire surface of the immerged heat exchangers, in its final configuration these valves are maintained in a fixed position. Thus LN_2 saturated pressures (e.g. temperatures) provide the manipulated variables for controlling the liquid

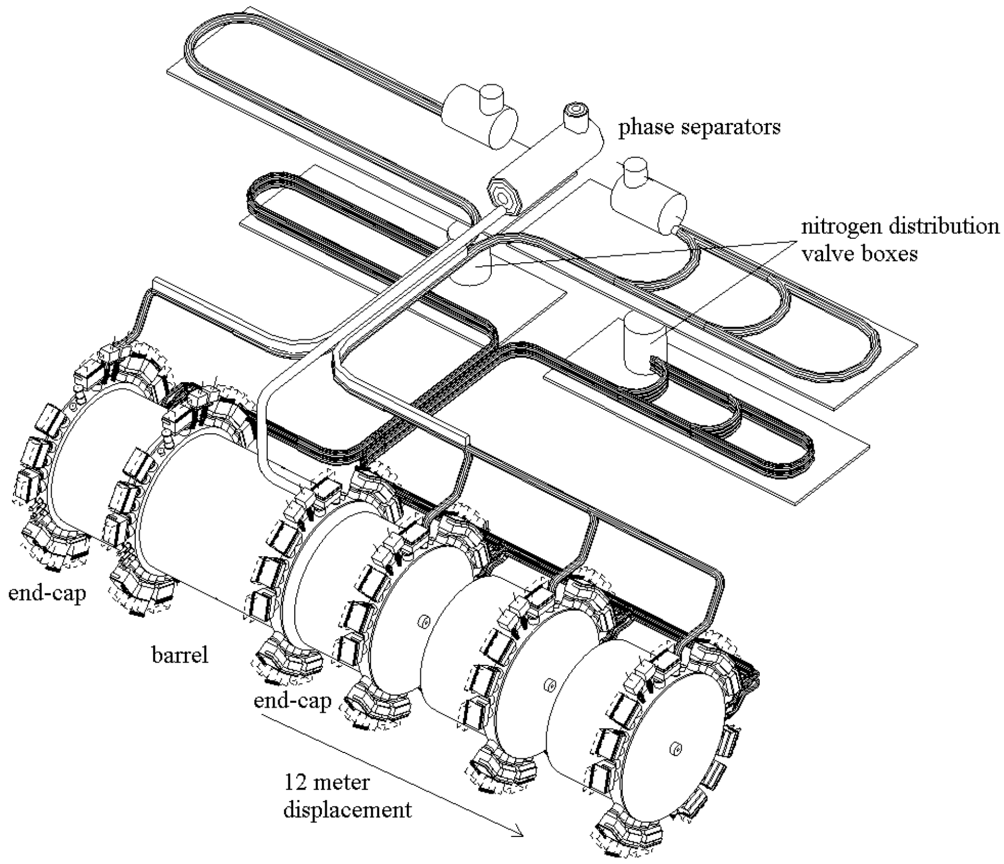

Figure 2.23: Overall view of the ATLAS cryogenic system.

Ar subcooled temperature in the cryostat. The saturated pressures within each heat exchanger needs to be optimisely controlled in order to improve the overall liquid Argon temperature stability. The set up for these tests has been carried out using the *UNICOS* based cryogenic control system in its final configuration see Fig. 2.25.

2.2.3 MIMO model identification of the barrel Ar bath temperature

The architecture system for recording data and permitting the retrieving of themselves is based on a long term data archive (ORACLE) technology [36] and with CERN based retrieving tools capable of storing several hundred signals. The cryogenic temperature sensors linked to the control system of the Ar bath in the calorimeter have shown a significant rough precision limitations. Due to this limitations we should considering of

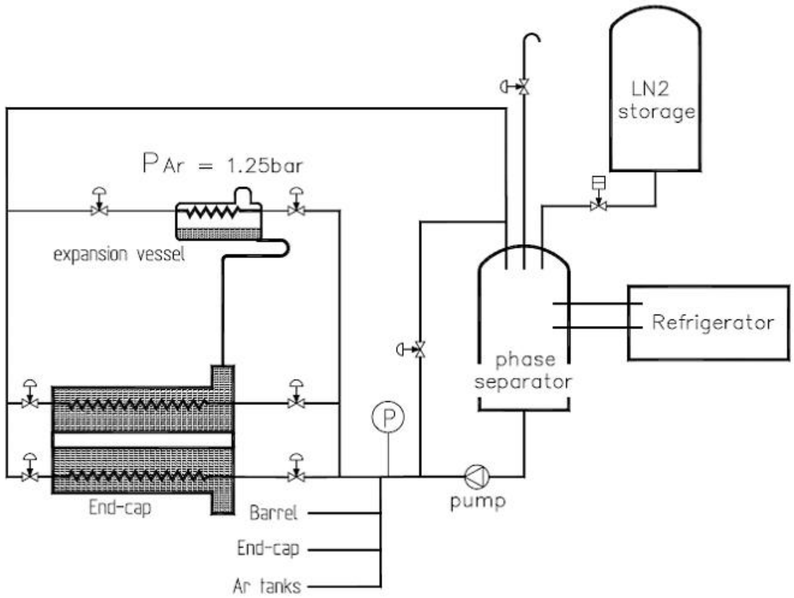

Figure 2.24: Nitrogen cooling circuit principle.

using the thermal sensors of the physic part of the ATLAS experiment, these sensors are not available for the next future. We consider having an experiment "slot" during only the next year. An accurate description of the test campaign for the multivariable identification tests will be reported in the following.

The cryogenic process can be classed [37] in a continuous process type around a stability point which uses linear time-invariant dynamic models for control. It is a large scale and complex process, it has 6 MVs (manipulated variable or input) and 10 CVs (controlled variables or output) with oscillating behaviour and time delays. Dominant slow dynamics, time ranges of several hours, dictate relative long time for identification test. Identification must respects important constraints as a duration of 10-15 times the longest response time, an operation control for security reasons, and a wide spectrum test signals.

The test protocol should include all the inputs that have to be uncorrelated between themselves and their autocorrelation should be also close to a white noise. Generally, a white noise cannot be applied on a real process due to the actuators. Hence, the stimulation input chosen is a parameterized PRBS (Pseudo Random Binary Signal) as explained in Section 3.2. An automatic function has been developed in the supervision system capable

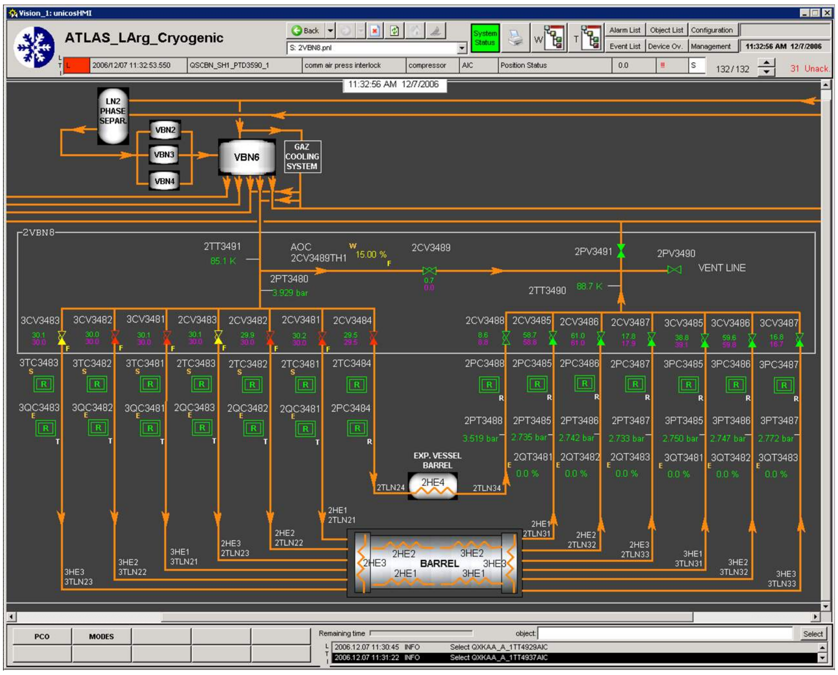

Figure 2.25: *UNICOS* synoptic of cryogenic barrel circuits.

to recreate these signals where the amplitudes and switch times are parameterized. This functionality results to be an asset for the procedure of the identification because of the dominant slow time process, the control engineer will not organize night-shift in order to follow the test protocol which could last several weeks. Moreover, this functionality is based on the *UNICOS* supervision system and his implementation will not compromise the security of the control system layer [38].

The temperatures variations of the liquid Argon calorimeter and their distributions have been simulated by a numerical estimation using LES method (Large-Eddy Simulation) [39]. Moreover, the constant time of the cryogenic system face some uncertainties. A preliminary pre-test should be performed on the system permitting the verification of the cryogenic system time constant and delay. The measuring data recording for the studies would stretch over approximately 2 weeks 24 hours per day continuously. The average switch time of all the PRBS signals are set to 120 minutes. Amplitude variation set point for LN_2 pressure was set in a range of ± 0.10 *bar* around the stability position, good enough signal-to-noise ratio and not disturbing the stability point of the cryogenic liquid inside the barrel calorimeter (Fig. 2.26). The first step after the data taking is to remove the continuous component of all signals.

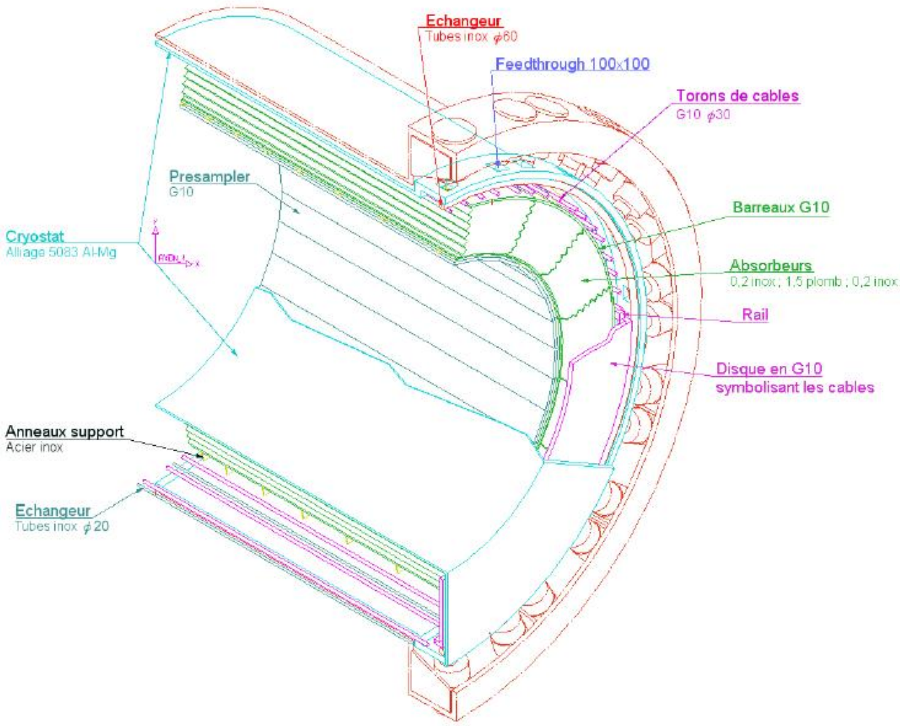

Figure 2.26: Cross section of the Barrel Calorimeter.

The multivariable process with m manipulated variables (inputs) and p controlled variables (output) will produce, during an identification test, the data sequences as shown in Section 2.1.2

So if the system to identify has a model $y = \phi \cdot \theta$, the optimal θ can be calculated with the pseudo inverse of ϕ 2.15:

$$\theta = \left[\phi^T \phi\right]^{-1} \cdot \phi^T \cdot y$$

with $[\phi^T \phi]$ invertible. After this step we should proceed in a comparison with RLS algorithm to see if parameter results change, as well as doing a comparison of results using higher order model. This algorithm takes more calculation time than the LS algorithm but it can provide better results. Then, an analysis of residues is necessary (errors between model and process). Residue values can be estimated by the calculation of the Final Predicted Error (FPE):

$$FPE = \frac{1}{N} \cdot \frac{1 + \frac{d}{N}}{1 - \frac{d}{N}} \sum_{t=1}^{N} (y(t) - y_m(t))^2 \tag{2.54}$$

where d is the number of parameters estimated and N the sample number.

At this stage, a validation of the model has to be proceed with other experimental data, with a new test campaign. If these values are consistent we can consider the identification process done, in the other case a re-identification guideline would be necessary. Although we deal most of the times with MIMO systems, in cryogenics the considered dynamics either do not influence each other significantly, or they do to an extent that is hardly assessable in a quantitative way. Therefore, the MIMO approach is often left out and replaced by a SISO technique. As in this case, a complex multidimensional problem is split into a set of decoupled monodimensional problems to be solved separately.

2.2.4 Combination of industrial and scientific solutions

In order to perform the data record and the identification of the model, we have used an industrial solution developed by Schneider for SISO system, Optireg© [40], the tuning procedure for recursive identification and optimisation method including data acquisition, filtering system, modeling, uncertainty estimation and tuning methods for applied cryogenics PI controller has been developed in a MATLAB © environment [32].

SISO model identification for Nitrogen heat exchanger of ATLAS Argon barrel calorimeter

There are two times three different types of heat exchanger, vertical, bottom horizontal and top horizontal. The tests has been performed for each type of heat exchanger using a series of command on the open loop. It aims was to analyse pressure response according to the valves positions as single-variable step in different time period, under different disturbance conditions. Tests have been done manually, expansion vessel heat exchanger in the saturated Ar gas has not taken into account in the test procedure to maintain a high level of security for the Ar bath [7] (see Fig. 1.7). Manual steps on valves have been done within their operational safety limit, and optimal signal spectrum variation. Thus, reducing disturbance effects and representing an advantage for learning and understanding the step responses of the Ar cryogenic process. The duration of each identification test per heat exchanger took 8-10 hours. The data record has been processed with a digital low-pass filter to match the desired closed-loop bandwidth. The choice of the digital low-pass filter was a compromise between the attenuation of the noise and maintaining the signal dynamics in order to use reliable data for identification [41]. Fig. 2.27 presents the different steps of the identification procedure.

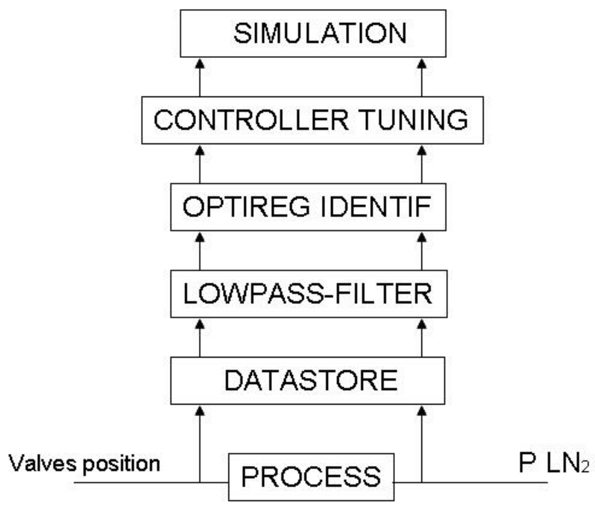

Figure 2.27: Data taking, filtering and analysis procedure.

We consider one transfer function per heat exchangers, which has its own response to its connected outlet valve, depending of several variables such as dimensions, installed measurement variables and geographical presence in the Ar bath. Regarding this assumption, we define $[H_1, H_2, H_3,..., H_6]$ and $[PI_1, PI_2,..., PI_6]$ corresponding respectively to the 6 immersed heat exchangers transfer functions and their corresponding designed controllers (see Fig. 2.28).

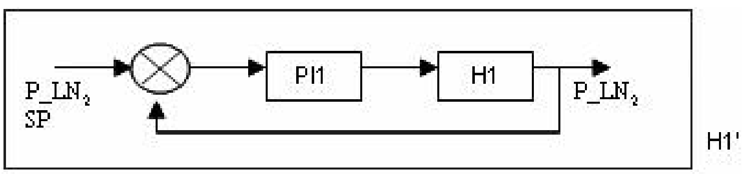

Figure 2.28: Closed loop control of liquid Nitrogen pressure.

Based on the quadratic mean errors analysis different order model has been compared to the process data. The result has shown a first order model is sufficient to represent pressure dynamics inside the heat exchanger tube. The transfer functions are characterised by a large time constant, a small gain and a constant time delay as it is shown in the Eq. (2.55) obtained using Optireg with sampling time of 30s:

$$H(z^{-1}) = \frac{-4.13 \cdot 10^{-4} \cdot z^{-1}}{1 - 0.94 \cdot z^{-1}} \cdot z^{-2} \tag{2.55}$$

Smith controller for time delay compensation based on *UNICOS* PI controller

As said in Chapter 2.1, the Smith Predictor is a PID controller adding an internal model intended to cope with larger delay. The principal aim is to provide a correction to the PID by removing the effect of delay inside the closed loop response. This type of controller can be used for first and second order (double pole) transfer function or an unstable system with delay see Fig. 2.29.

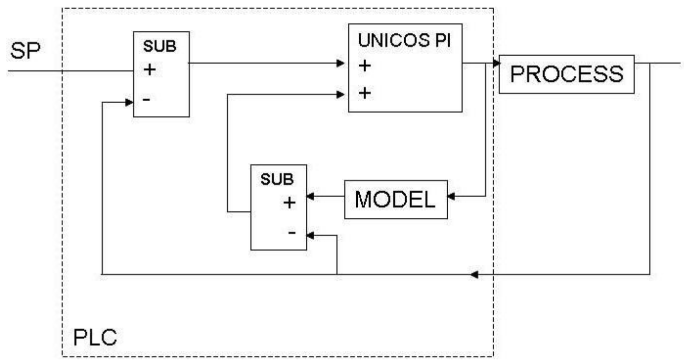

Figure 2.29: Smith predictor closed control loop.

In our work we have simulated this controller with experimental data record and have compared the results.

2.3 Results

In this Section, simulation results of parametric identification and PID optimization for a real large scale system, the ATLAS Nitrogen heat exchanger, are presented. The performance comparison encompasses three different control configurations: (*i*) a classical PI controller, (*ii*) a PI controller tuned after the identification phase without considering time delays, and (*iii*) a Smith predictor-based controller tuned to compensate the time delays.

2.3.1 Discussion on PI controller and model based Smith Predictor controller

In Fig. 2.30 dynamic responses of simulated controller model with different configurations are compared using experimental data record. On one hand the first controller, a classical PI, tuned from cryogenic operator (gain=1, $T_i = 300\ s$), the second a PI controller also but tuned after the identification process without taking into account time delay and a third controller based on Smith predictor approach [42] to compensate the time delay.

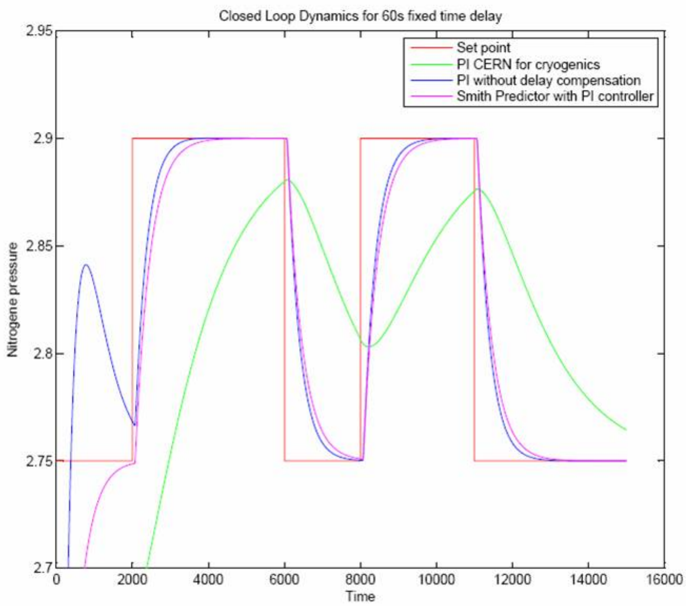

Figure 2.30: Closed loop dynamics for 60 s fixed time delay.

For a time delay less than 2 minutes the PI controller tuned to obtain a first order response of the closed loop is adapted to the process as well as the Smith Predictor controller. The installed PI controller shows a very slow response to the dynamic excitation which will be more amplified by larger time delay processes. In Fig. 2.31 a 300 seconds process time delays have been simulated.

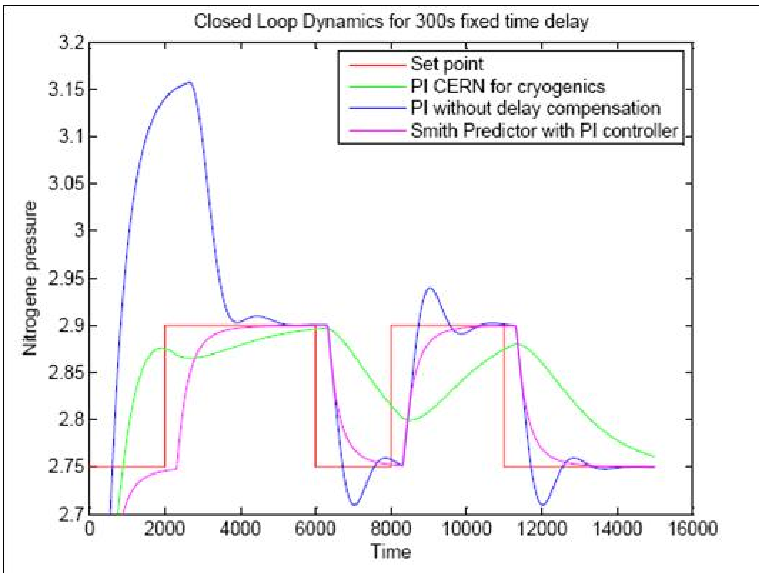

Figure 2.31: Closed loop dynamics for 300 s fixed time delay.

The typical tuning of CERN cryogenic PI, which is done for a PI by cryogenics engineer, faces time delay or inverted response problems FOR increasing the T_i coefficient. This widely spread methodology gives modest dynamic response but combined with dominant slow dynamics processes such cryogenic, the final results obtained is acceptable. The reason can be understood looking at the curve of the optimised PI controller facing a larger time delay (300 s) in Fig. 2.31, obtained in comparison to the results with a time delay of 60 s (see Fig. 2.30).

In this configuration only the Smith Predictor keep its combines precision, velocity and zero overpass, the installed PI controller stays in an acceptable region even if it is not precise and the tuned PI controller response could bring, if applied, the cryogenic system to an instability operation region.

2.3.2 HIDEN Matlab toolboxes for MIMO model identification

Based on liquid Ar temperature measurements and LN_2 pressure (MV), a multivariable identification process[43], has been studied. HIDEN toolbox [44] is a classical scientific multivariable identification toolbox from Valladolid University (Spain). In our work, the identification will create a model which relates directly the LN_2 pressures with LAr barrel cryostat temperatures. The resulting output of the optimized control of the P_{LN_2} (pressure of liquid Nitrogen) will go directly into the transfer function which links the LN_2 pressures and the overall temperature of the liquid Ar in the barrel cryostat, cf Fig. 2.32.

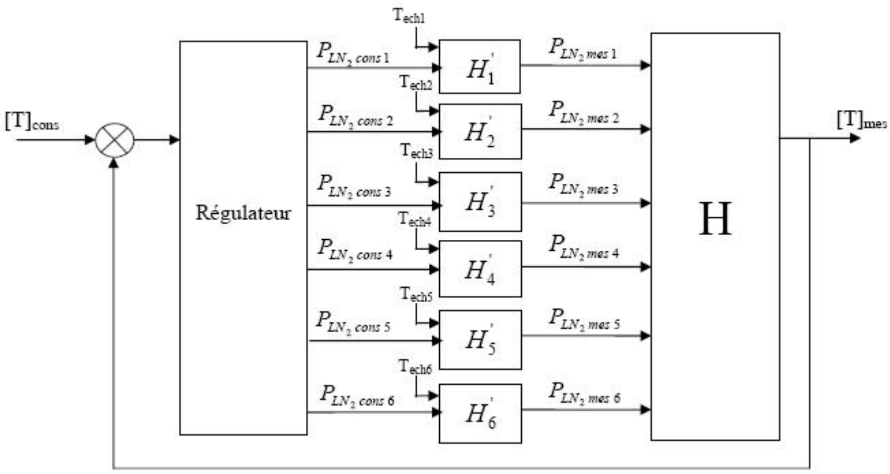

Figure 2.32: Temperature multivariable model combined with the pressure closed loop transfer function.

2.3.3 Discussion

This work presents an identification procedure applied to a large cryogenic process, using CERN/UNICOS standard. Different functionalities have been defined in a specific procedure using scientific identification toolbox (HIDEN©) and industrial tools (Optireg©) reducing application time and manpower; i.e. automated script for MV movements in the supervision system (control engineer are free from watching test continuously during identification) plus the development of an automatic interface for cryogenic PI tuning with and without delay compensation.

In SISO identification tests, the result have given us an appreciation about the type of control applied without a proper identification. The response behaviour of the typical cryogenic tuned PI controller (with large T_i coefficient) remains acceptable in dominant slow time process such as cryogenics. The comparisons between different controls have given us also the necessity to propose a new controller based on Smith predictor model in order to ameliorate the control of the individual Nitrogen saturated pressure in the heat exchanger. In MIMO identification a specific identification procedure has been established and it is planned in future (when ATLAS-DCS and their very accurate temperature sensor operational) to proceed with a multivariable identification applied to the barrel Argon bath.

The multivariable identification of the system will be the base for future scientific studies in advanced controlled field in order to obtain a high efficient advanced controller for the Argon bath temperature stability. Other methods such as multiple model approach [45] for multiple controller design [46][47][48], state estimation [49][50] or diagnosis [48][51] are not considered in this manuscript.

Chapter 3

Physical model of advanced controls for cryogenics

3.1 Introduction to the NA62 system and its renewal

The NA62 experiment carried out at CERN was already introduced in Section 1.2.5. This Section provides insight into the experiment aims and requirements, along with the problems to be faced by the related cryogenic applications. Furthermore, it provides the reader with much wider information on the modeling effort carried out as a preliminary step for the control of the cryogenic system. The components of the process under control are: (*i*) a Krypton condenser based on an Argon bath, and (*ii*) a liquid Nitrogen two phase heat exchanger. In the following a detailed physical description of the system is given.

3.1.1 Introduction

The NA62 experiment (Fig. 3.1) is a continuation of the NA48 experiment, which was designed at CERN to measure the direct CP violation in the K^0-$\bar{K}^0$ system (Neutral Kaon and Antikaon). Part of the experiment is an electromagnetic calorimeter filled with 9000 liters of liquid Krypton. For 10 years, the cryogenic system has operated under good conditions, controlled by Siemens S5 PLC. Recently, a new proposal in the use of the NA48 detectors, has implied to consider an upgrade needs of the cryogenics control system. Moreover, CERN faces technical support problems, due to the laboratory lack of expertise and changes on actual control algorithms are risky. Consequently, the research collaboration plans to replace the cryogenics control system by CERN standardized interface and object-oriented programming. The complexity of the system evolution procedure comes mainly from short time period available to operate the change without neither stopping, nor disturbing the cryogenic cooling process. To avoid commissioning problem, it implied to simulate part of the system behaviour to validate control loops efficiency.

Figure 3.1: The Liquid Krypton cryostat overview.

3.1.2 Process Description

The purpose of the cryogenic system is to provide stable thermal conditions (120 K) in the liquid Krypton when the calorimeter is in operation, and to ensure safe and loss-free storage of the liquid during long idle periods [52]. Direct cooling of the Krypton with liquid Nitrogen is only used in emergency cases because it makes the precise temperature control difficult due to the large temperature difference between the two liquids. To overcome this problem, a Krypton condenser using liquid Argon as intermediate coolant, has been installed. It forms a separate unit outside the cryostat to re-liquefy the gas evaporating from the calorimeter. The cold surface, around 3 m^2, is made of 230 vertical pipes, which tops are connected to the Argon reservoir. The evaporated Krypton gas (around 450 L/min of gas under a static heat input of approximatively 3.3 kW, equivalent to 0.64 L/min of liquid) is brought in thermal contact with the heat exchanger cooled from the bath of saturated liquid Argon at 10 bar (117 K), slightly above the triple point of Krypton [53].

During data taking, the Krypton pressure needs to be regulated to a value of (1.05 ± 0.01) bar. The Argon is cooled by liquid Nitrogen flowing through a heat exchanger in the gas space of the vessel. The Nitrogen flow is controlled by the inlet valve such as to maintain the Argon bath pressure constant to tend to a stable equilibrium point under a constant heat input. To compensate varying dynamic heat loads, the Argon pressure needs to be part of the global approach in the modeling process. The outlet valve of the Nitrogen heat exchanger regulates the inner pressure. A schematic of the Krypton condenser is shown Fig. 3.2. In order to improve the efficiency of the cryogenic fluids and their control, in the following the modeling steps to prepare control loops validity are developed, and the integration in the new control architecture is proposed. A parallel station exchanging data with the PLC is used for state observation, with the aim of estimating several parameters related to the liquid Nitrogen heat exchanger and of optimizing Krypton condensation and Nitrogen evaporation through a suitable model of the component.

3.2 Dynamic condenser model

Several condenser models have been proposed, but most of them are not developed in a control perspective. The purpose of this Section is to obtain a first principle model from balance equations, i.e. low order model of a Krypton condenser in terms of ordinary differential equations (ODE) which represent the heat transfer between the cryogenic fluids. Due to the large variations of some thermal coefficients close to the saturation, it

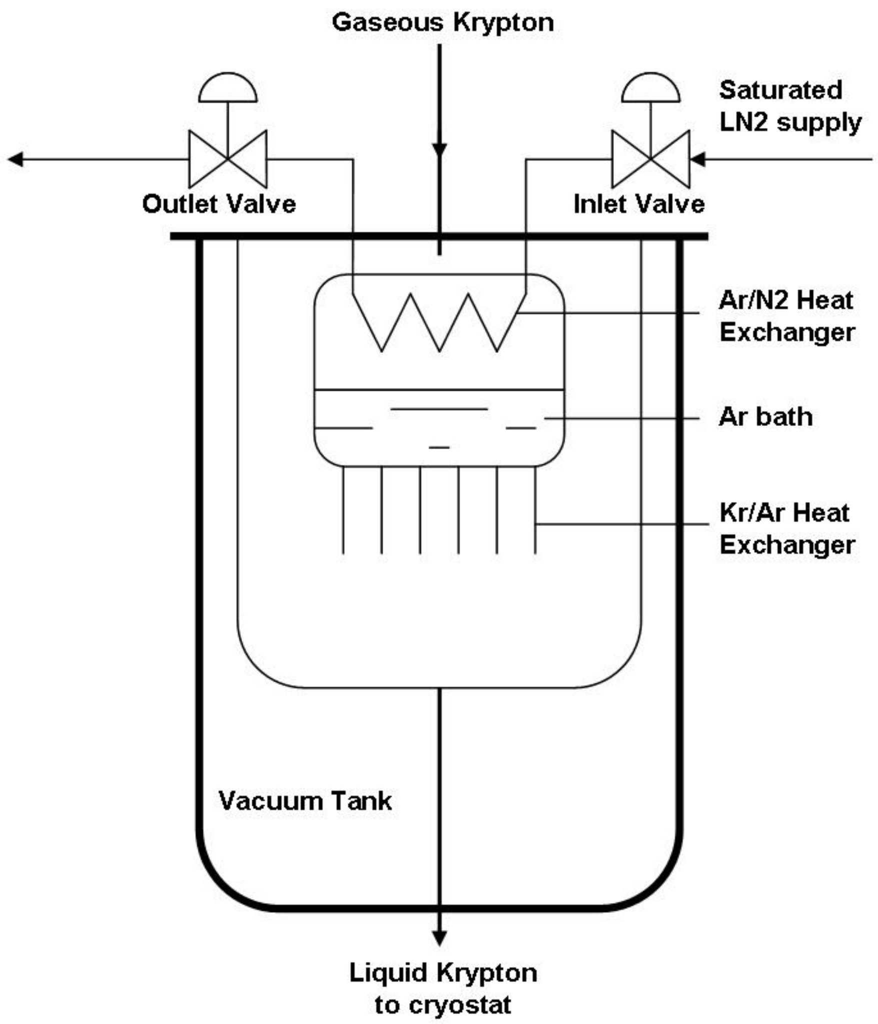

Figure 3.2: The Liquid Krypton condenser.

is sometimes necessary to take them into account, but not as a time derivative variable. Consequently, their values have to be determined by means of a "cryogenic fluid library" which contains the interesting parameters for Krypton, Argon and Nitrogen. Considering the changes in Argon and Krypton as isochoric (constant density), vapor quality is directly related to saturated temperature. In the following, we do not include neither the pressure drop in the heat exchanger, nor the losses in the Argon cooler, i.e. we consider the vacuum isolation as perfect.

To face the limitations of the PI controller currently employed, a state space model with unknown terms, integrating thermal coefficients data, is used to show the improvement possibilities in terms of thermal stability through a Time Delay Control approach, integrating a state observer in the control architecture.

3.2.1 Heat transfer coefficients estimation

One of the main problem is to find an approximation for the heat transfer coefficients between fluids. Several researches on this coefficient have been proposed for microfin tubes such as L. Dorretti et al. [54], and Kandlikar and Raykoff [55]. For the following determination, we will consider two heat transfer areas: 1) area between Argon and Krypton, 2) area between Argon and Nitrogen.

On the one hand of the first area, the "heating surface" is immersed in liquid Argon. Regarding the phase change of Argon, and the similarity with natural convection, "Pool boiling" phenomenon occurs. Several surveys for cryogenic applications on boiling heat transfer have been presented in [56]. Pool boiling curve is given in [57] where the heat transfer coefficient is a function of temperature difference between the heating surface and the saturated temperature of the boiling liquid. High nonlinearities in this function can be reduced to 4 linear regions determining the boiling regime.

On the other hand, Krypton condensation appears. The correlation of the condensation heat transfer coefficient was developed by Nusselt in 1916, as shown in [57], as a function of the Nusselt number, the length of the tubes and the liquid thermal conductivity.

In the second area, the Nitrogen mass flow and the evaporation process inside the heat exchanger tube induce a “forced convection boiling”, and outside the heat exchanger, an Argon condensation occurs. In our approach, the heat transfer coefficients between Argon and Krypton, and between Argon and Nitrogen, are defined as global exchange coefficients H_1, and H_2 as shown in Eq. (3.1), where L is the heat exchanger length, λ the thermal conductivity of the solid interface, R_i and R_e are respectively the internal and external radii, and h_i and h_e the internal and external heat transfer coefficients.

$$\frac{1}{H_2} = \frac{1}{2\pi \cdot L}\left[\frac{1}{h_i \cdot R_i} + \frac{\ln \frac{R_e}{R_i}}{\lambda} + \frac{1}{h_e \cdot R_e}\right] \tag{3.1}$$

Consequently, for the H_1 correlation, h_i represents the Argon boiling heat transfer coefficient and h_e the Krypton condensation heat transfer coefficient. h_i and h_e for H_1 and H_2 are determined from [57, 58, 59]. If the exchange area has not the same surface on both side, typically in our case between Argon and Krypton, we report H to the “hot side”, noted H_h, and to the “cold side”, noted H_c.

3.2.2 Balances equations

Models for pressure vessels of different levels of complexity using thermal modeling approaches have been developed by S. Estrada-Flores in [60]. Rigorous thermodynamic approach, where the transitions between states for liquid and vapor zones are detailed, is confronted with less complex models. In control engineering, modeling is used to improve the control system ability to follow the given set points. In two-phase fluids systems, the interactions between gas and liquid are causing non linear behaviour and might easily bring the system outside the validity envelope of a linearized model. Low order models for two-phase fluids systems are not so implicit and require some assumptions. E. Skogestad et al. [61] observed the macro-scale behaviour rather than the detailed physics that governs flow to easily use their model in a control perspective, such as G. Nygaard and G. N[62] who focused on pressure and mass balances to design their model of two-phase flow for an oil well drilling.

The governing choice in our model equation must be the degree of precision we aim. We consider the exchanges between fluids following the Newton empirical law with global heat transfer coefficient, which represents vaporization on one side, condensation on the other side, and thermal conduction of the interface. We assume that axial heat conduction in liquid Nitrogen and heat conduction in Argon between fluid layers are negligible and liquid and gas temperature for each fluid are the same. The two main variables in saturated fluids are temperature and quality. We can easily correlate them with their respective pressure. We will reduce our model to the temperatures control $[T_{Kr}, T_{Ar}]$ using mass variation. In our first modeling approach, the manipulated variable is only Nitrogen mass flow.

First, we consider “Argon system” through vapor mass balance equation detailed in Eq. (3.2), where $M_{g,Ar}$ is Argon vapor mass.

$$\frac{\mathrm{dM_{g,Ar}}}{\mathrm{dt}} = \frac{q_{1c}}{h_{lg,Ar}} - \frac{q_2}{h_{lg,Ar}} \tag{3.2}$$

$q_{1c}/h_{lg,Ar}$ represents the rate of liquid Argon evaporating into vapor and $q_2/h_{lg,Ar}$ the rate of gaseous Argon liquefying. $h_{lg,Ar} = h_{g,Ar} - h_{l,Ar}$ introduces h_l and h_g, respectively Argon saturated liquid and vapor enthalpies. From Eq. (3.2), we can substitute Argon vapor mass variations by respective volume and density. Argon vapor volume is much larger than liquid volume and considered as almost constant.

$$V_{Ar}\frac{d\rho_{g,Ar}\left(T_{Ar}\right)}{dT_{Ar}}\frac{dT_{Ar}}{dt} = \frac{q_{1c}}{h_{lg,Ar}} - \frac{q_2}{h_{lg,Ar}} \tag{3.3}$$

$\rho_{g,Ar}$ is the Argon saturated vapor density in a function of the evaporating temperature T_{Ar}. According to small root mean squared error, curve fitting tools provide by regression a second order polynomial expression of density in a function of Argon saturated temperature. We observe that first derivative vary from 2.04 to 3.86 $kg \cdot m^{-3} \cdot K^{-1}$ between 110 K and 124 K, and cannot be assimilated to a constant. We introduce k_1 as described in Eq. (3.4).

$$k_1 = V_{Ar}\frac{d\rho_{Ar,g}\left(T_{Ar}\right)}{dT_{Ar}} \tag{3.4}$$

Assuming Nitrogen temperature is constant between inlet and outlet valves, we describe the heat transferred from Argon to Nitrogen as the percentage of Nitrogen mass flow evaporated along the heat exchanger tube. Nitrogen saturated pressure inside the heat exchanger is controlled by the outlet valve and modifies Nitrogen latent heat of vaporization, as shown in Fig 3.3. As a result, Nitrogen pressure can change Argon condensation

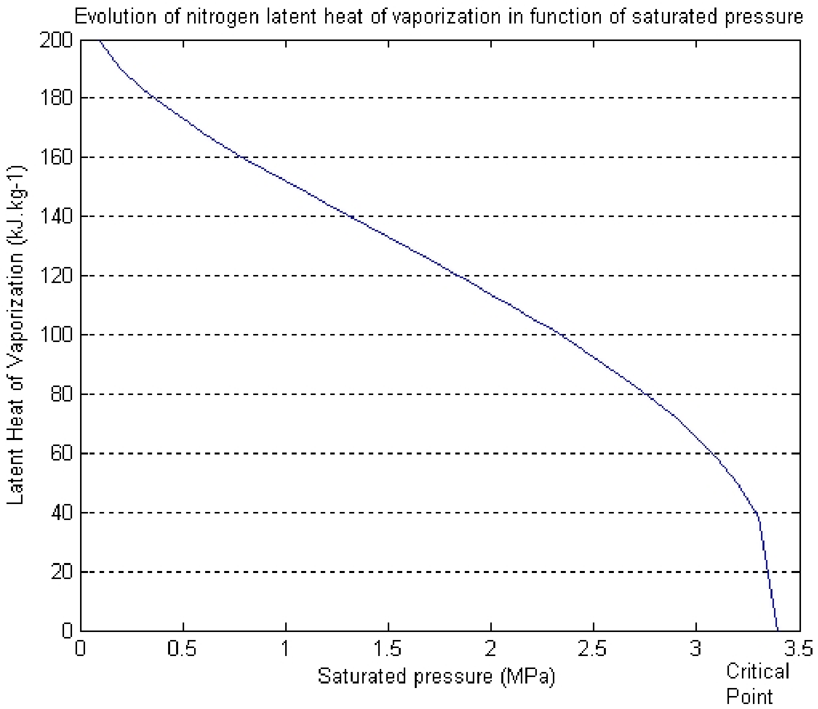

Figure 3.3: Nitrogen latent heat of vaporization in a function of respective saturated pressure.

velocity, in extracting more or less heat, and so, system velocity. In our first model, we do not include Nitrogen pressure control. Parallel studies and identification on pressure control inside heat exchanger have converged to first order model, well regulated by its own PI controller.

Based on the same development done previously for Argon system, Krypton saturated temperature variation is written in Eq. (3.5).

$$\frac{dT_{Kr}}{dt} = \frac{q}{k_2 \cdot h_{lg,Kr}} - \frac{q_{1h}}{k_2 \cdot h_{lg,Kr}} \tag{3.5}$$

q introduces heat inputs in the calorimeter we can divide into two terms: the static heat inputs q_s, which are approximately 3.3 kW, and the dynamic heat inputs q_d. $q/h_{lg,Kr}$ can be related to Krypton vaporization per time unit. Dynamic heat inputs are not directly measurable and difficult to estimate, but need to be compensated.

3.2.3 Modeling

q_{1c} and q_{1h} in Eq. (3.3) and Eq. (3.5) can be written following empirical newtonian law as function of global heat transfer coefficient, exchange surface and temperature difference, both reported to the cold and hot surface. Based on this equations, the state space representation for the condenser model is given below in Eq. (3.6), where $\dot{m}_{l,N_2}$ is liquid Nitrogen mass flow and the input to the system, and x_{vap} the percentage of liquid Nitrogen evaporating inside the heat exchanger tube. We assume Nitrogen quality at the input is close to 0%.

$$\begin{bmatrix} \dot{T}_{Kr} \\ \\ \dot{T}_{Ar} \end{bmatrix} = \begin{bmatrix} \frac{q_s + q_d}{k_2 \cdot h_{lg,Kr}} - \frac{q_{1h}}{k_2 \cdot h_{lg,Kr}} \\ \\ \frac{q_{1c}}{k_1 \cdot h_{lg,Ar}} - \frac{x_{vap} \cdot \dot{m}_{l,N_2} \cdot h_{\mathrm{lg},N_2}}{k_1 \cdot h_{lg,Ar}} \end{bmatrix} \tag{3.6}$$

The differential equations can be expressed under the following model of representation, described in Eq (3.7).

$$\dot{X} = A \cdot X + B \cdot U + \mathrm{w} \tag{3.7}$$

Where X is the state vector, $[T_{Kr}, T_{Ar}]$, U is the command vector and w contains the *a priori* unknown dynamics. This representation has the advantage to take into account the imperfection of the *a priori* known modeling part. A and B are two matrix which provides a commendable result. A and B are respectively describes in Eq (3.8) and (3.9).

$$A = \begin{bmatrix} -\frac{H_{1h} \cdot S_{1h}}{k_2 \cdot h_{\mathrm{lg},Kr}} & \frac{H_{1h} \cdot S_{1h}}{k_2 \cdot h_{\mathrm{lg},Kr}} \\ \\ \frac{H_{1c} \cdot S_{1c}}{k_1 \cdot h_{\mathrm{lg},Ar}} & -\frac{H_{1c} \cdot S_{1c}}{k_1 \cdot h_{\mathrm{lg},Ar}} \end{bmatrix} \tag{3.8}$$

$$B = \begin{bmatrix} 0 & -\frac{x_{vap} \cdot h_{\mathrm{lg},N_2}}{k_1 \cdot h_{\mathrm{lg},Ar}} \end{bmatrix}^T \tag{3.9}$$

Analysing matrix A, one of the eigenvalues is equal to zero providing an instability of the system. By numerical application, we notice the system is commendable for approximative values of A and B. To satisfy dynamic set point of Argon temperature, the term in function of T_{Ar} is in matrix A in the equation related to $\dot{T}_{Kr}$ is moved to matrix B. u becomes the new command vector containing $[u_1, u_2]^T$, respectively Argon temperature set point command and Nitrogen mass flow.

3.2.4 Time Delay Control approach

"Time Delay Control" has been developed 20 years ago for systems described by differential equations including unknown terms. Proposed by Youcef-Toumi and Ito [63], it was applied on nonlinear systems under two main conditions: all state variables must be measurable and a continuous signal conserves a quite constant value on a sufficiently small time period. This terms are estimated from past commands and state variables information. The estimator principle of the unknown term is defined in Eq. (3.10) as the output of a delay operator D.

$$\hat{\mathrm{w}}\left(t\right) = D \cdot \left(\dot{X}\left(t\right) - AX\left(t\right) - BU\left(t\right)\right) \tag{3.10}$$

The corresponding Laplace transform of time delay is e^{-Ls}, which can be estimate by Padé approximant. According to our model, we define a second order Padé approximation, developed in Eq. (3.11). The resulting transfer function has to be stable, causal and with a unitary static gain.

$$G_{m/n}\left(s\right) = \frac{d_0 + p_1 s}{d_0 + d_1 s + d^2 s^2} \tag{3.11}$$

In parallel, we arbitrary choose a reference linear model implying the trajectory to follow, according to the follow equation :

$$u = B^{+}\left[B_r c + \left(A_r - A\right) X - \hat{\mathrm{w}}\right] \tag{3.12}$$

where matrix A_r and B_r are constant, A_r is stable and the couple (A_r, B_r) is commendable. The command signal is developed in Eq. (3.12) where B^{+} is matrix B pseudo inverse. c is the set points vector, containing Krypton temperature static set point and Argon temperature dynamic set point directly linked to u, the command vector.
$\hat{\mathrm{w}}$ in Eq. (3.12) can be substituted by the Laplace transform of its expression in Eq. (3.10) with Padé approximants. u can be expressed as in Eq. (3.13), where c_1 and c_2 comes from Padé approximants after simplification.

$$u\left(s\right) = B^{+}\left[c_1 \cdot \left(B_r c + A_r X\right) - AX - c_2 \cdot X\right] \tag{3.13}$$

As shown in Fig. 3.4, the controller model uses state variables, consequently, they have to be available, physically or by a state rebuilder.

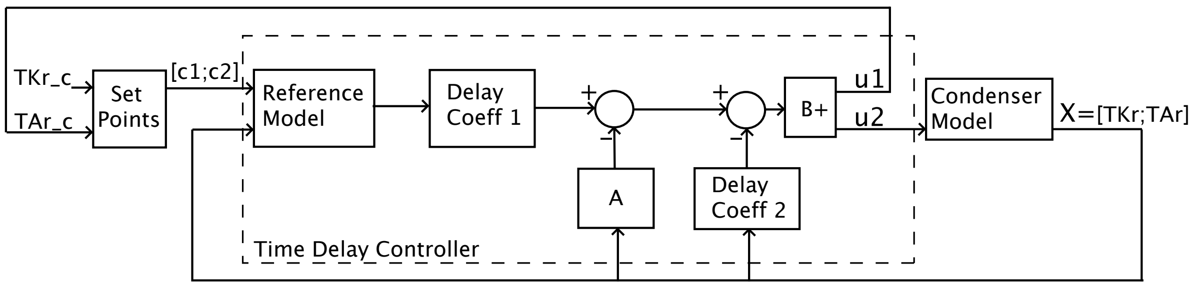

Figure 3.4: Simulated Model with Time Delay Control.

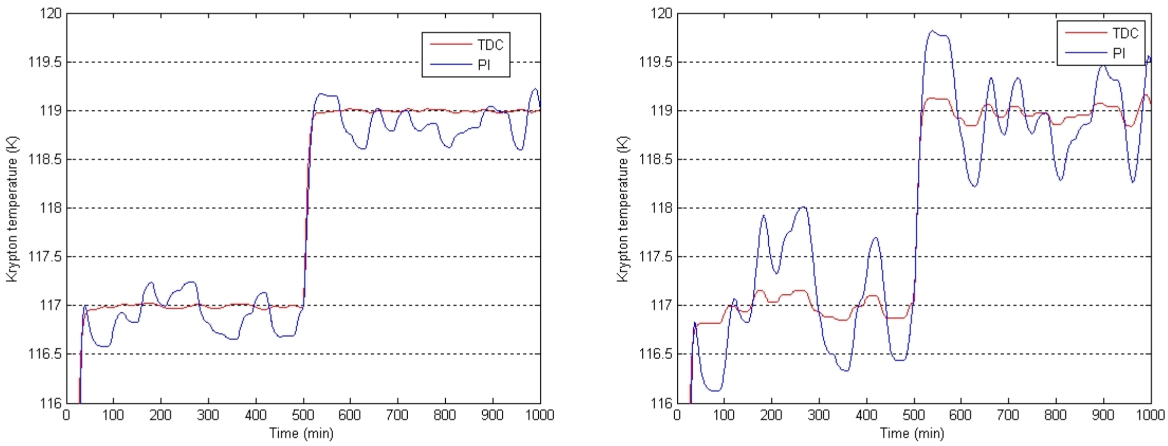

Figure 3.5: Comparison between PI controller and TDC with set point variation for small dynamics (on the left) and for enhanced dynamics (on the right).

3.2.5 Discussion

The modeling step developed a better overview and knowledge of the cryogenics process and of its nonlinearities. We are conscious that several assumptions have been done but the results, working with Time Delay Control, were able to compensate a part of the approximations.

Performance comparison

Fig. (3.5) shows on the left, stability differences between classical PI controller tuned as in cryogenics process (characterized by a large integration time, which is a compromise between set point tracking, inverted response and dynamics compensation) and a Time Delay controller. Both responses are based on the same model, included random parameters to represent the static and dynamic heat inputs in liquid Krypton. Fig. (3.5) on the right, presents a simulation with exaggerated dynamics to face the reactivity of Time Delay Control. In both cases, it occurs that TDC has a better efficiency on Krypton temperature regulation and keep T_{Kr} variations between ± 0.1 K. Krypton temperature set point is varying between 117 K and 119 K. Saturated pressure can easily be reported to saturated temperature. Between 116.5 K and 118 K, saturated pressure difference is close to 100 $mbar$.

The estimation of w from first order and second order Padé approximants, on Fig. (3.6), gives satisfying results. The approximation by first order transfer function is closer to the unknown dynamics but do not improve significantly the state variables stability. In both cases, the static part of w is clearly identified and the dynamic is well followed.
The model presented so far includes a discretization of the physical process only in the time domain, neglecting the dynamics in the spatial domain. Although this approach usually grants satisfying performance, in this particular case, due to the demanding requirements of the application, it is not sufficient to completely remove undesirable effects such as oscillations. Advanced control techniques are used to replace the traditional PID controllers to overcome these limitations.

3.3 Modeling workstation and communication time delay

This Section presents the modeling workstation (MAWS), designed to simulate the Krypton condenser discussed in the previous chapters, in order to validate the control algorithms before its application to the NA62 experiment. The implementation of this control strategy requires a reliable estimation of the actual time delays found during operation. To this purpose, in the following a dedicated section addresses the problem of communication time delay assessment by means of a statistical approach, for which experimental results are finally provided.

3.3.1 Introduction

CERN, during last decade, has extensively applied the CERN/UNICOS framework to large scale cryoplant control system. As previously explain an increase of interested to advanced control techniques and innovative simulation environment applied to cryogenic processes has also occur. Since new control algorithm development into *UNICOS* framework requires significant time, a control testing platform which can be externally

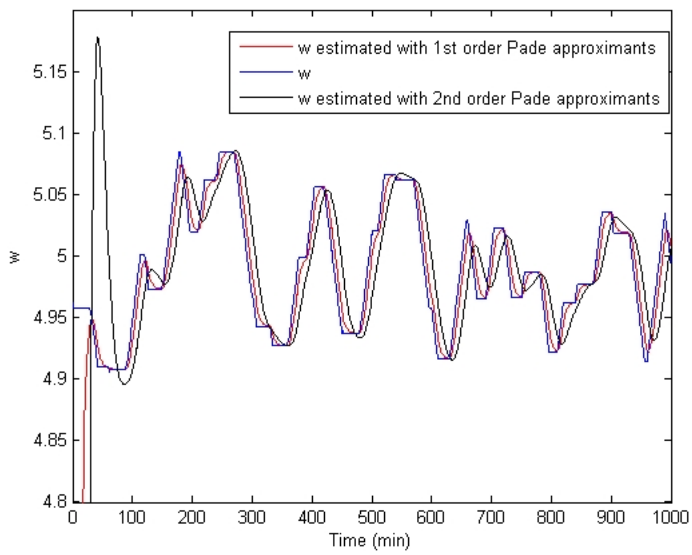

Figure 3.6: Estimation of unknown parameters linked to dynamic heat inputs.

connected can improve and simplify the procedure of testing advanced controllers implementation. In this context, the present work describes the development of a control testing tool at CERN, which allows rapid control strategies implementation through the Matlab/Simulink® [64] environment, coupled with the large scale cryogenics *UNICOS* control system or with the CERN PROCOS simulation environment. The time delays which are inherently introduced by network links and communication protocols are analyzed and experimentally identified. Security and reliability issues are also discussed.

During the last few years, CERN has shown increasing interest on the application of advanced control techniques to cryogenics processes [65]. However, the application of such techniques has been limited to the set of controllers which are available in the local automation standard, the *UNICOS* [13]. The integration of a new control technique to the framework can require months of development, what is undesirable when one wants to test a new control technique without guarantees of future use.

In order to provide a universal control testing platform, easy to use and allowing rapid control implementation for testing purposes, the simulation software Matlab/Simulink® was integrated to the CERN control architecture allowing the control of cryogenic process, which typically have large time constants (order of magnitude of minutes), directly from Simulink models. This facility is referred as Virtual Control Platform (VCP).

As one can expect, the VCP introduces time delays due to the network link between Matlab/Simulink® and the real processes, and also due to the finite calculation time required by the control algorithm implemented on Simulink. This part focuses on the study of such delays, identifying and measuring them in real operation. It also discusses how we can assure that the delays will not degrade control performance into unacceptable levels.

Another important issue put in spot is the platform's security of operation. Without precautions, a network breakdown could freeze the control of the process and possibly cause serious damages to the plant. The strategy adopted by the VCP in order to eliminate this risk is also presented.

3.3.2 Facility description

In normal operation, a programmable logic controller (PLC) is in charge of several control tasks, as sequential operations, security interlocks, alarm triggering and process variables regulation.

Fig. 3.7 describes how the VCP was set up to communicate with an industrial process. A PLC runs the program which is normally used to control a given process. A short set of

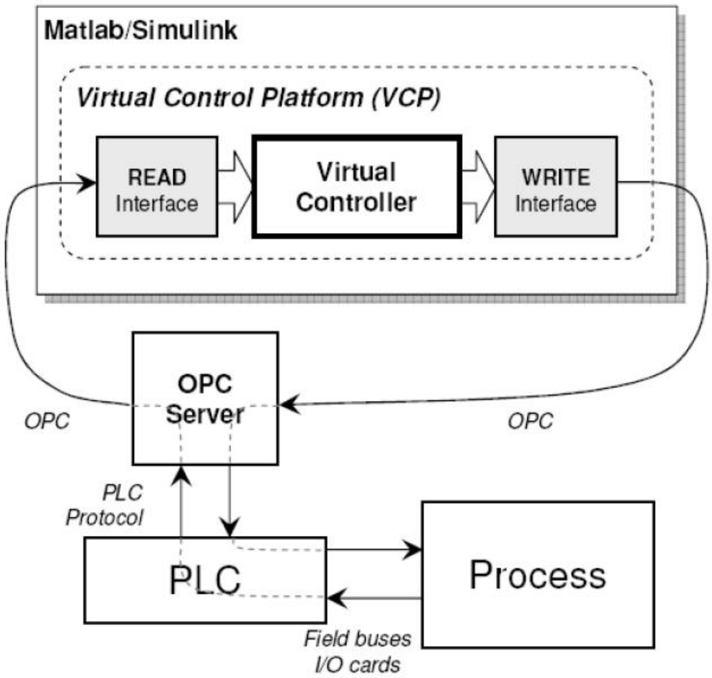

Figure 3.7: Interface between VCP and process.

adaptations replaces the original controller's outputs by the outputs of the Virtual Controller. The objective is to modify PLC programs as less as possible, only by by-passing the PLC-based *UNICOS* controllers (commonly PIDs) with the new commands provided by the controller implemented in Simulink. In case of communication or Matlab/Simulink® failure, the original controllers are switched on and normal operation is restored. Transitions from VCP to PLC control loop algorithm (and vice versa), and tracking mode are not described in this Section. All PLC functionalities are kept unchanged. The ""OLE" for Process Control" (OPC), which stands for "Object Linking and Embedding" (OLE) for Process Control standard, is used as a high-level communication protocol to exchange measurements and commands between the virtual controller and the process. In order to implement the expected behaviour of a digital control system, a new OPC interface blockset was written for the VCP prototype. The operation sequence is: read controller's input variables with a synchronous OPC transaction; wait for the read values; calculate the control algorithm outputs; write the controller outputs with an asynchronous OPC transaction.

3.3.3 Communication time delay

A control-loop which is implemented through the VCP can be theoretically defined as a Networked Control System (NCS), i.e. the interface between controllers and processes are done through a network link with associated time delays. NCSs have been studied since 1980s, when first works aimed to determine stability criterions for such systems [66, 67]. In recent years, researchers focuses on compensating the network delays with advanced control techniques [68, 69].
The time between sampling the input variables and writing the corresponding outputs to the PLC is herein referred as output delay. Since the read and write time delays can have significant variations due to the network communication, the output delay is modeled as a probabilistic distribution. In addition, equal-distance sampling cannot be guaranteed and thus the sample time can slightly fluctuate around the user-specified read period. VCP operation is synthesizes as shown in Fig. 3.8.

3.3.4 Tests and results

In order to identify experimentally the probabilistic distribution of the output delay and the sample time variation, several tests were run with the VCP prototype inside CERN control architecture. The scan time of the PLC was set in four different values (50, 100, 150 and 200 ms) and the read period was specified in 0.5 s. The PLC program which was continuously running during the tests was not linked to the real process but in a simulation framework [70] for security reasons.

Basal output delay

Since the calculation time required by the control algorithm depends on the complexity of the user-specified virtual controller, it is impossible to determine the VCP's output delay objectively. Thus, we only calculate the basal value of the output delay. It is done by adding the distributions of the read and write delays, which can be obtained experimentally. To find the output delay itself, one has to add an estimate of the algorithm's calculation time to the basal value.

Tab. 3.1 shows the mean and the standard deviation of the basal output delay for each hosting approach and each PLC scan time used in the tests. Each distribution is obtained from 8'000 measures of the read and writes delays.

	Scan Time of the PLC			
	50 ms	**100 ms**	**150 ms**	**200 ms**
Mean	167 ms	193 ms	268 ms	320 ms
Deviation	33 ms	47 ms	68 ms	89 ms

Table 3.1: Basal Output Delay Distribution.

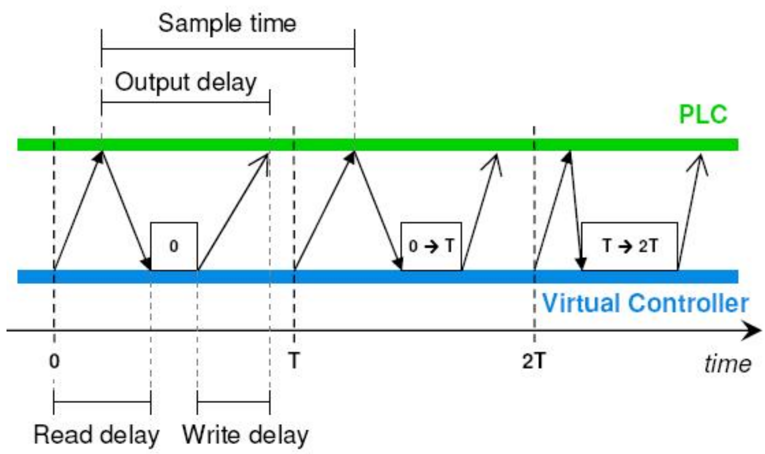

Figure 3.8: Timeline of VCP operation.

We also observe that the scan time of the PLC is a fundamental factor on determining the output delay.

Sample time variation

Ideally the sample time variation around the read period should be equal to 0, with standard deviation null. Since Simulink does not operate perfectly in real-time and since OPC read requests can be processed by the OPC server at non-equal-distanced intervals, the sample time of VCP presents some fluctuations. In order to measure these fluctuations, the timestamp information of each OPC read was retrieved for 2'000 sample instants of platform's operation. The chosen read period was 0.5 s. Tab. 3.2 shows the mean and the standard deviation of the variation of the sample time around the read period.

Despite a biased result for the scan time of 100 ms, we note that the sample time variation mean tends to be null (near 1 ms). On the contrary, the standard deviation increases with the scan time of the PLC.

	Scan Time of the PLC			
	50 ms	**100 ms**	**150 ms**	**200 ms**
Mean	1 ms	17 ms	1 ms	1 ms
Deviation	10 ms	40 ms	77 ms	110 ms

Table 3.2: Sample Time Variation when the Read Period is 0.5 s.

3.3.5 Discussion

The main contributions of the work herein presented are (i) an optimized prototype of VCP, which uses OPC communication to interact Matlab/Simulink® with largescale cryogenic processes; (ii) an experimental survey of the time delays which are associated to platform's operation. Further studies will be necessary to define the theoretical criterion to ensure reliability when VCP is applied to real processes. These criterions encompass process time constant and delays, and PLC cycle time.

The Virtual Control Platform is still a concept in development at CERN. The first results show that, under certain conditions, the platform can be safely used to control real cryogenic plants. The experimental campaign focused on the PLC cycle time impact, but it has also emphasized on the correlation between time delay introduced by the VCP use and system time constant, which needs to be the subject of a more detailed approach.
As a testing tool, the VCP can serve as an efficient guide in the development of the *UNICOS* framework, allowing control engineers to seek promising advanced control techniques for cryogenics with short development times.

Chapter 4

Object-based industrial controls for cryogenics

4.1 The UNICOS object model

This Section presents the UNICOS framework, developed in the past years at CERN in the frame of a project aiming to provide a unified homogeneous control system for the cryogenics plants of the Organization. In the following, (*i*) the background and (*ii*) the basic concepts of the framework are presented, with particular emphasis on its object model and the related pros and cons.

4.1.1 Background

Cryogenics has been extensively used in LHC, both in the accelerator and in the detectors. In order to rationalize the control effort a common project was launched in 1999. This project called UNICOS for UNified Industrial COntrol System, had to provide an homogeneous control system for the cryogenics plants supplying liquid Helium to the LHC accelerator, the cryogenic equipment in the machine tunnel, and the ATLAS and CMS cryogenic systems. During the past years controls and cryogenics groups have developed an expertise in the control of cryogenic and other systems for LEP, LEP2, LHC String test and other R&D facilities. A synthesis of the different approaches was made and led to the elaboration of a technical design both for hardware and software. The hardware architecture is based on a three-layer model using distributed I/O connected to PLC via field-networks, PLC to hold the process control software and a *SCADA* System as operator interface. The software design is an evolution of the “object oriented” philosophy used with former control system [71, 72]. In this approach each process component (I/O channel, actuator, set of sensors and actuators constituting a process entity) is modeled in an object. This object integrates the process behaviour and the Human Machine Interface (HMI) .

4.1.2 HMI and PLC repartition

In the UNICOS concept the object is split in two parts (fig. 4.1):

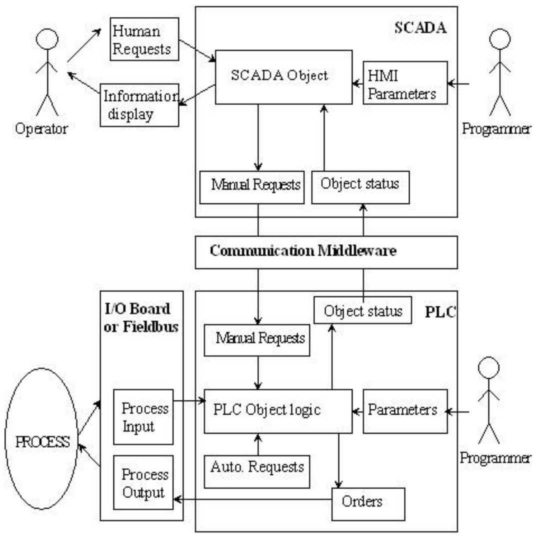

Figure 4.1: PLC/SCADA Object interface.

- The process behaviour, programmed in the PLC.
- The HMI functionality programmed in the *SCADA*

The HMI part includes the interaction with the operator by mean of widgets and dedicated panels called faceplates; these graphical elements inform the operator on the object status, and allow him to send orders. The PLC part contains the process behaviour of the object. The programmer can parameterize this process behaviour. The object is linked to the plant through the Input/Output (I/O) board that may be linked to the PLC via either a fieldbus or the backplane

Both parts are connected together thanks to the communication middleware.

4.1.3 Object integration

An object receives:

- Requests from the operator via the *SCADA* part of the Object, these requests are transmitted to the PLC by the Manual Requests through the middleware (see Fig.4.1).

- Configuration parameters (HMI or PLC) set during the programming phase and accessible for modification by a program specialist (see Fig.4.1).

- Information from the process (process inputs), consisting of analogue or binary values from sensors and statuses of other objects (see Fig.4.2).

- Order from the control logic programmed into an object of a higher hierarchical level via the Auto Requests (Fig. 4.2).

According to its internal states (driven by the PLC/driven by the Operator, interlocked or not, started or stopped etc.) the PLC Object logic processes the inputs and the requests and emits orders either to the process outputs or to other objects(fig. 4.2).

The PLC object logic publishes the status of the object to inform the operator or any other objects to trigger coherent action in the control logic.

4.1.4 Main object types or classes

Three main types of objects are defined in the UNICOS architecture:

- **Input-output objects**: These objects provide the interface to the plant. They link the devices and actuators to the control system. Some basic treatments may be embedded in this object class. (I/O) channels shall be accessed through such objects exclusively.

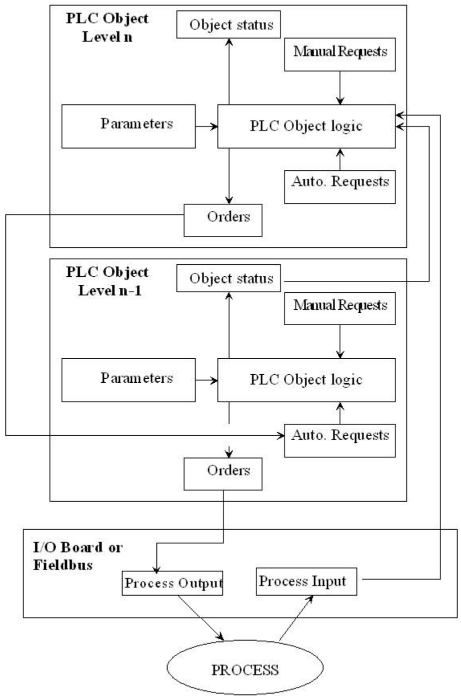

Figure 4.2: PLC object/PLC object hierarchy.

- **Field objects**: These objects are the images of the hardware elements such as valves, heaters, motors, and other devices. For each type of Field object an Object standard logic is defined. This logic integrates specific functions (alarm generation, ramping, interlocking).

- **Process control objects (PCOs)**: These objects control equipment units grouping several Field objects and/or other process control objects. The PCO object logic is split between a standard part insuring an homogeneous interface to the environment, and a specific part to cope with the process to control.

4.1.5 Implementation

From the above design the implementation of the control system requested :

- The supply of the control hardware

- The development of PLC and *SCADA* components for each type of object

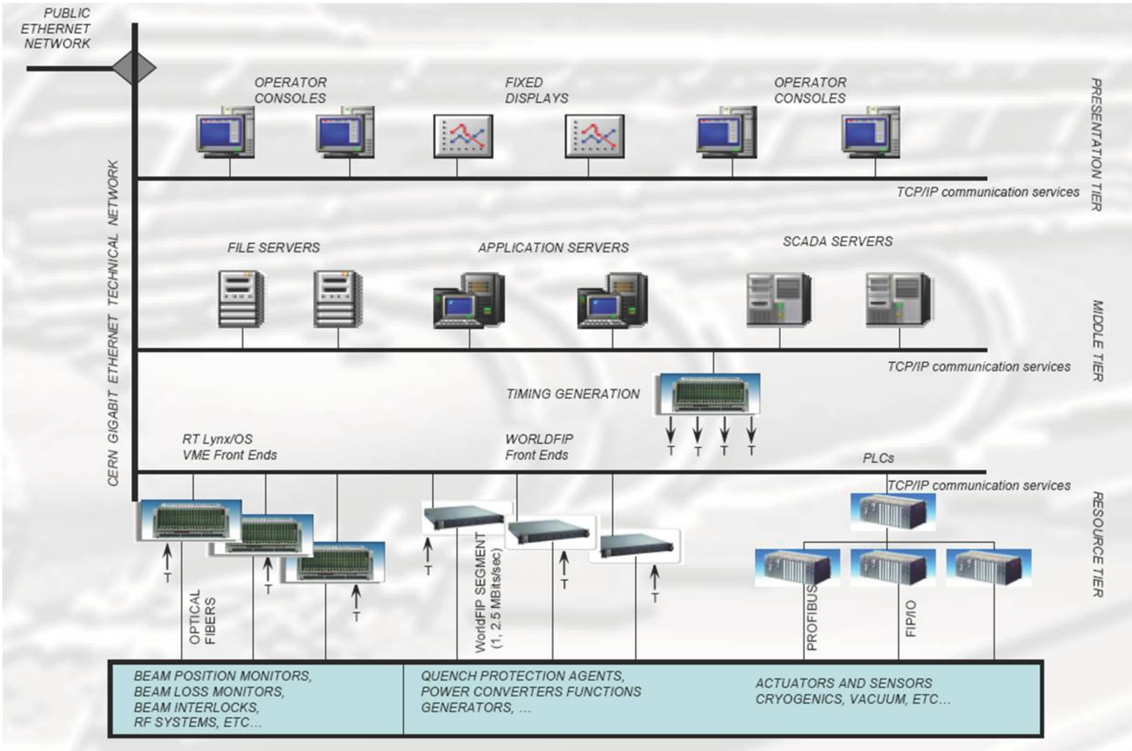

Figure 4.3: CERN control architecture.

- A communication middleware between PLC and *SCADA*
- A *SCADA* framework to offer an homogeneous User interface
- The realisation of Control

Contract Award The contract which, includes the delivery of the above items was awarded to a European consortium (GTD SA Spain, CEGELEC France & Belgium). Hardware architecture This implemented Architecture is a classical three layers control architecture (fig.4.3).

The Supervision Layer: The HMI is located in this layer. The chosen implementation relies on Operator Workstation (OWS) as human interface and client of a redundant data server holding the real time database, the chosen *SCADA* software is PCVue32 from ARC Informatique.

- Control Layer: All process control duties are performed in this layer in Schneider Quantum PLC;the programming is done via an Engineering Workstation (EWS)

- Field Layer: Schneider Premium PLC are used to connect the process channels to the control system. An alternative solution using a proprietary Schneider bus technology and Quantum remote I/O can also be used.
- Communication: Based on the Ethernet TCP-IP CERN infrastructure this network must be highly reliable as control loops are closed trough it.

4.1.6 Framework deployment

The framework has been deployed Using ESA PSS-05 methodology [73]. The first phase for the consortium was to reformulate the framework requirement exposed in the call for tender. Then based on this analysis an Unified Modeling Language (UML) study of the object behaviour has been produced from which the PLC objects were developed in IEC 61131-3 language [74]. In parallel to the PLC object all *SCADA* modules have been developed using ActiveX and proprietary *SCADA* script.
Finally a prototype integrating all layers and the communication middleware has been delivered and validated.
In order to optimise the communication bandwidth an event-driven protocol based on MODBUS on TCP-IP has been developed by the consortium between the PLC and the *SCADA*.

4.1.7 User application development

- Phase 1: Specification
  - Object list: from the process specifications one has to establish a complete list of the I/O and field object. We have provided spreadsheet templates to capture all relevant information.
  - Object hierarchy: the process engineer analyze his system and proposes a hierarchical organization down to the field objects
  - Control logic: for each PCO specific logical modules have to be developed, these modules contain typically the interlocks and the logic used to control dependant

objects. A specification template has been elaborated with guidelines.

- Phase 2: Software development
  - Database generation: From the object list spreadsheet an automated tool generates all variables together with their memory assignment into the PLC and the *SCADA*
  - PLC Object instantiation: The same tool generates the code instantiating all object in the PLC. Then 100% of the premium code is automatically generated, and a large part of the Quantum
  - Control logic: The programmer has to fill the program sections following the programming guidelines.
- Phase 3: Acceptance and Maintenance
  - Acceptance tests to check the conformity to specification. Then the commissioning of the cryogenic system can be made; this includes a large amount of the process logic modification
  - Maintenance, follow up during the lifetime of the application of all medication using a case tool "5 lessons drawn from applications". From the first application commissioning since July 2001, several pros and cons can be noted.

4.1.8 UNICOS pros and cons

- PROS
  - Easiness of modification during commissioning due to the readability, the modularity and reusability of the code.
  - Once mastered, the specification template are easy to use by the programmer and few errors are generated allowing a good quality of the produced control software.
  - Excellent stability of the PLC.

  - Easy and efficient creation and modification of Process display
  - The operator can interact with any objects through a standardized interface. This possibility allows troubleshooting flexibility during tests, or in case of equipment failure.

- CONS
  - This model needs an appropriate training to be understood and deployed. Mainly for the process engineer.
  - Programming templates have to be established in order to optimize the object interactions.
  - The use of objects implies extra memory usage and additional CPU load. Hence this method is not suitable for time critical control ($< 10\ ms$).
  - Necessity of an automated tool to generate the database in PLC and *SCADA*.
  - Stability problem in the present version of the *SCADA* implementation but work undergoes with good preliminary results.

4.1.9 Discussion

Over the past decade almost UNICOS framework has provided the expected results and more. The teething problem has been solved and the mass production of the user application software has smoothly follow. In order to face CERN recommendation a migration to another *SCADA* has been performed and a technological evolution in the PLC has implied few framework upgrade steps. These evolutions have been executed in agreement with the project schedule and have not compromise any dead lines. Moreover, these evolutions and other developments (UNICOS for Siemens PLC, Premium PCO & Field objects) have open the use of the UNICOS framework out of the cryogenic systems trough CERN industrial control activities.

4.2 Cryogenics UNICOS project development at CERN

This Section presents the development activities carried out at CERN for the LHC control system, with details on its architecture, instrumentation, tests, commissioning, and deployment. Subsequently, the installation and commissioning of the refrigeration system of the CMS magnets are discussed. Finally, a simulation study for the virtual commissioning of the CERN central Helium liquefier, the off-line commissioning of the Helium cryogenics plants and the operator training are introduced.

4.2.1 The development of the control system for the cryogenics in the LHC tunnel

The LHC (Fig. 4.4) is the world's largest and most powerful particle accelerator, designed to collide two proton beams head-on at the energy of 7 TeV per beam. Four main detectors: ATLAS, ALICE, CMS, and LHCb have been built to identify the particles produced in collisions.

The LHC is a 27 km ring located about 100 meters underground. It is divided into eight 3.3 km long sectors. A single sector is made of a curved part (ARC) with one long straight section (LSS) at each extremity. The beams are guided along the tunnel by superconducting magnets and accelerated by superconducting radio frequency cavities (RF). The current is supplied to the magnets through electrical feed boxes (DFB). All cryogenic equipment is maintained at 1.9 K or 4.5 K by Helium supplied trough a cryogenic distribution line, which runs along the magnets and is linked to 8 cryogenic plants, grouped in 5 technical sites. Each plant is comprised of warm compressors, refrigeration units, transfer lines and cold interconnection boxes.

Controls architecture

The process automation for the cryogenics in the LHC tunnel follows a hierarchical industrial control system architecture (Fig.4.5). It is composed of remote Input/Output modules (RIO), Programmable Logic Controllers (PLC), and a Supervisory Control And Data Acquisition ($SCADA$).

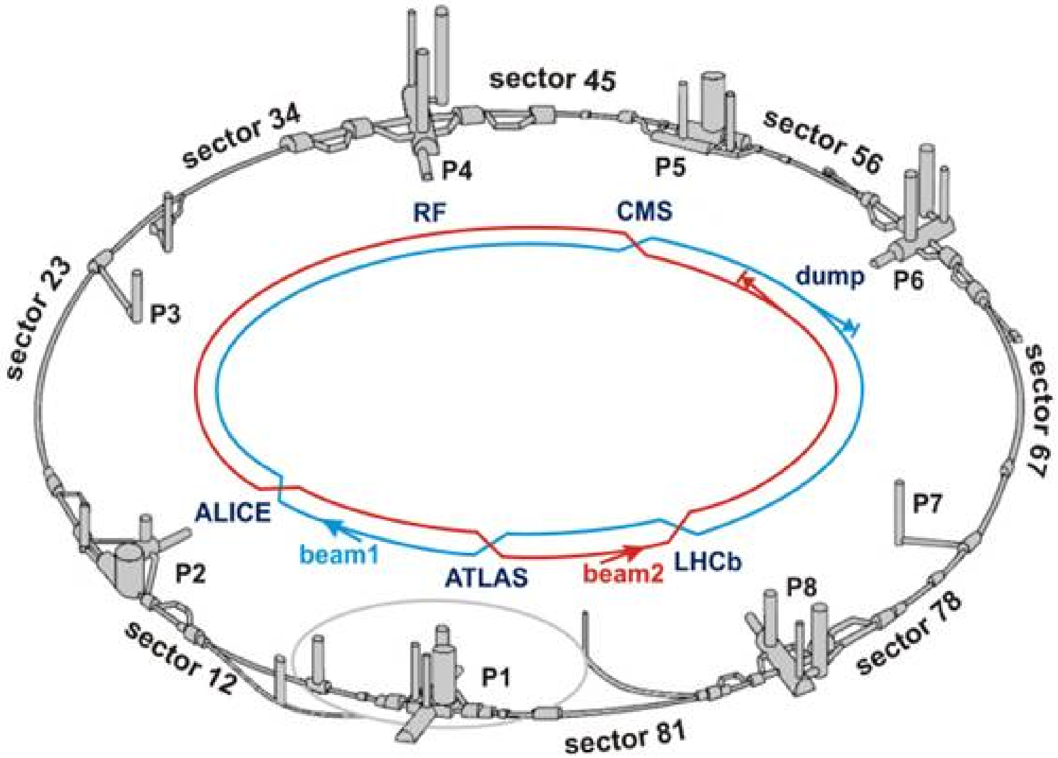

Figure 4.4: Layout of 8 LHC sectors, RF and main detectors.

Cryogenic instrumentation and remote I/O

About 10'000 sensors and 5'000 actuators have been installed, in order to keep the LHC tunnel cryogenics at nominal conditions (Table 4.1).

Cryogenic process status is provided by sensors measuring temperature (TT), pressure (PT) and the level of liquid Helium (LT). The process is controlled via analog and digital cryogenic valves and analog heaters. Additionally, the control system is equipped with several types of diagnostic devices and hardware interlocks, both represented by digital signals.

To cope with the distributed instrumentation, the Profibus-DP (Decentralized Periphery, Fig. 4.6), Profibus-PA (Process Automation, Fig. 4.7) and WorldFIP (Fig. 4.8) fieldbuses are employed.

The Profibus-DP RIO modules, driving digital valves or reading diagnostic signals, have been placed in those areas. The Profibus-PA intelligent valve positioners, normally attached to the pneumatic actuator, have also been moved into protected areas. To commu-

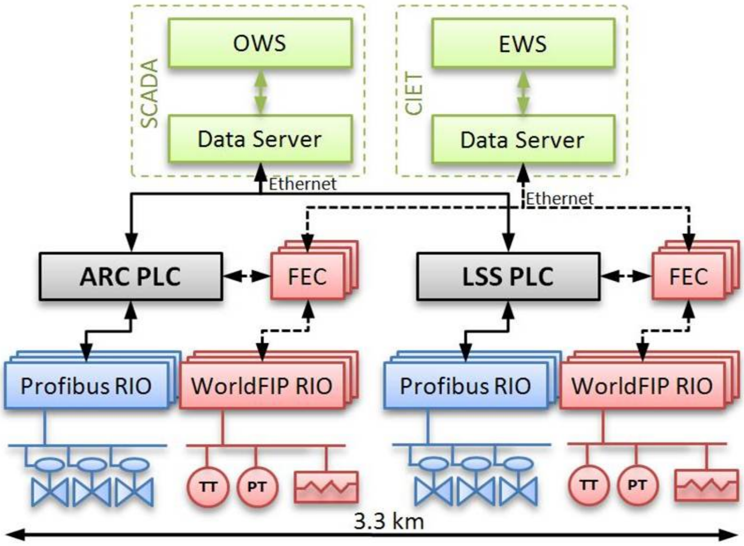

Figure 4.5: Control system layout for one LHC sector.

Instruments	**Range**	**avg/sector**	**RF**	**Total**
TT (temperature)	1.6 - 300 K	868	168	7 118
PT (pressure)	0 - 20 bar	105	14	855
LT (level)	Various	52	16	436
EH (heaters)	Various	297	10	2 392
CV (Control Valves)	0 - 100 %	323	18	2 606
PV/QV (OnOff Valves)	On - Off	83	10	681
Digital status signals	0 - 1	500	214	4 214

Table 4.1: Profibus DP, Remote IO Profibus is used whenever the front-end electronics can be housed in radiation protected areas.

nicate with the upper level of the control system, it needs industrial computer gateways, called Front End Computers (FEC). The FECs capture raw signals from the conditioners and convert them into physical sensor information; and vice versa for commands.

Each sector is controlled by two SIEMENS S7-400 PLCs (Fig. 4.9).

The tunnel cryogenics is protected by 5 500 alarms and software interlocks and controlled by 3 600 Closed Control Loops (CCL) with a PID algorithm. The phases of the process have been classified as four operational modes: cool-down; emptying; stand-by at 75 K and warm-up. To handle the cool-down steps and transitions between them a phase sequencer has been designed. Around 35 000 functions, function-blocks and data-blocks

Figure 4.6: Profibus DP, Remote IO Profibus is used whenever the front-end electronics can be housed in radiation protected areas.

Type	**avg/sector**	**RF**	**Total**
SCL source files	1 792	544	14 884
Functions, funct-blocks, data-blocks	4 193	1 482	35 032
Alarms & interlocks	679	98	5 536
Closed Control Loops	444	51	3 610
SCADA synoptic panels	204	10	1 650

Table 4.2: WorldFip: Remote IO 2.2 DCS and *SCADA* Considering the large scale of the cryogenic system, it was necessary to distribute the PLCs over the eight LHC sectors.

were automatically generated in 15 000 source files, written in Structured Control Language (SCL) (Table 4.2).

The *SCADA* layer is based on PVSS II®; it provides the classical features of a *SCADA* including the Human Machine Interface (HMI), through which the operators monitor and act on the cryogenic facilities, from local or central control rooms, It comprises around 1'650 panels with process synoptics, alarm and interlock handling, event logging, real-time and historical trend monitoring, navigation and global operation tools. A specialized tool was created to configure and diagnose all the sensors located in the tunnel: the Cryogenics Instrumentation Expert Tool (CIET). This tool was developed using the same *SCADA* environment: PVSS II®; it allows instrumentation engineers accessing the full data of

Figure 4.7: Profibus PA, drawers of intelligent valve positioners WorldFIP , being radiation tolerant, is used where the front-end could not be moved away from radiation.

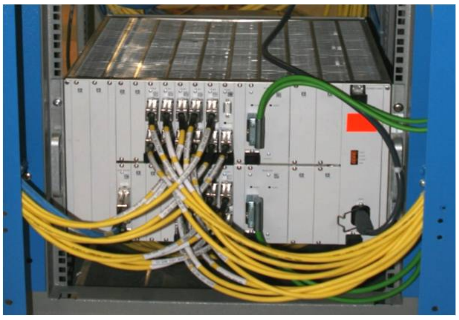

Figure 4.8: WorldFip, Remote IO 2.2 DCS and *SCADA* Considering the large scale of the cryogenic system, it was necessary to distribute the PLCs over the eight LHC sectors.

the WorldFIP devices.

Hardware commissioning

In order to validate the FIP instrumentation, 4 Mobile Test Benches (MTB) were built and several test procedures were designed. The MTB automatically validates the signal conditioner cards, the communication interface and the attached sensors (PT, TT, and LT) and actuators (EH). A dedicated testing sequence is set up by the MTB for each RIO, according to information obtained from a Layout Database. The testing procedure is split into a consistency test and an electrical test. During the consistency test, the MTB checks whether there is a correlation between the crate descriptions stored in the Layout

Figure 4.9: Rack with 4 PLCs for 2 sectors (1 cryogenics site).

Database and the components installed in the crate. The electrical test contains four parts: an instrumentation test that verifies the physical existence and proper wiring of sensors and heaters; verification of the electrical connection between sensors and crates; validation of the correct functionality of each of the electronic cards housed in the crate; and a check of all the components together. Finally, all test results are stored automatically in a database. The results are described by Penacoba et al (2008) [75].

Profibus RIO test

The test procedure of the control valves comprises two stages: the first is executed in the laboratory, and the second one executed in the LHC tunnel. In the laboratory, the configuration and automatic initialization of the positioner units are performed with a reference valve. In the tunnel, after the positioners have been connected to the corresponding valves, they are again initialised; the motion direction and the min-max positions were verified by manually operating each valve's positioner from its local command panel. The Siemens PDM tool provides remote initialization or restart of any valve positioner, in case of failure and despite tunnel access restrictions. A dedicated CERN application was also developed to use PDM for campaigns of simultaneously changing, automatically modifying or saving the parameters of several positioners. Digital valves require a 24 V DC command, reaching the valve farthest from the alcove, where the power supply is localized. These valves' operation was verified using a tool simulating the driving signal and simultaneously reading feedback from end switches. Positioner units are connected to the Profibus DP through DP/PA Link + Coupler modules, while the command signals for the digital valves and the digital input signals are managed by Profibus DP RIO modules. All this equipment is housed in crates, which were electrically tested in the laboratory before installation. Once installed in the alcoves, the network parameters were set up and the test procedure was executed using a portable PLCs. During the test, each RIO module was connected to the Profibus network in order to check consistency between the database and the physically installed components. The parameters verified include: module type and version, address, and channel assignment. All test results were archived for future reference.

Valve automatic test

After the accessibility of each Profibus RIO component has been checked from the PLC, extensive tests of actuators operability were performed. The procedure aimed to repeatedly check the valve reaction time and the accuracy of the reaction to requests sent by PLC. Every second, for each tested valve the following information was registered: occurrence of an IO-error, valve reaction time, request-feedback difference, feedback position range. All data is gathered in the PLC and later copied into a spreadsheet for further analysis.

Coherence test

The final stage of hardware commissioning was the coherence test of all the instruments, using the complete system configuration. The aim of this test was to verify if all valves respond correctly to requests. The verification was performed by a team consisting of an operator responsible for sending requests and checking feedbacks on the *SCADA* synoptic and a technician present in front of the tested devices in the LHC tunnel.

Software production

The cryogenics controls software relies on various automatic generation tools developed at CERN. The software is generated using data coming from several databases (DB) containing definitions of the cryogenic instrumentation, controls system components and process logic. The software production process (Fig. 4.10) begins with the Specifications generation, using the view which combines data from several DBs and external spreadsheets. It extracts information required to produce a specification document and associated hardware configuration for PLC and then applies a set of rules and calculations to complete the objects, their parameters and dependencies.

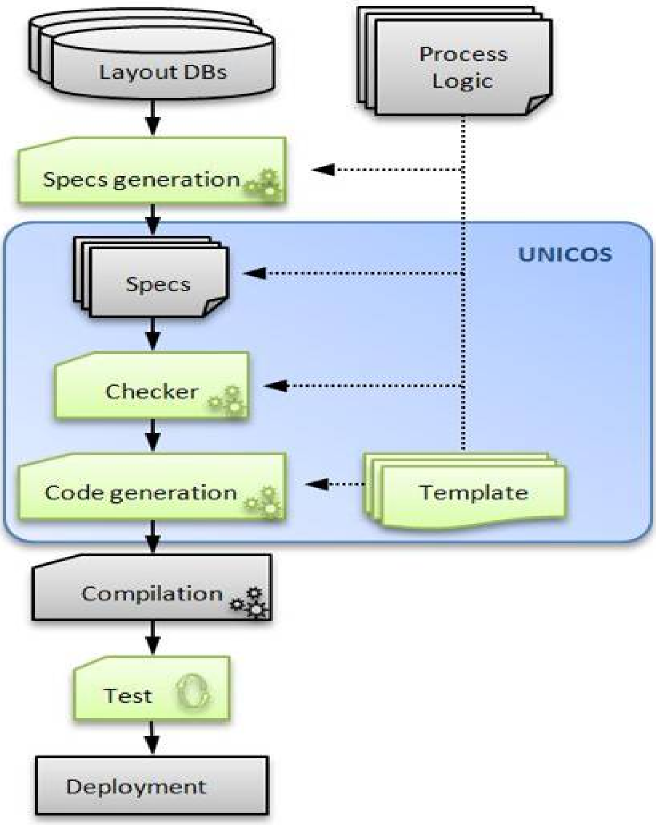

Figure 4.10: Software production diagram.

The UNICOS automatic validation of the specifications was extended by a PERL checker. The aim of this tool was to shorten the code production cycle, by detecting most of the specification's errors at the very beginning. This way, we minimized the risk of having to repeat the software generation procedure. The PERL checker covers most of the aspects of the project, analyzing the specification for compliance with different rules i.e.: object dependencies and parameters, interlocks for given devices and completeness of the data. Due to the specificities of the cryogenics process, a substantial piece of code had to be manually prepared by a programmer. Another PERL tool extends the UNICOS generator capabilities, in order to replace the programmer as much as possible. An example of automatically generated code is the calculation of minimal, average and maximal values for every cryogenic cell, where each calculation may be derived from one hundred arguments. Automatic software generation required the creation of around 80 templates, based on the process logic and on the UNICOS skeleton. Any process logic modification forces the subsequent regeneration and compilation of the group of objects affected by the change. In order to avoid such situations, all recurrent pieces of code have been extracted from the templates and moved to external functions; as a result only a single function is touched in case of logic update. The last step before field deployment is the test of PLC and *SCADA* software, carried out by the process engineer on the development machines, to ensure the correctness of the translation from process functional analysis to machine code. Those development machines are not connected to the real instrumentation in the field; thus the check is performed by exploiting the UNICOS process state simulation features, by forcing the instruments status.

In the cryogenics system there are circuits recurring multiple times; therefore, special generation tools were developed to replicate the corresponding panels (Fig. 4.11). Each sector has around 50 panels automatically produced from templates and around 150 static panels manually created on the basis of machine technical drawings and information collected in the Layout Database.

Keys for challenging large applications

Even if UNICOS was a mature framework in the development of process control systems, a large adaptation was needed. The high-performance PLCs used in the cryogenics control were driven to their limits in terms of cycle-time and resources (memory and

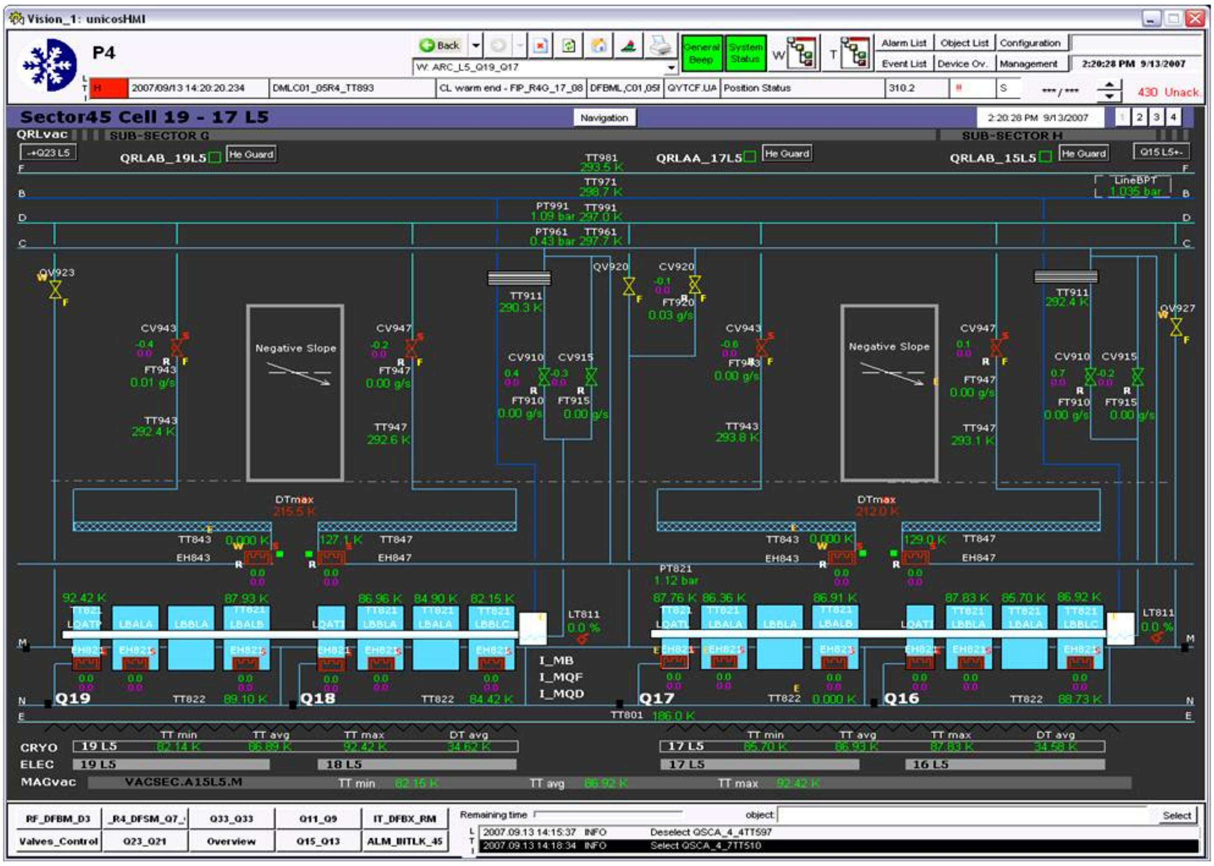

Figure 4.11: Synoptic in *SCADA*.

communications). UNICOS for SIEMENS S7 PLCs was totally revamped with the aim of optimizing resources and performance. This allowed the full deployment of the process control application. The Industrial PCs, included in the control system layer, run a real time application based in a CERN in-house framework (FESA: Front-End Software Architecture). The development of this application imposed a block-design instead of a classic device-design. Dealing with such a large number of instruments imposed a logical grouping to keep treatment times coherent with a WorldFip sampling time of 500 *msec*. The application also included the automatic specification of the cryogenic instrumentation, both, sensors and actuators. Dedicated generators were developed to provide the required capabilities and to accelerate the procedure of deployment. Demanding performance in the communication between PLCs and FECs also imposed an improvement of the Ethernet mechanisms and protocols. The *SCADA* layer of the tunnel cryogenics is part of the complete LHC cryogenic control system. A distributed and high scalable system was designed due to the large quantity of exchanged data between the control and supervision layer (about 1 million of tags). A data server is employed to supervise each LHC sector. The whole *SCADA* includes 16 PVSS data servers (DS). The mechanisms for long-term archiving data, based on an Oracle database, have been largely improved in terms of performance. A nominal flow of 3.5 $Gbytes/day$ is stored in such database.

Commissioning

Dealing with large systems imposes automatic procedures, not only during the developing phase but also for the commissioning; the time spent in this activity could be reduced as much as possible while keeping a high quality assurance standard. Having a common specification source as in the UNICOS framework is a key for coherence within the different controls components (PLCs, FECs, DSs). Moreover, the technical coordination of the commissioning became a challenging task, due to the involvement of several very specialized technical groups, solving highly complex problems. The experience shown that a great deal of problems were much easily solved when there was tight coordination of all commissioning teams, and effective communication between the responsible of the different equipment, such as: radiation-hard electronic crates, PROFIBUS & WorldFIP field bus, PLC architecture and PLC source codes and finally the Human Machine Interface. This approach has improved a lot the commissioning process showing its best results for the rapid comprehension of the origin of the different errors and the dispatch of the required solutions. The long commissioning phase started with a detailed inspection aimed at detecting installation and cabling errors, and was followed by automatic tests to ensure coherency between databases and the field. The commissioning of the instrumentation was done from the surface by using CIET; thanks to this tool, most of the channels of the cryogenic instrumentation used by the controls and cryogenic operation are monitored and validated. After a period of cryogenic operation, the cool-down sequence was simplified, by organizing it in only two phases instead of the original eight, in order to improve the global operability. The improvement of the behaviour of the system was reached in different ways: through the implementation of median filters on all sensors, to avoid spikes; through first-order low-pass filter at the input of control loops; through control loops identification; and through optimisation of software interlocks list, where the non-essential ones were moved into the actuators' logic.

Deployment

Due to frequent changes in the LHC schedule, the tasks related to hardware commissioning had to be executed simultaneously in all LHC sectors. In 2007 it turned out that the period allocated to software preparation was not sufficient to take into account all the requirements coming from the functional analysis of the process and new proposals coming from LHC operators aiming to improve the system. After examining possible scenarios, the decision was to prioritize the main tasks. The software responsible for human and machine safety was given the highest priority. The process automation software was defined as necessary to operate system with second priority. Finally it was reasonable to assume that all system improvements that addressed only the comfort of work for the operators were postponed to future updates. As a result, in March of 2008 the software production procedure for the last LHC sector was put into practice. The LHC cryogenics control system was deployed and fully operational before the LHC beam start-up in 2008. After that, reorganization from development mode to maintenance mode was carried out. The resources were reduced to just a few people taking care of system maintenance and updates. In September 2008 one of the LHC subsystems was damaged, which resulted in stopping the collider for more than a year. This time period was used to redefine process logic, taking into account the experience gained in the preceding phase. The new functional analysis of the process (called Logic Phase II) brought improvements in safety, better operability through a major logic simplification and better availability of the LHC machine. The details are described by Gomes (2009) [76]. Preparing the redeployment took 6 months; during this time all databases, automatic generation tools and code skeletons were adapted to the new requirements. Regeneration of all software was performed during a period of 4 months, and the deployment time was reduced from 5 days in first sector to 3 days in the last 3 sectors. The presence of cryogenic temperatures in the tunnel and limited time window for deployment intervention forced all actions to be synchronized. The PLCs, *SCADA* and FECs software was uploaded simultaneously and started individually. The LHC tunnel cryogenics controls system was again fully operational, with the new logic, in 6 September, 2009.

Discussion

Since the beginning of the project we took advantage of the CERN/UNICOS main features, such as reduced effort and software production time, increased code reliability, minimized risk of human mistakes, and simplified long-term maintenance. Within the UNICOS framework, a large improvement of the process control systems was triggered by the specificity of the cryogenic installation in terms of: large number of instruments (physical IOs and IO software objects); integration of the WorldFip fieldbus (using FECs and FESA); optimization of PLC resources and performance; demanding communication mechanisms be-tween PLCs and FECs (using Ethernet). During the commissioning phase, the technical coordination resulted in a challenging task, due to the involvement of several very specialized technical groups dedicated to solve highly complex problems. A significant improvement was obtained by introducing a global coordination of all commissioning teams. During the operation phase, the main challenge has been to maintain a high-reliability standard, taking into account that some operational conditions might cause failure of the control system and, as a consequence, increase the downtime of the LHC machine. In the last 2 years, after the first LHC operation in nominal cryogenic conditions, we have evolved towards simplicity in process control, databases, and generator of specifications; the control system is now more reliable and user friendly and much adapted to regular operation. Taking into account the experience gained in the preceding phase, a major redefinition of the process logic was undertaken. The new functional analysis of the process brought improvements in safety, better operability through a major logic simplification and better availability of the LHC machine. Like any large scale system, the LHC cryogenic control system is a living machine, which needs continuous high-level controls support and a very accurate and detailed technical documentation, in order to minimize the interventions need in terms of time and manpower.

4.2.2 Installation and commissioning of the Helium refrigeration system for the CMS magnet

The overview of the CMS plant was already given in Section 2.3.1. The commissioning configuration is shown in Fig. 4.12.

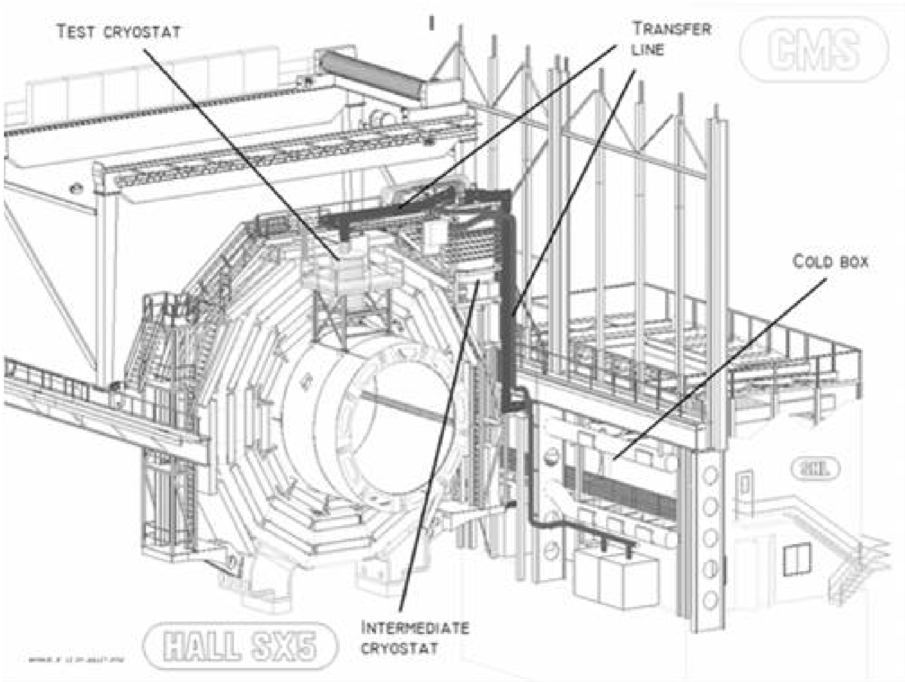

Figure 4.12: Commissioning configuration of Helium refrigeration plant in the CMS assembly hall.

All components, but the Helium storage tanks and the control system have been supplied by Air Liquide (Sassenage, France). Both, the gaseous Helium storage tanks as well as the control system have been procured in the framework of CERN wide contracts.

Installation

The installation of the Helium refrigeration plant components was achieved in the period from Apr. 2001 until Sep. 2003.

Infrastructure. The compressor hall and the assembly hall alcove have been purpose built and special requirements like sound proofing and oil retention provisions in the compressor hall and other installation particularities have been implemented. The buildings as well as all services, i.e. the ventilation, the crane, the water cooling circuit, the electrical power supplies, the instrument air compressor etc. have been handed over well in time by the CERN technical services.

Compressor Station. The compressor station has been delivered pre-assembled on four skids (Fig.4.13).

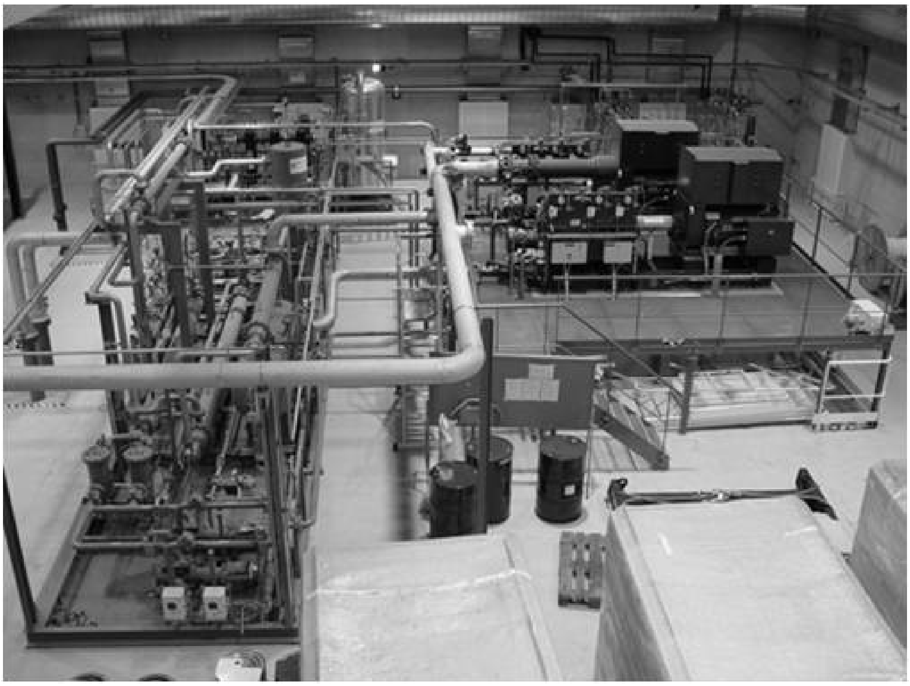

Figure 4.13: The compressor station.

The first and second stage compressor skids carry the screw compressor, the electric motor and the oil injection circuits. Each of these skids is mounted onto a 15 t concrete block which is decoupled from the ground by the means of anti-vibration pads. Access to the two compressor skids at 1.4 m height is provided by a common platform. All the remaining components of the compressor station are assembled on two further skids. One skid regroups the primary oil removal, the Helium coolers, the oil coolers as well as the doubled oil pumps and oil filters for both compressor stages. The other skid carries the final oil removal train comprising three coalescers, one adsorber and one dust filter, as well as the compressor station pressure controls and the Helium analyzer station. The two 250 m^3 Helium storage tanks, which have been supplied through an LHC-cryogenics wide contract, had already been commissioned by the mid of 2001.

Cold Box. For the surface tests, the cold box has been installed in a temporary position inside an alcove of the assembly hall (Fig.4.14).

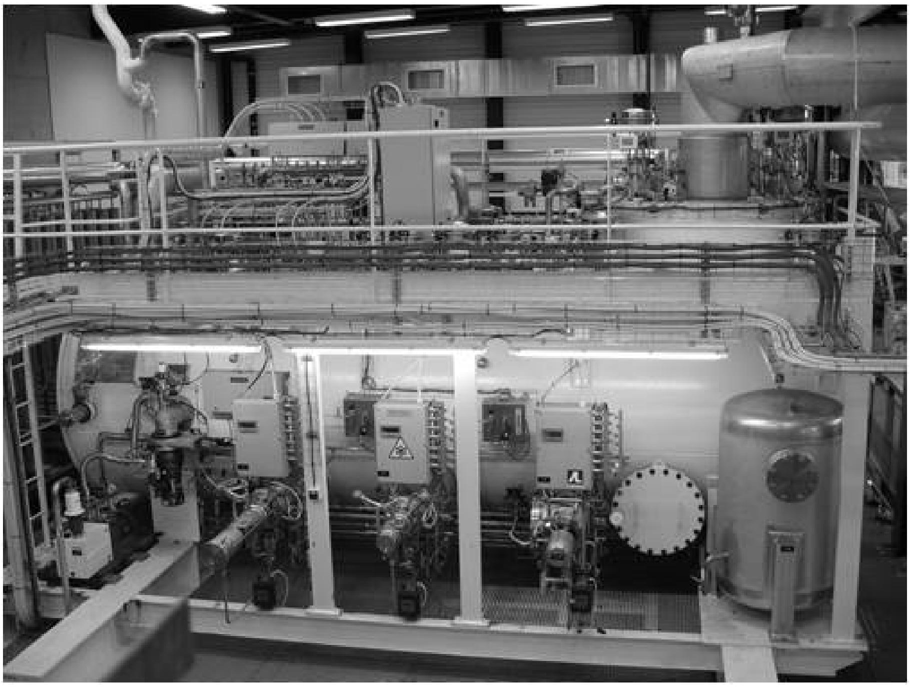

Figure 4.14: Cold box in temporary position inside assembly hall.

The cold box as well as its valve panel and the two atmospheric heaters have been installed by lowering them through an opening in the building roof, specially foreseen for this operation. Once all elements were in place, the piping and cabling has been terminated and the cryogenic valve stems and actuators as well as the three turbines have been installed.

Cryostats. A number of problems during manufacturing and installation of the intermediate cryostat have led to an important delay with respect to the original planning.

At first, due to the problems with the sub-contracted manufacturing, the assembly of the intermediate cryostat had to be terminated in Air Liquide workshop. Later an unfortunate damage to a cryogenic valve, which has occurred during the installation of the cryostat, required a repair of the cryostat in Air Liquide workshop and has added an additional 6 month delay. Fortunately these delays could be accommodated without consequences due to the early start of the refrigeration system contract. The test cryostat (Fig.4.15) has been installed on top of the cryostat vacuum vessel near the future position of the magnet phase separator.

Figure 4.15: Test cryostat located on top of the magnet vacuum vessel.

It allows therefore a test of the refrigeration system close to the operation configuration.

Controls. The controls hardware and software has been delivered in three batches, one for the compressor station, one for the cold box and one for the cryostats. Each batch of the controls hardware comprises the remote I/O cubicle, the power supply cubicle and the PLC cubicle. The remote I/O cubicles have been installed adjacent to the corresponding electrical cubicles. In the course of the project it was decided to receive external manpower in order to produce, from very precise technical specification the source code software concerning the compressor station and the cold box.

Commissioning

The commissioning of the Helium refrigeration system has been carried out in three stages. Within each stage, the commissioning has followed the same principle: after installation of both, the plant hardware and the controls hardware, the plant hardware is conditioned. The conditioning comprises drying, purging and evacuation of the Helium circuits and filling in of all process fluids (see fig.4.16).

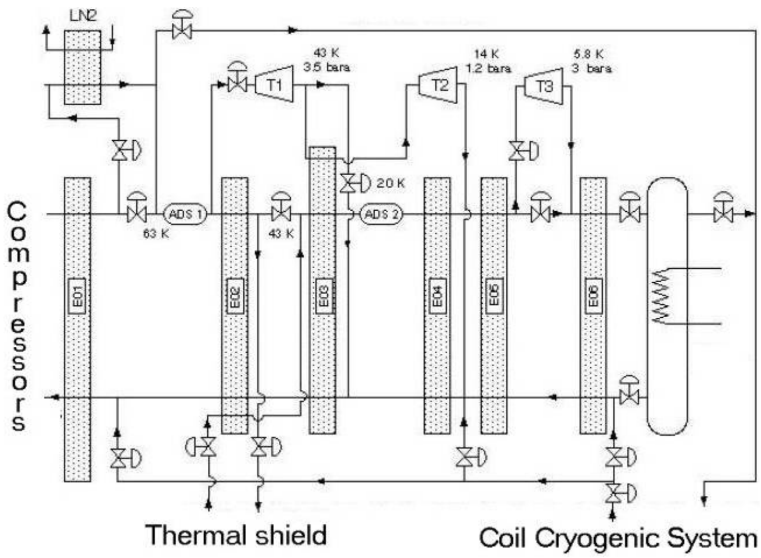

Figure 4.16: CMS cold box schematic.

In parallel, a synchronization test of the I/O signals is carried out to ensure the correct communication in between field objects and the plant software. At this stage also the well functioning of every field device is checked, this comprises checks of the range, the function, etc. With all signals in order, the software testing would be tackled by first operating each software module independently and then by running the sequencer automatically. Commissioning is then completed by carrying out the performance tests to verify the plant performance. The commissioning of the compressor station could be achieved without problems, after about 500 hours of operation a problem with the oil removal has become apparent as an excessive amount of oil was detected in the last coalescer. During the commissioning of the cold box and the cryostats together with the transfer line we have encountered some difficulties with the automatic controls of the turbines 1 and 2 which have been investigated and solved. The process software which is running on two PLCs is working reliably now for more then 6-7 years. Some adaptations that resulted from the commissioning and from a post mortem virtual commissioning have been implemented. The supervisory software which serves as operator interface and which deals with the data storage and the alarm tasks, however, has been accompanied by numerous teething troubles. This was due to the fact that the *UNICOS* framework [13] suffer at the time of not enough maturity (also because we have been used shortly after its introduction at CERN). These problems disappeared soon after the replacement of the supervisory software by the new CERN cryogenics wide supervisory system PVSS.

Cold-Box simulation and process logic validation

4.2.3

The cryogenic CERN control team has develop a dynamic simulator environment called PROCOS (PROcess and COntrol Simulator) [77] to improve the knowledge of the behaviour of these systems and to optimize their management. Other different work objectives consist in providing tools for operators training, being able to check control strategies before or after their implementation.The process is controlled by a PLC and data are exchanged through generic interfaces. All necessary process information collected by the PLC are sent in a data server via the ethernet network using a MODBUS protocol. The *SCADA* supervision clients using the software PVSS are connected to the data server to read process information and to send order to the PLC for manual corrective operations. The key advantage of this CERN system consist of being able to simulate large scale refrigeration plants using the real control architecture, the existing control policy and supervision systems.

The cryogenic plants and their control are highly complex due to the large number of correlated variables on different operation cryogenic scenario that goes from 300 K to 4.5 K [78, 79, 80]. Simulations have been effectuated with the coldbox alone and it is possible to compare the steady-state reached at the end of the Helium liquefaction with the design parameters of the cold box. Conception, design and the control of cryogenic systems are based on CERN and suppliers' experience on appropriate static calculations (4.17) [81].

Due to the system complexity (coupled partial differential equations, propagation and transport phenomena), dynamic simulations represent the only way to provide adequate data during transients and to validate complete cooldown scenarios. The process model is solved at each sampling time using numerical algorithms. The linear algebraic subsystems are solved by a linear equation solver and non-linear algebraic subsystems are solved with a tearing technique which finds a reduced subset of variables (tearing variables) to iterate over them. Then, remaining paired variables can be calculated explicitly as a function of these variables finding. Iterations are performed until residues between calculated values

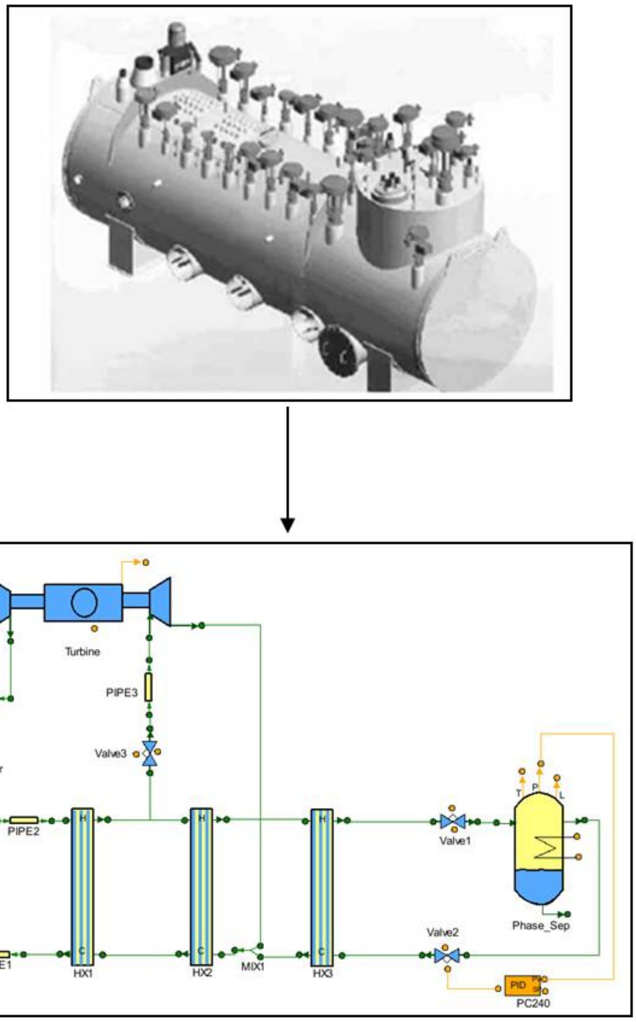

Figure 4.17: Real cold box and the simulated model.

and expected values are canceled. In the cold-box model, the subset of tearing variables are pressure drop ratios of valves. A DASSL algorithm (Differential-Algebraic System Solver)is used to solve numerically differential and algebraic equations. The solution method is based on replacing the time derivative $\ddot{y}(t)$ with an approximation by differences and then solving the resulting equations for time t_n using an implicit Newton-Raphson method by iterating.

Each cryogenic component is composed of Helium ports (inlets and outlets). In the model, an Helium port is represented by its pressure, mass flow, temperature and enthalpy. Helium properties are characterized by three state variables, so, properties have to be calculated from two known states, calculated for a given pressure and temperature. Helium properties are either extracted from a specialized library or a linear interpolations is done from tables. Interpolations with small intervals allow a faster calculation of Helium properties with a sufficient accuracy, for temperatures below 5 K or when Helium becomes liquid, interpolations are inaccurate due to the high non-linearities of Helium properties (like specific heat and density).

The Cold box contains 6 plate-fin counter-current heat-exchangers in brazed aluminum grouped in three blocks. Each heat-exchanger is defined by a set of parameters at designed condition: global heat transfer coefficient, pressure loss, temperature, pressure, mass flow, mass, volume and aluminum heat capacity of each stream. Heat transfer and mass flow are calculated as functions of design values using a space discretization (each HX is divided in several nodes).

CMS cold box is equipped with three expansion turbines to cooldown Helium by expansion. The model uses the design parameters: inlet and outlet pressures, inlet temperature, shaft speed, mass flow, adiabatic efficiency, rotor blade diameter and inertia moment of the rotor. The mass flow rate and the outlet temperature are functions of the pressure drop and of the inlet temperature. There is no mass accumulation inside turbines and forward flows only are taken into account. A hybrid model is used due to the different behaviours of the flow inside the turbine as the mass flow can be subsonic or sonic according to the pressure ratio.

Discussion

The simulation environment has been validated and it respect the real control architecture. The process and control engineers have successfully worked together with the simulator thank to the simulator behaviour close to the real plant (4.18).

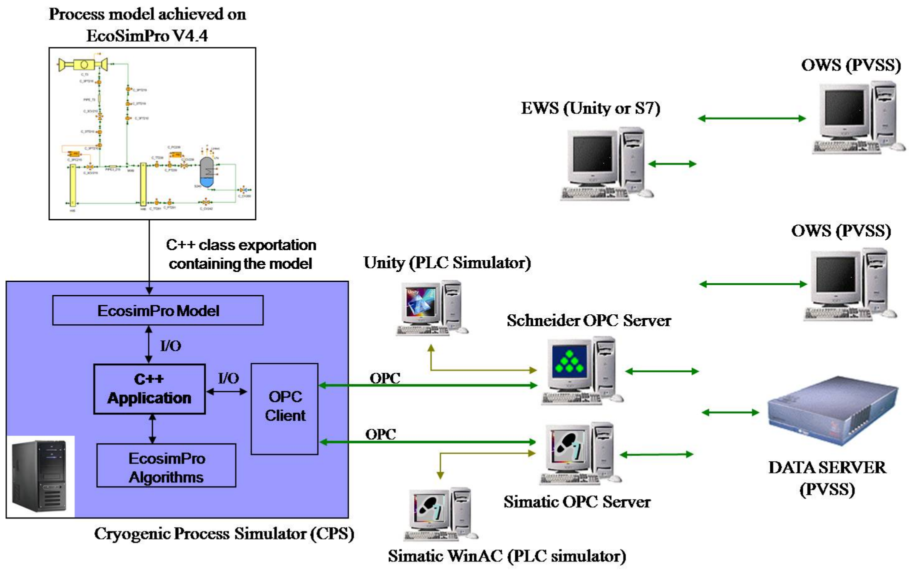

Figure 4.18: PLC code validation through simulation.

Thus it has permitted to finalized the process control system for the long LHC operation and to find new encouraging control strategies in order to optimized several cryogenic behaviour in case of disturbances. The control system and the simulator have bene installed in a cryogenic simulator room and it serve to operator either in training or investigative session.

4.2.3 A simulation study for the virtual commissioning of the CERN central Helium liquefier

The CERN cryogenics experimental infrastructure includes several cryogenic plants controlled by ABB-Master PLCs (automation Swiss company). These plants are spread through out different experimental areas around the CERN sites. In order to meet the requirements of the operation team, CERN has undertaken a major upgrade using the experience gained during the construction of the LHC cryogenic control system within the *UNICOS* framework [82]. Virtual commissioning has already shown its benefits on other large scale industrial systems such as LNG (Liquefied Natural Gas) plants [83] but has never been implemented on cryogenic plants due to the large functional span and the non-linearities involved. Our motivation takes its origin in the important time saving factor during plant re-start by minimizing unexpected errors in the program producing undesired process behaviour. The work focuses on the interaction between a cryogenic process simulator, a PLC and its supervision. It presents control adaptation problems on a simulator integrating physical models of valves, heat exchangers, turbines, phase separator and Helium data. The entire model encompasses 2'700 equations and has the capacity to reproduce the cold-box dynamic behaviour from 300 K to 4.5 K.

Simulation principles

Simulation architecture CERN has developed a simulation environment for cryogenic processes called PROCOS (Process & Control Simulator, see Section) to perform dynamic simulations for operator training, control optimization and control validation [84]. This environment uses the same three layers control architecture as the real processes, see Fig. 4.19. In simulation, the Cryogenic Process Simulator (CPS) is a C++ application embedding a model of the process in order to provide simulated input and output to the control layer. The Process and Logic Controllers are replaced by PLC emulators provided by manufacturers. The data server and supervision clients remain the same. All components are communicating on the Ethernet network using an OPC protocol.

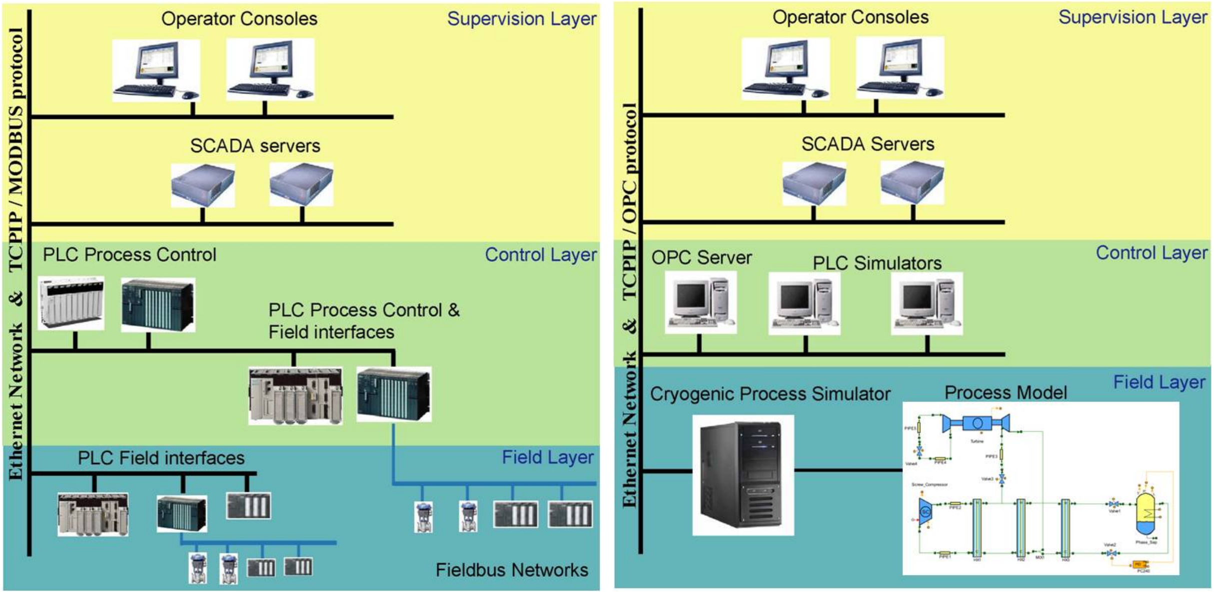

Figure 4.19: The real and the simulated control architecture for cryogenic processes.

Process models Models are designed with EcosimPro©, a commercial modeling and simulation software allowing to develop dynamic models from differential and algebraic equations.

Cryogenic systems are modeled using an object-oriented approach where each cryogenic equipment is an independent model. The models are based on thermodynamic and hydraulic equations. Helium properties are taken from data tables calculated offline with the specialized HEPAK library [80]. In this way a cryogenic library including all components (heat exchangers, turbines, valves, phase separators, pipe, compressors) used at CERN cryogenic installations was developed.

Process definition and model of the central liquefier - Cold-Box TCF50

The CERN Central Liquefier plant produces all year long liquid Helium at 4.5 K for distribution via mobile dewars to CERN-wide users. The Helium liquefier is composed of several units:

- A compressor station which compresses gaseous Helium from 1.1 bar to 12.5 bar.
- A TCF50 coldbox provided by Linde® cooling down Helium from 300 K until 4.5 K

with a 2 $g \cdot s^{-1}$ liquefaction rate. The scheme of the coldbox is shown in Fig. 4.20.

- An intermediate 5 m^3 dewar to stock the liquid Helium before distribution in small dewars.
- A liquid Helium distribution box dispatching the Helium dewars.

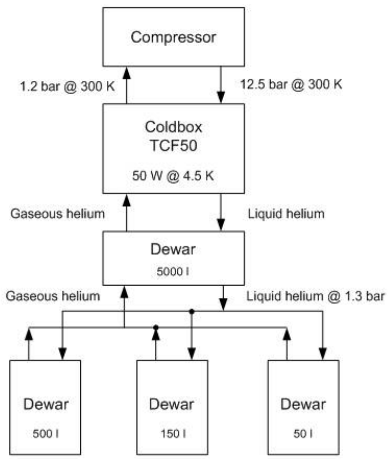

Figure 4.20: The CERN central liquefier.

The model of the coldbox is based on the information provided in Section 2.4 and depicted in Fig. 2.7.

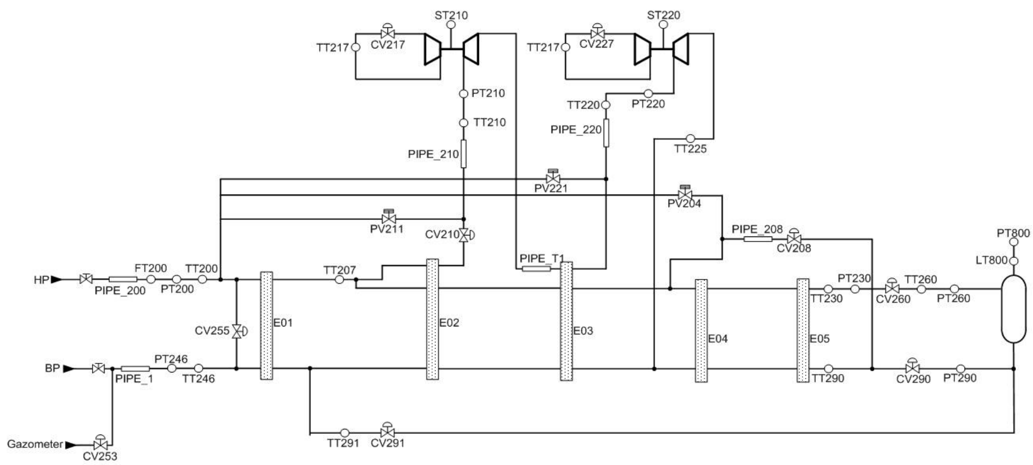

Figure 4.21: The TCF50 simulation model.

For our study, we have limited the simulation to the critical part of the installation. In this way, only the coldbox and the intermediate cryostat have been modeled. We consider that the compressor station and the vacuum system work perfectly under constant boundary conditions. In order to proceed to the virtual commissioning, the simulated coldbox behaviour must be as close as possible to the reality. For this reason, the model needs all the mechanical and cryogenic parameters. Heat exchangers are defined by their nominal pressures, mass flows, internal volumes and masses. Turbine models use the nominal values of speed, temperature, pressure, isentropic efficiency and power extracted by the break circuits. Pipes and dewars take as parameters their respective length, diameter, height and heat loss, and valve are modeled according to the valve coefficients (Cv or Kv). Using the CERN cryogenic component library, process modeling consists in reproducing the process architecture by object drag and drop on the EcosimPro graphical interface. Regarding the TCF50 technical datasheet and the modifications achieved on the apparatus to obtain a liquid Helium production unit, component parameters have been adjusted in the simulation model to fit with the real plant dynamics.

A simulator as an offline commissioning tool

The simulation process is calculated by 2 Intel Dual-core 1.86 GHz with 2 GB of RAM. One is dedicated to the process and the PLC simulator, and the other is used for the *SCADA* part (PVSS, process visualization and control system software) and the OPC© Server. Once the process simulation model has been finished, the data collected from the real cooldown achieved under the ABB PLC have been compared with the simulated data.

Based on know-how control specifications for such plants, the ABB control logic was transformed into a standardized structure, taking into account process singularities. Afterwards, the offline commissioning performed on the new control logic through the simulator allowed to correct and optimize the new PLC programs. Consequently, the control logic of the bypass valve, CV208, the Joule-Thomson valve, CV260, and the return valve, CV290, has been adjusted and validated. To enhance turbine safety, a new turbine program has been developed and checked using simulations. Therefore, the control of the 3 inlet valve and the brake circuit were modified, implying a review of valve ramp slopes, and turbine security interlocks. The previous and new turbine start sequence can be seen in Fig. 4.22.

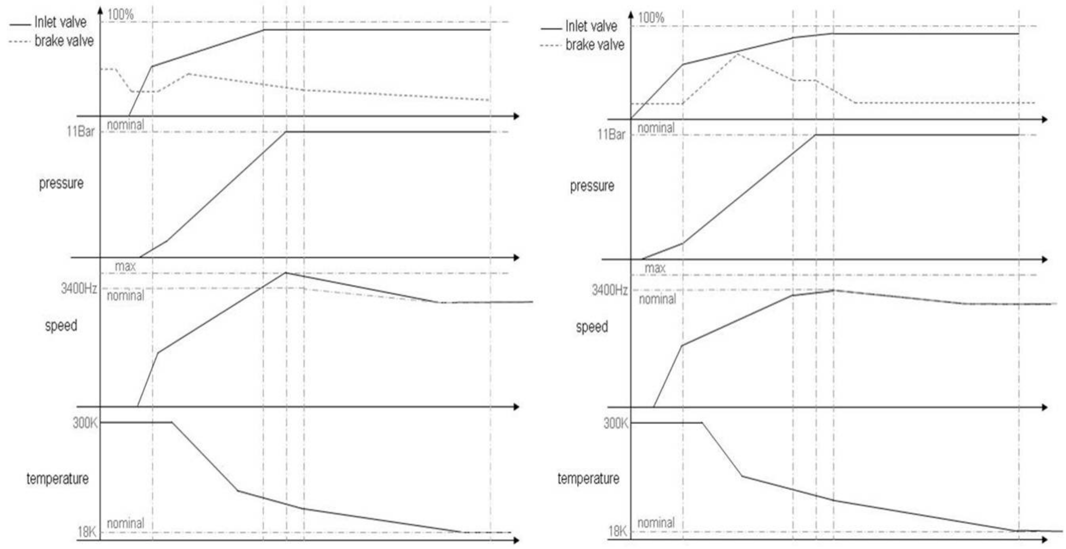

Figure 4.22: Turbine start sequence, previous (left) and new (right) control logic.

In a second time, after the completion of the installation, we have done the comparison between the real plant and the simulation to confirm the quality of the model. The results are shown in Fig. 4.23.

The offline commissioning also focused on the validation of PI controllers. According to the simulated responses, PI coefficients have been tuned and the reversed action parameters, allowing the inversion order from controller to the valves, have been tested and verified. The different simulated temperatures, pressures and mass flows agree with the ones observed during the cooldown from 300 K to 4.5 K, see Fig. 4.24 where the temperature after the first heat exchanger (TT207), the temperature after the second turbine (TT225) and the total mass flow obtained in simulation are plotted and compared. The simulation is around 5 times faster than the real time which is a relevant simulation speed for such a system. The simulated behaviour of the turbines is closed to the real turbine dynamics. Therefore, the turbine model used for the virtual commissioning reacts correctly. In the simulator, a small difference in the power of the brake circuit results in an amplification of the controller working on the brake valve but does not affect the turbine operation. We can observe a disturbance after 2 hours of simulation. This difference be-

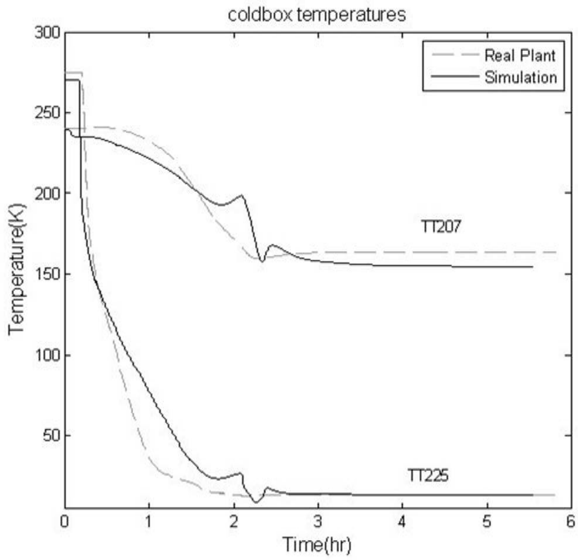

Figure 4.23: Coldbox temperatures.

tween the simulation and the real plant corresponds to the Joule-Thomson valve opening which leads to a different process reaction in simulation. This modification of the valve position provides a flow modification in the dewar and a return of warm gaseous Helium in the coldbox. This difference does not have any impact on the virtual commissioning which is not disturbed by undesired control interlock.

Discussion

Within the *UNICOS* framework, a dynamic simulator able to reproduce large-scale refrigeration plant behaviour has been used to perform a pre-commissioning of the entire control system. Based on our experience on cryogenic plant commissioning [85, 86], we were able to assess the utility of the simulator environment. This virtual commissioning minimizes the time for plant re-start and allows operators to anticipate unforeseen plant reactions, using it as a training test bench. The encouraging results obtained have clearly shown that we are able to avoid programming mistakes and perform control optimization through simulations. A long term perspective will consist in using the simulation environment to explore different control algorithms applied to the cryogenic systems.

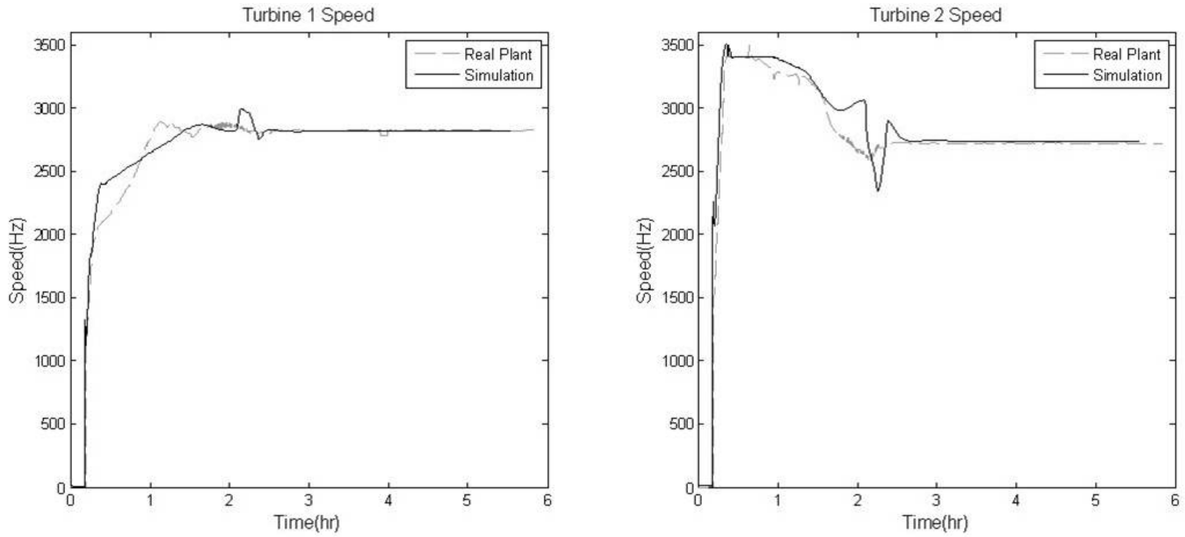

Figure 4.24: Turbine speeds.

4.2.4 Helium cryogenic plant off-line commissioning and operator training: two applications of the PROCOS simulation system at CERN

The CERN Helium cryo-plants [86] are controlled by several industrial Programmable Logic Controllers (PLCs) in order to ensure a high degree of reliability as required by cryogenic operation specification. Moreover, LHC cryogenic control architecture and control policy are based on the hierarchical multilevel and multilayer *UNICOS* framework [13]. CERN, during the last few years, has shown increasing interest on the real-time simulator techniques dedicated to large cryogenics processes. The resulting simulators have contributed to improve knowledge of cryogenic system [87, 88] but also they have been adapted in order to contribute for a new commissioning technique for Helium cryogenics plant. The virtual commissioning approached [70] has brought an important time saving factor during plant re-start by minimizing unexpected errors in the program producing undesired process behaviour.

Control system architecture for simulation

The architecture of the PROCOS simulation tools, based as UNICOS on a three-layer control architecture (field, control and supervision layers), is shown in Fig. 4.25. The

PLCs are replaced by PLC simulators which are software provided by PLC manufacturers and the supervision system (*SCADA*) remains the same. All variables are exchanged through an OPC server also provided by PLC manufacturers. Nevertheless, the fact to

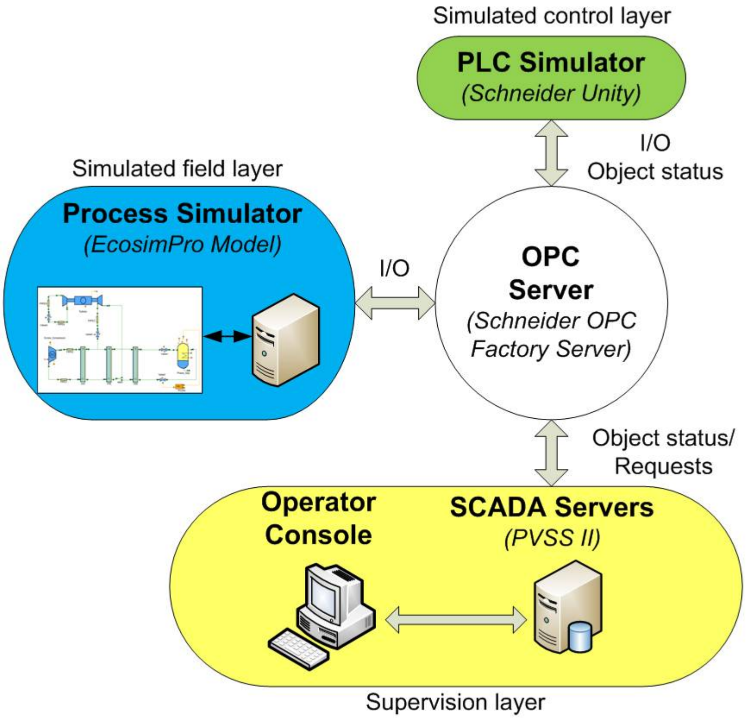

Figure 4.25: The PROCOS structure.

reuse this architecture implies several constraints for the good working of the virtual commissioning and for operator training. First, real systems are using field buses to exchange data whereas the simulator uses OPC protocol. Thus, all variables have to be mapped differently inside PLCs and *SCADA*. Fortunately, *UNICOS* is based on code generators (for PLC and *SCADA*) allowing us to generate automatically all modifications in an efficient and fast way. Moreover, about the half of the sensor signals are not simulated in such cryogenic systems because infrastructure facilities are not embedded in models (power switches, cooling water, compress air and vacuum). Hence, sensor signals which are simulated have to be selected one by one as first step in order to link correctly PLC and model variables through the OPC server and non-simulated sensors have to be forced to correct values in PLCs to ensure the absence of interlocks. Once again, this step is simplified by using automatic generation tools: only modifications in the inputs/outputs database are necessary in this case. We also have to point out the fact that the achievement of the process model is a difficult task that demands an important development time event if we are now able to construct such a model for a classical system in several weeks due to our experience on these processes. One of our objectives for the future is to alleviate this step by introducing simplified process dynamics and better generation tools. Figure 4.26 show an example of the EcosimPro model with the corresponding synoptic in the *SCADA* system.

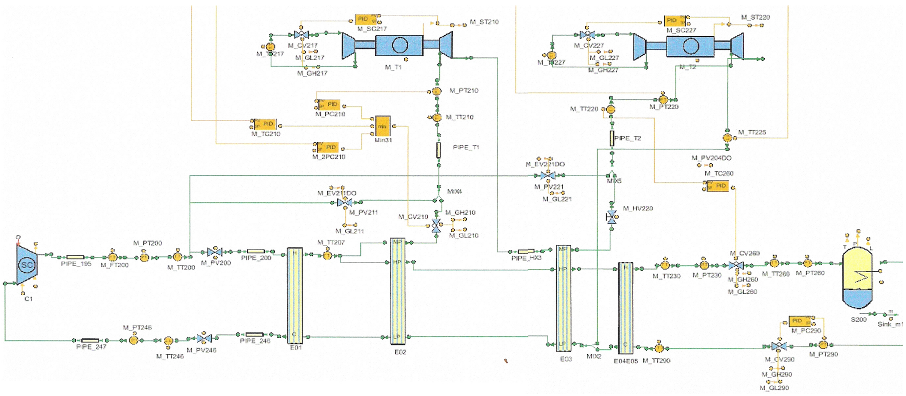

Figure 4.26: The FRESCA Helium refrigerator model.

Virtual commissioning experience

The virtual commissioning includes operational tests aiming at demonstrating all functions specified in the control system. Once commissioned and qualified for operation, sub-systems are used in a cascade way to commission subsequent sub-systems, allowing testing and tuning collective behaviour. This gives the possibility to progressively get experience and define eventual programming errors or adapt corresponding sequences.

Helium compressor set. The initial test started from the Helium compressor station which provides Helium flow to the cold box. Hence the compressor start-up sequence and the high and low pressure control have been verified and adjusted. This step allows us to detect wrong variable connections and wrong ranges of some sensors.

Moreover some step conditions were also modified in agreement with our requirements.

Refrigerator Helium flow circuit and turbines circuit. Once the refrigerator is receiving the Helium flow from the compressor it is divided in two streams: the Joule-Thomson circuit (J-T circuit) that goes to the heat exchangers and the phase separator; and the turbine circuit. Each circuit is controlled by a specific process control object managing different actuators. The control logic of the bypass valve in the J-T circuit has been tested with different configurations and the best solution has been chosen in order to achieve a better cool down speed of the system. Moreover the inlet and return valves of the phase separator have been adjusted in order to avoid, in a start up situation, abnormal oscillations caused by the warm Helium contained in a close circuit between the client dewar and the cold box.

Turbine safety and stability. To enhance turbine safety and stability, a new logic has been developed and validated. The control of the inlet and brake valves were modified according to the new refrigerators technology (Linde®) where the turbine speed is only regulated by the brake valve and the inlet valve regulates the pressures and the outlet temperature. In this work the review of valve ramp slopes, and turbine security interlocks as well as of the PID parameters of the different controllers has been optimised.

Operators training: familiarity within the ***UNICOS*** control framework

The *UNICOS* framework HMI interacts with operators by mean of widgets and dedicated panels called faceplates.

These graphical elements inform operators on the object status and provide dynamic trends, multi-trends, navigation functionalities, interlock diagnostics and allow him to send orders. These facilities make this framework a powerful standardized interface allowing troubleshooting flexibility during tests, and easiness of operation. The virtual operator training finds his best utilities when new technical personnel join the operation team and needs an appropriate and intensive training period for a global discovery of

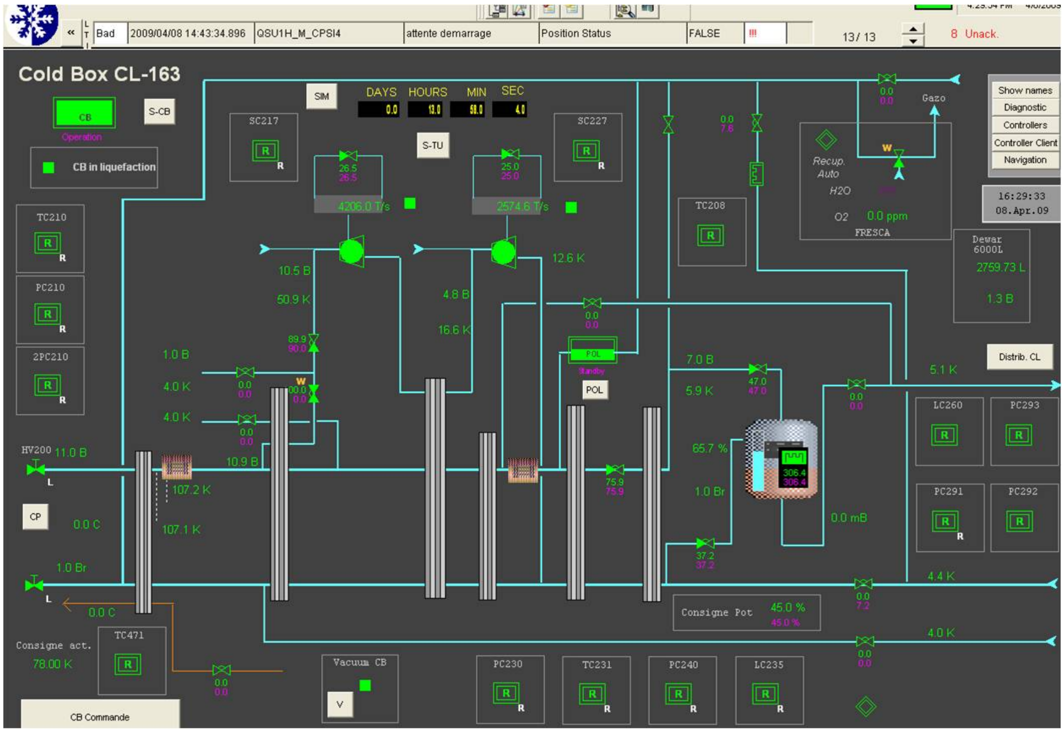

Figure 4.27: Refrigerator synoptic under PVSS-ETM®.

the operation tool. Training in the critical cryogenic scenarios PROCOS embeds different useful features for operator training such as the possibility to perform real-time or accelerated simulations and to run, freeze, save and restore predefined process states. It can also introduce malfunctions in order to trail the operator skills. For example, critical interlocks can be generated such as a turbine failure in order to evaluate operator reactions. Finally the PVSS supervision interface (Fig. 4.27) also lets the monitoring of the training session progress with trends of process sensors and allows the evaluation of how an identical critical scenario has been dealt under different operation constraints.

Discussion

The work has two main contributions: an optimized procedure for virtual commissioning of large-scale cryogenic processes and a starting project for setting up an operator training station. CERN experience has shown that a control system which has been virtually commissioned with the PROCOS environment shows a high efficiency in the global context and needs only insignificant logic modifications during the real commissioning. It will be useful to improve software tools in order to render the modeling step easier and faster. Off line commissioning is used only when the time constraint for a complete refurbishing of the control system is the critical factor. The first results show that the virtual cryogenic operator training is an efficient and pedagogic tool. It allows operators to be trained on the most critical phases of real cryogenic processes. It can also serve as an efficient HMI *UNICOS* framework guide allowing cryogenic operators to become familiar within a short training period.

Conclusions

The work presented in this thesis is the result of more than ten years of experience, acquired during the construction of the LHC cryogenic control and electrical systems. During this period, different approaches have been used: (*i*) a conventional industrial approach based on PID control loops, and (*ii*) an innovative scientific approach to control trough advanced algorithms, on which at the moment some studies are in progress but which is still used in extremely limited applications.

Even though the former approach has been much widely used so far at CERN, the significant nonlinearities of such systems due to extremely changeable gas properties over the pressure and temperature range of interest for cryogenic applications, strongly demand for more advanced solutions. Dead times, inverse responses and other features push to the limit the traditional PID-based controllers, and pave the way for the introduction of advanced control techniques, thus allowing to (*i*) increase system availability through the minimization of set-up and tuning times, (*ii*) enhance its reliability, and (*iii*) improve the capability to cope with transitions between different operating states which now result tricky to handle properly.

In this thesis a twofold contribution was given:

1. A synthesis of scientific and industrial approaches to identification and control, through their application to real large scale cryogenic systems employed at CERN and their implementation on Schneider PLCs. Within the frame of standard identification and control techniques, after a review of the state-of-the-art solutions proposed in literature, it was shown what kind of problem these traditional approaches may pose when used in real large scale applications. A solution was presented

through the activities carried out at CERN for parametric identification and control design of the ATLAS Nitrogen heat exchanger, which has been working in optimal condition since 2003 on industrial controllers. It is worth mentioning that the heat exchanger is normally unavailable for experimentation, and that the practical work carried out on it was made possible only by an exceptional authorization granted to the author during commissioning period. This constitutes an unprecedented case study and one of the main contributions of this thesis. A contribution to the implementation on industrial platforms of advanced control techniques within the CERN *UNICOS* framework was also presented: the *MultiController* object gives alternative solutions to standard PID controllers for the implementation of control loops on PLCs, thus increasing the available control solutions to solve highly complex problems.

2. A novel approach to modeling and control of the aforementioned systems through the definition and the simulation of (i) a suitable model based on mass flow and heat transfer equations, and (ii) the design of a Time Delay Control. A novel theoretical approach to modeling and control for large scale cryogenic systems was studied, whose formulation was applied to the liquid Krypton condenser of the NA62 experiment. The modeling phase was followed by a prior optimization of the parameters of the existing PID-based control loop and then by the design of an advanced control strategy, the Time Delay Control, whose performance obtained in simulation was presented in comparison with those of the traditional PID-based control loop, thus showing the improvement allowed by the new approach. The implementation of the proposed solution required a further phase of analysis in order to statistically estimate the communication time delays usually encountered during the operation of the system under control. The results of these analysis were also presented.

Finally, the last part introduced an optimized procedure for virtual commissioning of large-scale cryogenic processes, and a project to set up a cryogenic operator training station. CERN experience has shown that a control system which has been virtually

commissioned with the PROCOS environment has a high efficiency in the global context and needs only minor logic modifications during the real commissioning.
The first results showed that the virtual cryogenic operator training is an efficient and pedagogic tool. It allowed operators to get trained on the most critical transition phases of real cryogenic processes. It served also as an efficient *UNICOS* framework guide allowing cryogenic operators to become familiar with the Human-Machine Interface within a short training period.
Although off-line commissioning is used only when the time constraint for a complete refurbishing of the control system is the critical factor, it will be useful to improve software tools in order to make the modeling step easier and faster.

Perspectives

A novel approach to the control of cryogenic plants was previously proposed, including the phase of modeling a heat exchanger through balance equations, describing mass flows and heat transfer evolution in the time domain under the assumption of spatial uniformity of the physical properties of interest. On the basis of the resulting model, it was possible to design and implement a controller, estimate the model parameters, and evaluate the suitability of the control strategy.
Satisfactory results were obtained. Nonetheless, it was deemed useful to further investigate one of the basic assumptions made in the formulation of the model, namely that the equations describing the evolution of the system take into account only variations in the time domain, whilst a uniformity assumption is assumed to hold in the space domain. To this purpose, a new model was developed and presented in Appendix A by considering variations in both the aforementioned domains.
In the refined model, Nitrogen is considered as a perfect fluid: viscosity and thermal conductivity are neglected as it has a very low viscosity and a very low thermal conductivity. Moreover, gaseous Nitrogen is considered as a compressible gas. After developing the model equations and discretizing them through a suitable finite difference scheme, a numerical implementation available in commercial tools was proposed to solve the discrete

equations and simulate the system.

At the moment of submitting this thesis, the work was still in progress and it was therefore impossible to include in this dissertation any related results. Anyway, this parts plays a central role among the contributions of the thesis, since it constitutes the starting point of further developments of the proposed modeling and control approaches. In particular, as first step further investigation will be required to assess the possible benefits deriving from this approach, and to check whether the additional complexity it introduces is balanced by significant improvements both in the model prediction accuracy and in the possible enhancements of the control strategy.

Appendix A

Time and space approach to condenser modeling

In this Appendix, an improved model for a Nitrogen heat exchanger is presented. This model is based on the work of B. Bradu [89] and refines the results given in Chapter 3.2 by introducing partial differential equations describing the physical problem in the time and space domains, thus providing a starting point of further developments of the proposed modeling and control approaches. At the moment of closing this work, the modeling phase was still in progress and it was therefore impossible to include any results.
In the following, Nitrogen is considered as a perfect fluid: viscosity and thermal conductivity are neglected as it has a very low viscosity and a very low thermal conductivity. Moreover, gaseous Nitrogen is considered as a compressible gas. After developing the model equations and discretizing them through a suitable finite difference scheme, a numerical implementation available in commercial tools is proposed to solve the discrete equations and simulate the system.

A.1 Modeling of the flow

First, the main flow line is modeled, neglecting interconnections. According to previous assumptions, an inviscid flow in the header B is considered. Thus, the flow can be described by Euler equation which is obtained from Navier-Stokes equation neglecting the viscosity and the thermal conductivity [90]. The conservative form of Euler equations is the following:

$$\frac{\partial}{\partial t}\begin{bmatrix}\rho\\ \vec{M}\\ E\end{bmatrix}+\vec{\nabla}\cdot\begin{bmatrix}\rho\cdot\vec{V}\\ \rho\cdot\vec{V}^T\otimes\vec{V}+P\cdot I\\ \rho\cdot\vec{V}\cdot\left(u+\frac{P}{\rho}\right)\end{bmatrix}=\begin{bmatrix}0\\ 0\\ q\end{bmatrix}\tag{A.1}$$

where the different variables are described in Tab. A.1. These three equations represent mass, momentum and energy balances. The momentum is defined as $\overrightarrow{M}=\rho\cdot\overrightarrow{V}$ and the total energy per unit volume is $E=\rho\cdot(u+\frac{1}{2}\cdot(V_x^2+V_y^2+V_z^2))$.

Symbol	Description	Unit
c	Sound velocity	$m.s^{-1}$
D	Diameter	m
E	Energy per unit volume	$J.m^{-3}$
fr	Darcy-Weisbach friction factor	$-$
h	Specific enthalpy	$J.kg^{-1}$
h_c	Heat transfer coefficient	$W.m^{-2}.K^{-1}$
k	Thermal conductivity	$W.m^{-1}.K^{-1}$
L	Length	m
$\dot{m}$	Mass flow	$kg.s^{-1}$
$\vec{M}$	Momentum	$kg.m^{-2}.s^{-1}$
P	Pressure	Pa
Pr	Prandtl number	$-$
Re	Reynolds number	$-$
S	Hydraulic cross section	m^2
q	External heat inputs	$W.m^{-3}$
T	Temperature	K
u	Specific internal energy	$J.kg^{-1}$
$\vec{V}$	Gas speed	$m.s^{-1}$
μ	Viscosity	$Pa.s$
ρ	Density	$kg.m^{-3}$
$g = 9.81$	Gravity acceleration	$m.s^{-2}$
$R = 8.31$	Perfect Gaz constant	$J.mol^{-1}.K^{-1}$
$R_{He} = 2078$	Helium specific constant	$J.kg^{-1}.K^{-1}$
$C_v = 3148$	Helium specific heat	$J.kg^{-1}.K^{-1}$
$\gamma = 1.66$	Specific heat ratio, $\frac{C_p}{C_v}$	$-$

Table A.1: Main variables and physical constants.

The following assumptions on the flow are assumed:

- flux according to the x direction only (the main flow direction) : $V = V_x$ and $M=\rho\cdot V_x$;
- in operational conditions, the kinetic component can be neglected: $\rho\cdot|\overrightarrow{V}|^2\ll P$, which implies that $\rho\cdot\overrightarrow{V}^T\otimes\overrightarrow{V}+P\cdot I\approx P\cdot I$.

Considering the above approximations, Euler equation (A.1) can be expressed in 1D as:

$$\frac{\partial X(x,t)}{\partial t} + F(X) \cdot \frac{\partial X(x,t)}{\partial t} = Q(x,t) \tag{A.2}$$

where $X = [\rho, M, E]^T$ is the state vector, F is the Jacobian flux matrix and $Q = [0, 0, q]^T$ is the source vector.

A.1.1 Modeling for an ideal gas flow

To compute the Jacobian flux matrix, it is necessary to include an equation of state to link pressure, density and internal energy. First, an ideal gas is considered: it is assumed that $u = C_v \cdot T$, which leads to the following equation of state:

$$P = \rho \cdot R \cdot T = \rho \cdot u \cdot fracRC_v = \rho \cdot u \cdot \hat{\gamma} \tag{A.3}$$

where the constant $\hat{\gamma} = (\gamma - 1)$. For this case, the Jacobian matrix was calculated in [90, 91] as:

$$F = \begin{bmatrix} 0 & 1 & 0 \\ \frac{(\gamma-3)V^2}{2} & (3-\gamma)\,V & \hat{\gamma} \\ \hat{\gamma}V^3 - \frac{\gamma V E}{\rho} & \frac{\gamma E}{\rho} - \frac{3\hat{\gamma}V^2}{2} & \gamma V \end{bmatrix} \tag{A.4}$$

and the eigenvalues of the Jacobian are:

$$\begin{cases} \lambda_1 = V + c \\ \lambda_2 = V \\ \lambda_3 = V - c \end{cases} \tag{A.5}$$

where c is the speed of sound, defined by:

$$c = \sqrt{\gamma R T} = \sqrt{\frac{\gamma P}{\rho}} = \sqrt{\gamma\hat{\gamma}\left(\frac{E}{\rho} - \frac{V^2}{2}\right)} \tag{A.6}$$

All the eigenvalues of the Jacobian are real and distinct. This means that Eq. (A.2) is a strictly hyperbolic system of equations. Moreover, for subsonic flows ($V < c$) there are two positive eigenvalues and one negative eigenvalue: information is propagated forward and backward and the eigenvalues represent the different speeds of propagation.

A.1.2 Modeling for a gaseous Nitrogen flow

The previous equations cannot be directly applied to Nitrogen flows at low temperature as the equation of state (A.3) is not valid anymore. Hence, the following empirical formulation for the Nitrogen internal energy is considered:

$$u = u_0 + C_v \cdot T \tag{A.7}$$

where u_0 is a constant. This equation remains valid for gaseous Nitrogen at low pressure ($P < 10\ kPa$), with a relative error less than 1% in a wide temperature range. For higher pressures, this equation is still valid for gaseous Nitrogen far from the saturation line and far from the critical point.

We are interested in simulating the Nitrogen flow with the equipment in stable thermal conditions when the calorimeter is in operation. Within these ranges, Eq. (A.7) remains valid and the equation of state and the sound velocity for Nitrogen become respectively:

$$P = \rho \cdot R_{He} \cdot T = \rho \cdot (u - u_0) \cdot \hat{\gamma} \tag{A.8}$$

$$c = \sqrt{\gamma\hat{\gamma}\left(\frac{E}{\rho} - \frac{V^2}{2} - u_0\right)} \tag{A.9}$$

A new Jacobian flux matrix is computed with additional terms containing the constant u_0:

$$F = \begin{bmatrix} 0 & 1 & 0 \\ \frac{(\gamma-3)V^2}{2} - u_0\hat{\gamma} & (3-\gamma)\,V & \hat{\gamma} \\ \hat{\gamma}V^3 - \frac{\gamma V E}{\rho} & \frac{\gamma E}{\rho} - \hat{\gamma}\left(\frac{3V^2}{2} + u_0\right) & \gamma V \end{bmatrix} \tag{A.10}$$

and the eigenvalues are the same as for an ideal gas, see Eq. (A.5). Thus, the system of equations is still a strictly hyperbolic system with the same propagation speeds than for ideal gases but the dynamics is different.

A.2 Discretization scheme

To solve numerically the system of partial differential equations, the flow is discretized in N nodes, see Fig. A.1. A finite difference method was chosen to compute space and time

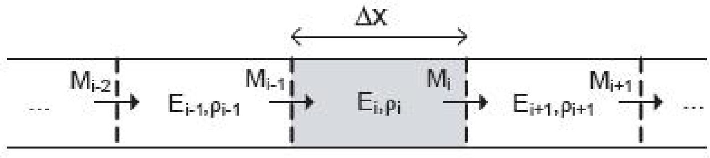

Figure A.1: Discretization of the main flow.

derivatives using a first order upwind scheme, as suggested in [91]. The time discretization is performed according to an implicit discretization scheme based on a backward Euler method. Dirichlet boundary conditions are set as follows:

- the input energy $E(0,t) = E_1(t)$;
- the input density $\rho(0,t) = \rho_1(t)$;
- the output momentum $M(L,t) = M_N(t)$.

Hence, mass and energy are propagated forward whereas momentum is propagated backward, which is in agreement with the signs of eigenvalues obtained in Eq. (A.5) and with the physics of the flow. As the compressors are "pulling" Nitrogen atoms in the line, the momentum propagation is backward whereas the mass (Helium atoms) and energy (heat) are naturally transported with the flow. Thus, in the framework of the upwind scheme, $\partial\rho/\partial x$ and $\partial E/\partial x$ are approximated by a first-order backward finite difference and $\partial M/\partial x$ is approximated by a first-order forward finite difference. The following algebraic system is then obtained:

$$\dot{X}_i(t) + \frac{A_i(X_i)}{\Delta x}X_{i-1}(t) + \frac{C_i(X_i)}{\Delta x}X_{i+1}(t) = Q_i(t) \tag{A.11}$$

where i denotes the value at x_i and:

$$X_i = \begin{bmatrix} \rho_i \\ M_i \\ E_i \end{bmatrix}$$

$$A_i = \begin{bmatrix} 0 & 1 & 0 \\ -\frac{(\gamma-3)V_i^2}{2} + u_0\hat{\gamma} & -(3-\gamma)V_i & -\hat{\gamma} \\ \hat{\gamma}V_i^3 - \frac{\gamma V_i E_i}{\rho_i} & \frac{\gamma E_i}{\rho_i} - \hat{\gamma}\left(\frac{3V_i^2}{2} + u_0\right) & \gamma V_i \end{bmatrix}$$

$$B_i = \begin{bmatrix} 0 & -1 & 0 \\ 0 & 0 & 0 \\ -\hat{\gamma}V_i^3 + \frac{\gamma V_i E_i}{\rho_i} & -\frac{\gamma E_i}{\rho_i} + \hat{\gamma}\left(\frac{3V_i^2}{2} + u_0\right) & \gamma V_i \end{bmatrix}$$

$$C_i = \begin{bmatrix} 0 & 0 & 0 \\ \frac{(\gamma-3)V_i^2}{2} - u_0\hat{\gamma} & (3-\gamma)V_i & \hat{\gamma} \\ 0 & 0 & 0 \end{bmatrix}$$

$$Q_i = \begin{bmatrix} 0 \\ 0 \\ q_i \end{bmatrix}$$

A.3 Heat transfer

The term q_i in the energy balance represents heat transfers between the fluid and its environments per unit volume in a node.
Heat losses can be divided in two parts: static losses q_{stati} due to radiation, conduction and vacuum barriers and dynamic losses q_{convi} due to convection between the stainless steel pipe and the fluid:

$$q_i = q_{stati} + q_{convi}(t, \rho_i, M_i, E_i) \tag{A.12}$$

To compute dynamically the convection heat transfer between the pipe and the fluid, supplementary variables are introduced to characterize the pipe properties: its temperature T_w, its specific heat C_{pw}, its mass M_w and its internal surface S_w. The specific heat can be computed from an empirical logarithmic polynomial of the 8^{th} order valid between 70 K and 300 K [92]. The convective heat transfer coefficient h_c is computed by:

$$h_{ci} = \frac{Nu_i \cdot k_i}{D} \tag{A.13}$$

where the Nusselt number Nu is computed from the Colburn formulation [93]:

$$Nu_i = 0.023 \cdot Pr_i^{1/3} \cdot Re_i^{0.8} \tag{A.14}$$

because the flow regime is always turbulent (Reynolds number $Re > 10^5$). Finally the convection heat transfer per unit volume is computed by the Newton law:

$$q_{convi} = \frac{h_{ci} \cdot S_{wi} \cdot (T_{wi} - T_i)}{S \cdot \Delta x} = \frac{M_{wi}}{S \cdot \Delta x} \cdot C_{pwi} \cdot \frac{dT_{wi}}{dt} \tag{A.15}$$

A.4 Pressure drops

The equipment is not perfectly horizontal, and it results a hydrostatic pressure. This hydrostatic pressure is not taken into account in previous equations and should be considered.

Moreover, friction phenomena are not embedded (the flow is considered inviscid) whereas frictions can lead to pressure drops not negligible in the case of a very low pressure flow. Thus, we propose to replace the momentum partial differential equation ($\partial M/\partial t + \partial P/\partial x = 0$) by an algebraic equation to compute the mass-flow $\dot{m}_i$ in each cell (compartmental approach).

The pressure in a cell is computed using the equation of state (A.8) and the total pressure drop in a cell can be computed as the sum of the hydrostatic pressure difference and the friction pressure drop:

$$\Delta P_i = P_i - P_{i+1} = \rho_i \cdot g \cdot dz_i + fr_i \cdot \frac{\Delta x}{D} \cdot \frac{\dot{m}_i^2}{2 \cdot \rho_i \cdot S^2} \tag{A.16}$$

where dz_i is the elevation over the cell i and fr_i is the Darcy-Weisbach friction factor. The line can be considered as a smooth pipe and the flow is always turbulent with a Reynolds number $Re > 2 \cdot 10^4$. In this case, the friction factor can be computed from the empirical formulation of Kakac, Shah and Aung [94]:

$$fr_i = 0.184 \cdot \mathrm{Re}_i^{-0.2} = 0.184 \cdot \left(\frac{D \cdot \dot{m}_i}{S \cdot \mu_i}\right)^2 \tag{A.17}$$

Combining (A.16) and (A.17) the mass flow is calculated as function of the total pressure drop:

$$\dot{m}_i = \left(\frac{(P_i - P_{i+1}) - \rho_i \cdot g \cdot dz_i}{0.184 \cdot \left(\frac{D}{S \cdot \mu_i}\right)^2 \cdot \frac{\Delta x}{2 \cdot D \cdot \rho_i \cdot S^2}}\right)^{\frac{1}{1.8}} \tag{A.18}$$

Finally, the momentum is simply deduced from $\dot{m}_i$ adding the interconnection momentum:

$$M_i = \frac{\dot{m}_i}{S} + M_i^{ext} \tag{A.19}$$

A.5 Numerical implementation

The modeling and simulations are performed on a commercial software called EcosimPro©, which is able to simulate systems of differential and algebraic equations (DAEs) [95]. Ecosimpro© uses a DASSL algorithm to solve the DAE system [96]. This method is based on an implicit time discretization scheme:

$$\dot{y}(t) = \frac{y_n - y_{n-1}}{t_n - t_{n-1}} \tag{A.20}$$

The non-linear system dynamics is then solved by iterations for time t_n using an implicit Newton-Raphson method. The iteration matrix required by Newton-Raphson method calculates a Jacobian matrix numerically using finite differences. Note that the use of an implicit scheme renders the time integration robust with respect to numerical errors but its main drawback is the associated lack of precision.

Bibliography

[1] Oxford University Press. *Oxford English Dictionary.* 2nd edition, 1989.

[2] IIF. *New International Dictionary of Refrigeration.* INF, Paris, 3rd edition, IIR-IIF Paris edition, 1975.

[3] J. Bremer, J.P. Dauvergne, D. Delikaris, N. Delruelle, G. Kesseler, G. Passardi, J.M. Rieubland, J. Tischhauser, and F. Haug. Cryogenics for CERN experiments: past, present and future. Number CERN-LHC-96-006-ECR, page 7. CERN, Jun 1996.

[4] CERN Press Office. Achievements with antimatter. *CERN courier*, Nov 1983.

[5] European Organization for Nuclear Research (CERN). www.cern.ch.

[6] CERN TDR. Technical proposal for a general-purpose pp experiment at the large hadron collider at cern. Technical Report 43, CERN/LHCC/94-43, LHCC/P2, ATLAS, CERN, 1994.

[7] CERN TDR. Atlas liquid argon calorimeter technical design report. Technical Report 41, CERN/LHCC/96-41, ATLAS TDR 2,CERN, 1996.

[8] A. Herve, B. Blau, P. Bredy, D. Campi, P. Cannarsa, B. Cure, T. Dupont, P. Fabbricatore, S.Farinon, and F. Feyzi. Status of the construction of the cms magnet. *IEEE TRANSACTIONS ON APPLIED SUPERCONDUCTIVITY ASC*, 14(2):542–547, 2004.

[9] The compact muon solenoidal technical proposal. CERN/LHC 9438, 1994.

[10] F. Kircher et al. CMS coil design and assembly. *IEEE Transactions on Applied Superconductivity*, 12:395–398, 2002.

[11] G. Perinic, A. Caillaud, F. Dagut P. Dauguet, and P. Hirel. The helium cryogenic plant for the cms superconducting magnet. *AIP CONFERENCE PROCEEDINGS*, 613(A):232–238, 2002.

[12] Ph. Lebrun. Cryogenics for the large hadron collider. *IEEE Trans App Superc*, 10:1500–1506, 1999.

[13] Ph. Gayet and R. Barillère. UNICOS a framework to build industry like control systems: Principles and methodology. page 9, Geneva, Oct 2005. ICALEPCS'2005.

[14] M. S. Sozzi. *Discrete symmetries and CP violation*. 2008.

[15] G.D. Barr et al. Performance of an electromagnetic liquid krypton calorimeter based on a ribbon electrode tower structure. Number NIM A370, pages 413–424, 1996.

[16] ESIEE. *Identification paramétrique*, Polycopié ESIEE, Amiens, 2004.

[17] I.D. Landau. *Commande des systèmes : conception, identification et mise en oeuvre*. Paris, Jun 2002.

[18] M. Mattsson. *Evolution and Composition of Object-Oriented Frameworks*. PhD thesis, University of Karskrona/Ronneby, Sweden, 2000.

[19] I. Jacobson, M. Christerson, P. Jonsson, and G. Overgaard. *Object-Oriented Software Engineering - A Use Case Driven Approach*. 1992.

[20] O.J. Smith. A controller to overcome dead band time. 6(2):28–33, Feb 1959.

[21] M. R. Matausek and A. D. Micic. On the modified smith predictor for controlling a process with an integrator and long dead-time. *IEEE TRANSACTIONS ON AUTOMATIC CONTROL*, 44(8):1603–1606, 1996.

[22] D.W. Clarke, C. Mohtadi, and P.S. Tuffs. *Generalized predictive control - Part I. The basic algorithm*, volume 23. Elsevier Ltd., 1987.

[23] D.W. Clarke, C. Mohtadi, and P.S. Tuffs. *Generalized predictive control - Part II. Extensions and Interpretations*, volume 23. Elsevier Ltd., 1987.

[24] E.F. Camacho and C. Bordons. A generalized predictive controller for a wide class of industrial processes. *IEEE TRANSACTIONS ON CONTROL SYSTEMS TECHNOLOGY*, 6(3):372–387, 1998.

[25] G. Dreyfus, J. Richalet, and G. Lavielle. *La commande prédictive, Mise en oeuvre et applications industrielles*. Lavoisier, Dec 2005.

[26] J. Richalet. *Pratique de la commande predictive*. 1993.

[27] P. Boucher and D. Dumur. *La Commande Prédictive*. Méthodes et Pratiques de l'Ingénieur. 1996.

[28] A.W. Pike, M.J. Grimble, M.A. Johnson, and S. Shakoor A.W. Ordys. *Predictive Control: The Control Handbook*. 1996.

[29] P. Borne, G. Dauphin-Tanguy, J.-P. Richard, F. Rotella, and I. Zambettakis. *Analyse et régulation des processus industriels (Tome 2 - Régulation Numérique)*, volume 2 of *Méthodes et Pratiques de l'Ingénieur*. 1993.

[30] L. Ljung. *System Identification - Theory for the user*. Prentice Hall, Sweden, 1987.

[31] D. Graupe. *Identification of Systems*. 2nd edition. New York, 1972.

[32] The Mathworks company. Matlab.

[33] P. Borne, R. Ben Abdennour, M. Ksouri, and F. M'sahli. *Identification et commande numérique des procédés industriels*. Paris, 2001.

[34] F.F. Jimenez. *Conception sure des automatismes industriels : modélisation synchrone de langage d'automates programmables de la norme CEI-61131-3*. PhD thesis, Université Rennes 1, Rennes, France, 2001.

[35] J. Bremer. The cryogenic system for the atlas liquid argon detector. In *ICEC 18*, Bombay Mumbai, India, 2000.

[36] R. Greenwald. *Optimizing and Protecting Storage with Oracle Database*. Oracle, 11g, fourth edition, 2009. Optimizing and Protecting Storage with Oracle Database.

[37] L. Ljung. *System Identification: Theory for the User*. Prentice Hall, New Jersey, 1987.

[38] P. Gayet and al. Unicos: a framework to build industry-like control systems, principles and methodology. In *ICALEPCS 2005*, number 41, Geneva, Switzerland, 2005.

[39] Y.C. Fraigneau and P. Le Quere. Etude numerique des echanges thermiques et estimation de la distribution de temperature moyenne dans le cryostat du barrel de l'expérience atlas. Technical report, UPR CNRS 3251 LIMSI, 2000.

[40] P. Delesalle. Manuelle d'utilisation de tsx optireg. Technical report, Schneider.

[41] E. Poulin and al. Development and evaluation of an auto-tuning and adaptative pid controller. *IEEE Trans. Autom. Control*, (32):71–82, 1996.

[42] S. Cabaret and al. LHC gcs process tuning: selection and use of pid and smith predictor for the regulations of the lhc experiments' gas systems. In *ICALEPS*, Geneva, 2005.

[43] Y.C. Zhu. Multivariable process identification for mpc: the asymptotic method and its applications. *Journal of Process Control*, 8(2):101–115, 1998.

[44] M. Sanzo and C. Prada. Hiden - una interfase grafica para identificacion de sistemas. In *CONAI'96*, volume 41, La Habana, Cuba, 1996.

[45] M. Chadli. *Stabilité et Commande de Systèmes décrits par des Structures Multi-modèles: Approche LMI*. INPL-CRAN, Nancy, France, 2002.

[46] M. Chadli. On the stability analysis of uncertain fuzzy models. *International Journal of Fuzzy Systems*, 8(4):224–231, 2006.

[47] M. Chadli and P. Borne. Design of robust static output controller for uncertain fuzzy model: an lmi formulation. *Studies in Informatics and Control*, 16(4):421–430, 2007.

[48] M. Oudghiri, M. Chadli, and A. Elhajjaji. Robust observer-based fault tolerant control for vehicle lateral dynamics. *International journal of vehicle design*, 48(3-4), 2008.

[49] M. Chadli. State and an lmi approach to design observer for unknown inputs takagi-sugeno fuzzy models. *Asian Journal of Control*, 12(4), 2010.

[50] *et. al* M. Chadli. State and unknown input estimation for discrete time multiple model. *Journal of the Franklin Institute*, 346(6):593–610, 2009.

[51] *et. al* M. Chadli. Fuzzy observer for fault detection and reconstruction of unknown input fuzzy models. *International Journal of Modelling, Identification and Control*, 3(2):193–200, 2008.

[52] J. Bremer, D. Cundy, J.P.Dauvergne, A.Gonidec, G. Kesseler, W. Kubishta, G. Linser, D. Schinzel, H. Taureg, and P. Wertelaers. The liquid krypton calorimeter cryogenics for the na48 experiment. In *International Cryogenic Engineering Conference*, number 17, pages 892–904, 1998.

[53] Richard T Jacobsen, Steven G. Penoncello, and Eric W. Lemmon. *Thermodynamics Properties of Cryogenic Fluids.* Plenum Press, New York, 1997.

[54] A. Cavallini, D. Del Col, L. Doretti, G.A. Longo, and L. Rosetto. A new computational procedure for heat transfer and pressure drop during refrigerant condensation inside enhanced tubes. *Journal of Enhanced Heat Transfer*, (6):441–447, 1999.

[55] S.G. Kandlikar and T. Raykoff. Predicting flow boiling heat transfer of refrigerants in microfin tubes. *Journal of Enhanced Heat Transfer*, (4):257–268, 1997.

[56] Y.Y. Hsu. A review of film boiling at cryogenic temperatures. *Advances in Cryogenic Engineering*, (17):361–381, 1972.

[57] Randall F. Barron. *Cryogenic Heat Transfer.* Taylor & Francis, Philadelphia, 1999.

[58] N. Özisik. *Heat transfer: a basic approach.* McGraw-Hill, 1985.

[59] J.F. Sacadura. *Initiation aux transferts thermiques.* Plenum Press, Tech et Doc, 1993.

[60] S. Estrada-Flores, D.J. Cleland, A.C. Cleland, and R.W. James. Simulation of transient behaviour in refrigeration plant pressure vessels: mathematical models and experimental validation. *International Journal of Refrigeration*, (26):170–179, 2003.

[61] E. Stoorkas, S. Skogestad, and J.M. Godhavn. A low-dimensional dynamic model of severe slugging for control design and analysis. In *Multiphase'03*, San Remo, Italy, 2003.

[62] Gerhard Nygaard and Geir Nævdal. Modelling two-phase flow for control design in oil well drilling. In *IEEE Conference on Control Applications*, pages 675–680, 2005.

[63] K. Youcef-Toumi and O. Ito. Controller design for systems with unknown dynamics. In *Proceeding of American Control Conference*, 1987.

[64] Mathworks. *Using Matlab version 5.* The Mathworks Inc., Natick, 1998.

[65] S. Cabaret, A. Burmyakov, H. Coppier, A. Rachid, and R. Barillere. Multicontroller: an object programming approach to introduce advanced control algorithms for the gcs large-scale project. In *ICALPECS07*, page 538, Knoxville, USA, October 2007.

[66] Y. Halevi and A. Ray. Integrated communication and control systems: Part i - analysis and part ii - design considerations. *ASME Journal of Dynamic System Measurements and Control*, 110:367, 1988.

[67] W. Zhang. *Stability Analysis of Networked Control Systems.* Phd thesis, Case Western Reserve University, 2001.

[68] C. H. Chen, C. L. Lin, and T. S. Hwang. Stability of networked control systems with time-varying delay. In IEEE, editor, *IEEE Communication Letters*, volume 11, page 270, March 2007.

[69] Y. Xia et al. Stability analysis of networked predictive control systems with random network delay. In IEEE, editor, *IEEE International Conference on Networking, Sensing and Control*, page 815, London, UK, April 2007.

[70] E. Rogez, B. Bradu, A. Moraux, M. Pezzetti, P. Gazet, and H. Coppier. A simulation case study for the virtual commissioning of the cern central helium liquefier. In IEEE, editor, *ICEC-ICMC08*, Seoul, Corea, July 2008.

[71] P. Gayet, S. Claudet, P.K. Frandsen, and A. Juillerat. Architecture of the lep2 cryogenics control system: conception, status, and evaluation. *CRYOGENICS -LONDON-*, 34(sup):83, 1994.

[72] N. Delruelle, A. Juillerat, H.K. Kuhn, and G. Passardi. Innovative aspects of the controls for the helium cryoplants in the CERN SPS accelerator. *CRYOGENICS -LONDON-*, 34(sup):77, 1994.

[73] ESA Board for Software Standardisation and Control (BSSC), editors. *ESA software engineering standards*, number 2, Paris, Feb 1991. European Space Agency.

[74] K.H. John and M. Tiegelkamp. IEC 61131: Programming industrial automation systems. volume 3, 2001.

[75] G. Penacoba, C. Balle, J. de la Gama, P. Gomes, E. Goussiou, N. Jeanmonod, A. Lopez Lorente, E. Molina, A. Suraci, and N. Vauthier. Outcome of the commissioning of the readout and actuation channels for the cryogenics of the lhc. LHC-PROJECT-Report-1134, page 4, Genoa, Italy, Aug 2008. CERN. Proceedings of EPAC08.

[76] P. Gomes, E Blanco, J. Casas, C. Fluder, E. Fortescue, E., P. Le Roux, G. Penacoba, M. Pezzetti, M. Soubiran, A. Tovar-Gonzales, and L. Zwalinski. The control system

for the cryogenics in the lhc tunnel [first experience and improvements]. volume CERN-ATS-2010-012, page 4, Geneva, Jan 2010. CERN.

[77] EA International, Madrid, Spain. *Mathematical algorithms and simulation guide.*, 2007.

[78] I. Butkevich, E. Idnic, and V. Shpakov. Cryogenic helium units simulation model. Prague, Czech Republic, 2006. ICEC21, CryPrague.

[79] R. Avezuela. *Cryogenic helium Library Reference Manual.* CERN, Geneva, Switzerland, 2001.

[80] Crodata Inc, Louisville, Colorado, USA. *User's guide to HEPAK Version 3.4.*, 1999.

[81] R. Maekawaa, K. Oobaa, M. Nobutokib, and T. Mitoa. Dynamic simulation of the helium refrigerator/liquefier for LHD.

[82] J. Casas-Cubillos, P. Gayet, P. Gomes, M. Pezzetti, C.H. Sicard, and F.J. Varas. Application of object-based industrial controls for cryogenics. volume CERN-LHC-2002-007-IAS, page 2013, Paris, Jun 2002. EPAC'02.

[83] H. Krause. Virtual commissioning of a large lng plant with the dcs 800xa by abb. 6th Eurosim Congress on Modelling and Simulation, Ljubljana, Slovenia, 2007.

[84] B. Bradu, P. Gayet, and S.I. Niculescu. Modeling, simulation and control of large scale cryogenic systems. volume Proceedings of the 17th World Congress The International Federation of Automatic Control, Seoul,Korea, 2008.

[85] G. Perinic, T. Dupont, D. Legrand, and M. Pezzetti. *Installation and Commissioning of the Helium Refrigeration System for the CMS Magnet*, volume 14, pages 1708–1710. 2004.

[86] G. Passardi and L. Tavian. Cryogenics at CERN. Divisional Report CERN LHC/2002-15, CERN, Grenoble, France, 2002.

[87] B. Bradu, P. Gayet, and S.I. Niculescu. Dynamic simulation of a 1.8 K refrigeration unit for the LHC. In *Proceedings of the 22nd International Cryogenic Engineering Conference*, 2008.

[88] B. Bradu, P. Gayet, and S.I. Niculescu. A process and control simulator for large scale cryogenic plants. *Control Engineering Practice*, 17:1388–1397, 2009.

[89] B. Bradu. *Modelisation, simulation et contrôle des installations cryogeniques du CERN*. Ph.D. Thesis in Physics, Université de Paris-Sud XI, Laboratoire des Signaux et Systèmes (CNRS-Supélec), 2010.

[90] C. Hirsch. *Numerical Computation of Internal and External Flow*, volume 2, chapter 3. John Wiley and Sons, 1990.

[91] E.F. Toro. *Riemann Solvers and Numerical Methods for Fluid Dynamics.* Springer, 2nd edition, 1999.

[92] E.D. Marquardt, J.P. Le, and R. Radebaugh. Cryogenic material properties database. In *Proceedings of the 11th International Cryocooler Conference*, pages 681–687, June 2000.

[93] A.P. Colburn. A method of correlating forced convection heat transfer data and a comparison with fluid friction. In *Trans. AIChE*, volume 19, pages 174–210, 1933.

[94] S.R. Kakac, K. Shah, and W. Aung. *Handbook of Single-Phase Convective Heat Transfer*. John Wiley and Sons, 1987.

[95] EA International. *Ecosimpro mathematical algorithms and simulation guide*, 2007.

[96] L.R. Petzold. A description of dassl: A differential/algebraic system solver. Report SAND82-8637, Sandia National Laboratories, 1984.